Copyright Warning & Restrictions

The copyright law of the United States (Title 17, United States Code) governs the making of photocopies or other reproductions of copyrighted material.

Under certain conditions specified in the law, libraries and archives are authorized to furnish a photocopy or other reproduction. One of these specified conditions is that the photocopy or reproduction is not to be "used for any purpose other than private study, scholarship, or research." If a, user makes a request for, or later uses, a photocopy or reproduction for purposes in excess of "fair use" that user may be liable for copyright infringement,

This institution reserves the right to refuse to accept a copying order if, in its judgment, fulfillment of the order would involve violation of copyright law.

Please Note: The author retains the copyright while the New Jersey Institute of Technology reserves the right to distribute this thesis or dissertation

Printing note: If you do not wish to print this page, then select "Pages from: first page # to: last page #" on the print dialog screen

ABSTRACT

ARTIFICIAL DIELECTRICS: CHARACTERISTICS AT LOW AND MICROWAVE FREQUENCIES

by
Nitish Agrawal

Artificial Dielectrics have been characterized using transmission line and s-parameter measurements. The complex dielectric constant and loss of graphite filled and non-poled piezoelectric-aggregate (Polyvinylidene Fluoride, PVDF) filled plastic (PMMA) has been characterized at low (1kHz-10kHz range, i.e., the VLF, very low frequency, range) and microwave frequencies. The average diameter diameter of graphite particles used was thirty microns. Measurements were performed on very fine graphite (one micron diameter grains) and 30 micron sized grains for comparison purposes. Fine grain graphite particles exhibited a larger real dielectric constant, probably owing to a larger dipole effect. The dielectric constant characterization has also been done for PVDF-graphite-PMMA aggregates. Dissipation factors have been calculated in all cases.

The very low frequency measurements have been done using lossy capacitance principles. The very low frequency behavior of graphite-PMMA samples showed an anomaly at percolation point (about 15 % of graphite). PVDF-PMMA samples showed no anomaly within the range of concentration measured, probably owing to the fact that PVDF is a dielectric material. At microwave frequencies, it is found that both real and imaginary parts of the dielectric constant experience an increase with the increase in graphite/PVDF loading.

ARTIFICIAL DIELECTRICS: CHARACTERISTICS AT LOW AND MICROWAVE FREQUENCIES

by
Nitish Agrawal

A Thesis
Submitted to the Faculty of
New Jersey Institute of Technology
in Partial Fulfillment of the Requirements for the Degree of
Master of Science in Electrical Engineering

Department of Electrical and Computer Engineering

October 1994

APPROVAL PAGE

ARTIFICIAL DIELECTRICS: CHARACTERISTICS AT LOW AND MICROWAVE FREQUENCIES

Nitish Agrawal

Dr. Haim Grebel, Thesis Advisor — Date
Associate Professor of Electrical and Computer Engineering, NJIT

Dr. Edip Niver, Committee Member — Date
Associate Professor of Electrical and Computer Engineering, NJIT

Dr. Shih Chang Wu, Committee Member — Date
Assistant Professor of Electrical and Computer Engineering, NJIT

BIOGRAPHICAL SKETCH

Author: Nitish Agrawal

Degree: Master of Science in Electrical Engineering

Date: October 1994

Undergraduate and Graduate Education:

- Master of Science in Electrical Engineering,
  New Jersey Institute of Technology, Newark, NJ, 1994
- Bachelor of Engineering in Electrical & Electronics,
  Manipal Institute of Technology, Manipal, India, 1992

Major: Electrical Engineering

This thesis is dedicated to my parents and my brother whose constant love and support helped me throughout my education.

ACKNOWLEDGMENT

I convey my sincere thanks to my thesis advisor, Dr. Haim Grebel, whose constant guidance helped me carry out the thesis work satisfactorily. My heartiest thanks to Dr. Jan Opyrchal for helping me throughout the research and for constant moral support. Thanks are due to Mr. Amy of Physics Machine shop who carefully machined samples of PVDF-PMMA used in the research.

I thank Dr. Edip Niver for help and guidance in the thesis work and for letting me use the rectangular waveguide setup and the Network-analysis equipment in the Center for Microwave and Lightwave Engineering. Special thanks to Dr. Shih Chang Wu for constantly supporting me throughout my work and enlightening me through useful discussions.

I would also like to acknowledge the use of the Network Analysis equipment at Epitaxx Inc., West Trenton. I would also like to thank my senior, Mr. Jim Rue, at Epitaxx for allowing me the time to work on my thesis. Last but not the least, I would like to thank all those whose names have not been mentioned but who have directly or indirectly helped me in my thesis work.

TABLE OF CONTENTS

Chapter Page

LIST OF FIGURES

Figure Page

Figure Page

Figure Page

Figure Page

CHAPTER 1

INTRODUCTION

This chapter will introduce artificial dielectric materials. Terms used in describing the dielectric constant behavior of dielectrics under the influence of an alternating field will be described. The materials studied in this thesis will be described.

1.1 About artificial dielectrics

An artificial dielectric is obtained by arranging a large number of identical conducting obstacles in a three-dimensional pattern. The conducting obstacles are held together by a binder material. The binder material used in this study was a homogeneous, non-polar polymer, Polymethyl Methacrylate (PMMA), commercially known as plexiglas. Under the excitation of an external applied electric field, the charges on each conducting obstacle are displaced so as to setup an induced field that will cancel the applied electric field at the obstacle surface. Each obstacle thus simulates the nature of a molecule in an ordinary dielectric in that it exhibits a dipole moment. The combined effect of all the obstacles in the material is to produce a net average dipole polarization P per unit volume. If E is the net average field in the medium, the displacement D is given by:

$$\mathbf{D} = \epsilon_o \mathbf{E} + \mathbf{P} = \epsilon \mathbf{E} \tag{1.1}$$

From the above equation it is apparent that the effective permittivity ϵ will be different than ϵ_o. A detailed account on the approaches used to analyze artificial dielectrics can be found in [1]. There has been a growing interest in conductive polymers and artificial dielectrics for microwave use such as in absorbers and shielding and also for high frequency polymeric integrated circuits. These applications served

as the motivation for characterising the complex dielectric constant of such materials. A number of methods can be used for estimating the dielectric constant and many papers have been published on these methods [15] [16] [18] [19] [14]. Two major methods have been used to calculate the complex dielectric constant and the loss at high frequencies (up to 18 GHz). The high frequency measurements are done using S-parameter techniques as well as rectangular waveguide theory. The rectangular waveguide technique works well for low loss materials whereas the S-parameter technique works well for characterization of relatively high loss materials. This is because higher order modes cannot be supported in a rectangular waveguide designed to operate in a certain frequency range and so the theory valid for the fundamental mode works well here. The S-parameter technique uses an air-line which becomes multimoded after a certain frequency depending on the dielectric constant of the material inside it. The single mode analysis thus does not yield satisfactory results under these conditions. The higher order modes, however, are not sustained if the dielectric inside the air-line is lossy. So, for high loss materials this method yields satisfactory results up to a relatively large frequency.

Low frequency characterization is done using a capacitance test fixture. The low frequency measurement technique used in this study gives satisfactory results for both low and high loss materials.

The conducting material used in this study is graphite powder and the base substance is a polymer, Polymethyl Methacrylate (PMMA), commonly known as plexiglas. A piezoelectric substance, Polyvinylidene Fluoride (PVDF) has also been used along with graphite to observe both graphite and PVDF's effect together.

1.2 Behavior of conventional dielectrics in alternating fields

The dielectric constant is a macroscopic manifestation of the polarization phenomena which take place at a microscopic or molecular scale, and which are essentially the

formation and orientation of dipoles within the material. When a dielectric material is subjected to an alternating field, the orientation of the dipoles and hence the polarization will tend to reverse every time the polarity of the field changes. As long as the frequency remains low ($< 1 \times 10^6 Hz$) the polarization follows the alterations of the field without any significant lag and the permittivity is independent of the frequency and has the same magnitude as in static field. When the frequency is increased, the dipoles will no longer be able to rotate sufficiently rapidly and their oscillations will begin to lag behind those of the field. As the frequency is further raised, the permanent dipoles, if present in the medium, will be completely unable to follow the field and the contribution to the static permittivity from this molecular process, the orientational polarization ceases; this usually occurs in the radio frequency range ($1 \times 10^6 - 1 \times 10^{11} Hz$). At still higher frequencies, usually in the infrared ($1 \times 10^{11} - 1 \times 10^{14} Hz$) the relatively heavy positive and negative ions cannot follow the field variations and so the contribution to the permittivity from the atomic or ionic polarization ceases and only the electronic polarization remains.

The above effects lead to a fall in the permittivity of a dielectric material with increasing frequency, a phenomenon which is usually referred to as anomalous dielectric dispersion. The dispersion arising during the transition from full atomic polarization at radio frequencies to negligible atomic polarization at optical frequencies is usually referred to as *resonance absorption* [2].

The dispersion arising during the transition from full orientational polarization at low frequencies to negligible orientational polarization at high or microwave frequencies is referred to as *dielectric relaxation* [2].

1.3 Brief review of the research and findings in artificial dielectrics

The rectangular waveguide technique has been used to investigate rubber compounds having different concentrations of carbon black content [3]. They reported an increase

in the dielectric constant with increasing carbon black content at all frequencies. Using this technique they were unable to measure the dielectric constant of graphite beyond a certain point owing to the high conductivity of graphite aggregates.

The dielectric constants, dissipation factors and dielectric losses of various polymers including PVDF have been listed in [6]. They have investigated the dielectric strengths of PVDF using DC and AC models. The DC measurements were done using a capacitance fixture with brass electrodes and PVDF films of thickness 12 microns. The orientation of the dipoles in PVDF have been determined by an approach that considers the equilibrium between the field induced torque and the elastic restoring torque generated by the excursion of the dipoles from their initial stable positions.

It was confirmed by Tsutsumi *et al* [7] that a melt-quenched and annealed blend of 80 wt% polyvinylidene fluoride and 20 wt% of polymethylmethacrylate has the β crystal form of PVDF with optical clarity and other properties that are desirable for a host material in a guest-host system where the guest is an optically nonlinear dye that is orientationally stabilized by the strong internal electric field of a poled ferroelectric. They have characterised the absorbance of PVDF/PMMA blends in the wavelength range 250-750 nm. They explained that the above blend was transparent in the visible region because the size of the crystallites was smaller than the wavelength of visible light. They concluded that the poling-induced internal fields in the PVDF/PMMA blend are greater than the nominal poling field (equal to the potential difference between the electrodes divided by the distance between the electrodes). The internal fields in the blend were due to both space charge and polarization.

Grebel and Jimenez [5] have measured frequency response of conditional artificial dielectrics in the microwave range and under illuminated conditions. In this paper they investigated optically controlled microwave devices and showed that

light induced electric and magnetic dipoles are created in the semiconductor obstacles which were embedded in the polymeric host material. The photo-generated dipoles induced a phase shift in the propagating microwave beam.

Wang *et al* [8] have proposed a new approach to describe the dielectric hysterisis behavior of polymeric ferroelectrics which had until now been described by an energy approach in which the redistribution of the crystal dipole orientation under an applied field was determined by the probability for the molecular dipoles to rotate about the long chain axes from energetically stable position to the other. By their new approach the orientation of the dipole is determined by the equilibrium between the field-induced torque and the elastic restoring torque generated by the excursion of the dipoles from their initial stable positions. They explain that the rotation of the chain segment takes place in a continuous manner in response to smoothly rising applied field, until a point is reached at which at which-the field induced torque equals the maximum value of the periodically varying restoring torque; at this point, which characterizes the threshold electric field, the chain segment makes a discreet rotational jump to the next stable position. They concluded that the advantage of their model was that it could readily be extended to account for switching experiments where inertial effects become important.

Krishna and Prasad [9] have investigated the iodine doped polymer, PBT, for microwave absorber use and as an EMI shield. They doped PBT by ion-implanting iodine in it. They also describe the cavity perturbation principle for the measurement of microwave conductivity and comment on the frequency dependence of the return loss and temperature dependence of microwave conductivity.

Yacubowicz and Narkis [11] report the results on the dielectric properties of carbon black filled cross-linked polyethylene composites. They state that the dielectric constant increases slowly with the increasing carbon black concentration at a measurement frequency of 8 MHz. They also report that the dissipation

factor increases initially with the increasing graphite concentration and then falls after the percolation point is reached. They report that carbon black-polymer systems deviate strongly from the predicted percolation concentration for dispersed conductive spheres.

Olmedo *et al* [10] have tried to show how conductive polymers can overcome the disadvantages associated with the preparation of microwave absorbing materials based on the dispersion of conductive additives (carbon black, graphite, metallic powders). They concluded that the latter suffer from such disadvantages as the requirement of control of both rate and addition of the conductive particles and the phenomenon of particle aggregation which make it difficult to obtain a high level of reproducibility. They used polypyrrole, polyaniline and polyalkylthiophene based absorbents.

Several models have been proposed to describe the behavior of artificial dielectrics under static and alternating conditions. The most accurate ones are based on the electron gas concept [20] [21] [22]. A good description of plasma resonance and electron gas can be found in [19]. Doremus [22] conducted a study on small silver particles embedded in glass. He tried to explain the observed dielectric constant assuming that the properties of the material were determined by free electrons. His model was to explain crystalline particles only. He reported that as the glass was annealed at high temperature after irradiation, a sharp absorption band developed with a peak at 0.406 microns, and the glass became yellow. As annealing continued, the band position remained fixed, but the band remained sharper. Without silver in the glass, no such band developed. He concluded that if the particles were not spherical (or equiaxial), the absorption band would be at longer wavelengths and would gradually shift to lower wavelengths as the particles become more spherical with long annealing at high temperatures as known for non-spherical gold particles.

Stookey and Araujo [21] have used a free-electron model to explain the dependence of absorption of light by small metal particles when suspended in a medium of a different refractive index. They showed that the position of the absorption bands depends strongly on the elongation of the silver particles used in their study. Their theoretical data indicated that if all the particles in glass were the same size, then glass would have very intense and very sharp absorption bands whose position in the visible spectrum would depend on the amount of stretching (in other words, the size of the particles).

The high frequency characterization of Graphite-PMMA, PVDF-PMMA and PVDF-Graphite-PMMA systems in terms of complex permittivity and dissipation factor has not been done previously.

CHAPTER 2

LOW FREQUENCY MEASUREMENT OF COMPLEX DIELECTRIC CONSTANT

The low frequency complex dielectric constant was measured using a lock-in amplifier and a parallel plate capacitance test fixture. These measurements were made at 1 kHz and 10 kHz. Planar samples (films) of graphite loaded PMMA, and PVDF loaded PMMA were made to be used for measurement of dielectric constant. In the case of graphite loaded PMMA, the samples were conductive after a certain concentration (percolation point). To prevent a short between the parallel plates of the fixture, a transparent thin tape was put on one of the faces of the film. The measurement setup consisted of a parallel plate capacitance test fixture connected to lock-in amplifier as shown in figure 2.1. Guarded electrodes were used in the measurement setup. A detailed note on the construction of guarded electrodes and low frequency dielectric constant measurement principles can be found in [12].

2.1 Theory of low frequency measurement

The theory of the low frequency measurement follows: The total current with dielectric and tape between the plates of the capacitor is I_{dt} where the subscript d stands for the dielectric and t stands for the tape. It is given as: $I_{dt} = |I_{dt}|exp(\jmath\theta_{dt})$ The impedance of the dielectric and tape together between the plates is found as:

$$Z_{dt} = V_{ref}/I_{dt} \tag{2.1}$$

The current through the capacitor placed with just the tape between them is also measured and is $I_t = |I_t|exp(\jmath\theta_t)$. The impedance of the tape would thus be $Z_t = v_{ref}/i_t$ where v_{ref} is the rms value of the voltage applied across the capacitor plates.

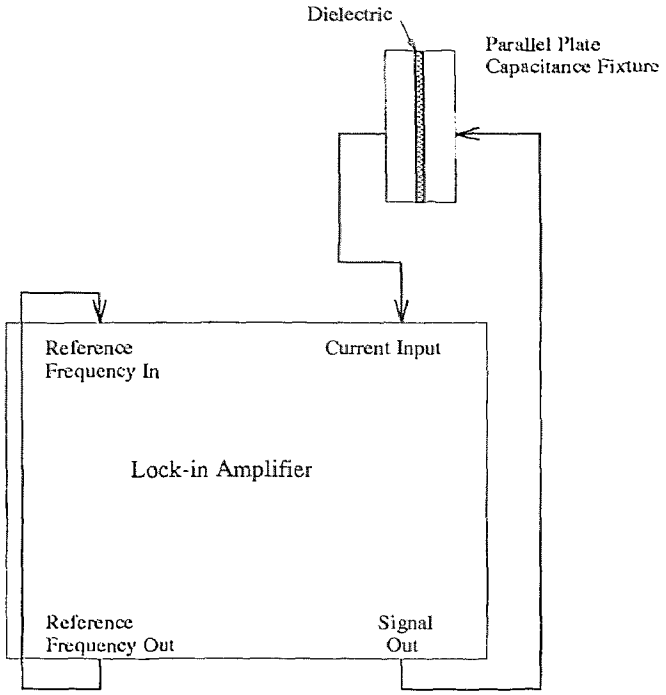

Figure 2.1 Capacitance measurement setup for the measurement of dielectric constant at low frequencies

The impedance of the dielectric alone would thus be Z_d:

$$Z_d = Z_{dt} - Z_t \tag{2.2}$$

The dielectric impedance is a parallel combination of its resistance, R and its capacitance, C, i.e.,

$$1/Z_d = 1/R + 1/jX \tag{2.3}$$

where, X is the parallel capacitive reactance and $X = 1/\omega C$ where, $\omega = 2\pi f$ (f is the measurement frequency) It follows that

$$R = 1/(Re(1/Z_d)) \tag{2.4}$$

and

$$X = 1/(Im(1/Z_d)) \tag{2.5}$$

$$C = 1/\omega X \tag{2.6}$$

The relative complex dielectric constant is defined as

$$\epsilon = \epsilon' - j\epsilon'' \tag{2.7}$$

The real part of the dielectric constant is found as

$$\epsilon' = (d)(C)/a\epsilon_o \tag{2.8}$$

where ϵ_o is the absolute electric permittivity of free space and has a value of $8.85 \times 10^{-12} F/m$. The dissipation factor (loss tangent) is defined as

$$tan\delta = X/R \tag{2.9}$$

The imaginary part of the relative dielectric constant is given by

$$\epsilon'' = (\epsilon')(tan\delta) \tag{2.10}$$

2.2 Experimental results

This section presents the computed values of the complex dielectric constant and the dissipation factor. The reflection coefficient magnitudes are also presented.

2.2.1 Graphite - PMMA composites tested at 1kHz

The variation of the real part of dielectric constant versus the weight percent of graphite in graphite-PMMA mixtures (at 1kHz) is shown in figure 2.2. It is seen that the real part of dielectric constant increases up to a certain frequency and then experiences a rapid rise after which it falls down again to assume its normal trend. The variation of the imaginary part of dielectric constant of the graphite-pmma composites (at 1kHz) as a function of the weight percent of graphite in the composites is shown in figure 2.3. It is observed that the imaginary part of dielectric constant stays approximately constant up to a certain concentration and then experiences a rapid rise after a certain concentration. After achieving its peak

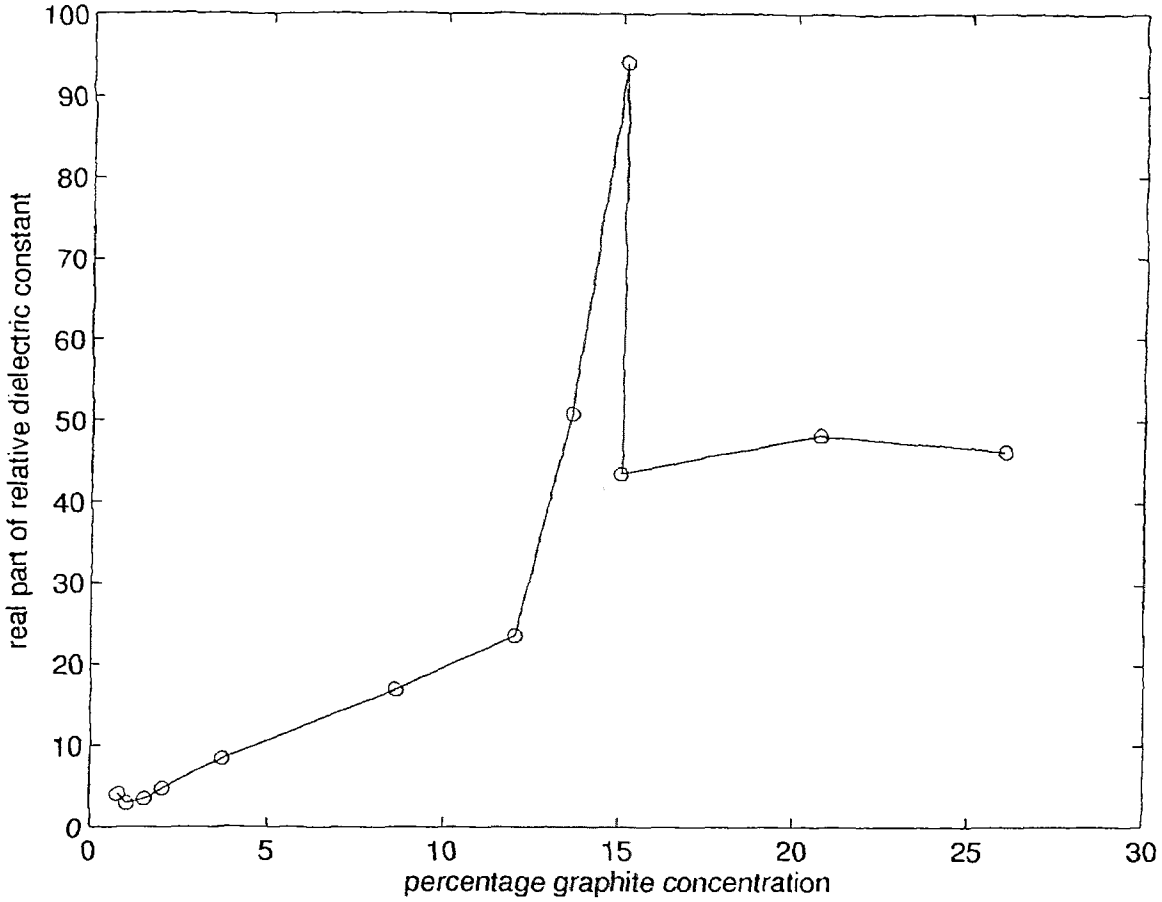

Figure 2.2 Variation of the real part of dielectric constant of the graphite-pmma composites (at 1kHz) as a function of the weight percent of graphite in the composites.

it falls down again but to a higher value compared to the values before it experienced the rise. The variation of the dissipation factor (loss tangent) in the graphite-pmma composites (at 1kHz) as a function of the weight percent of graphite in the composites is shown in figure 2.4. As explained in theory, the dissipation factor is the absolute value of the ratio the imaginary part of the dielectric constant to the real part of the dielectric constant.

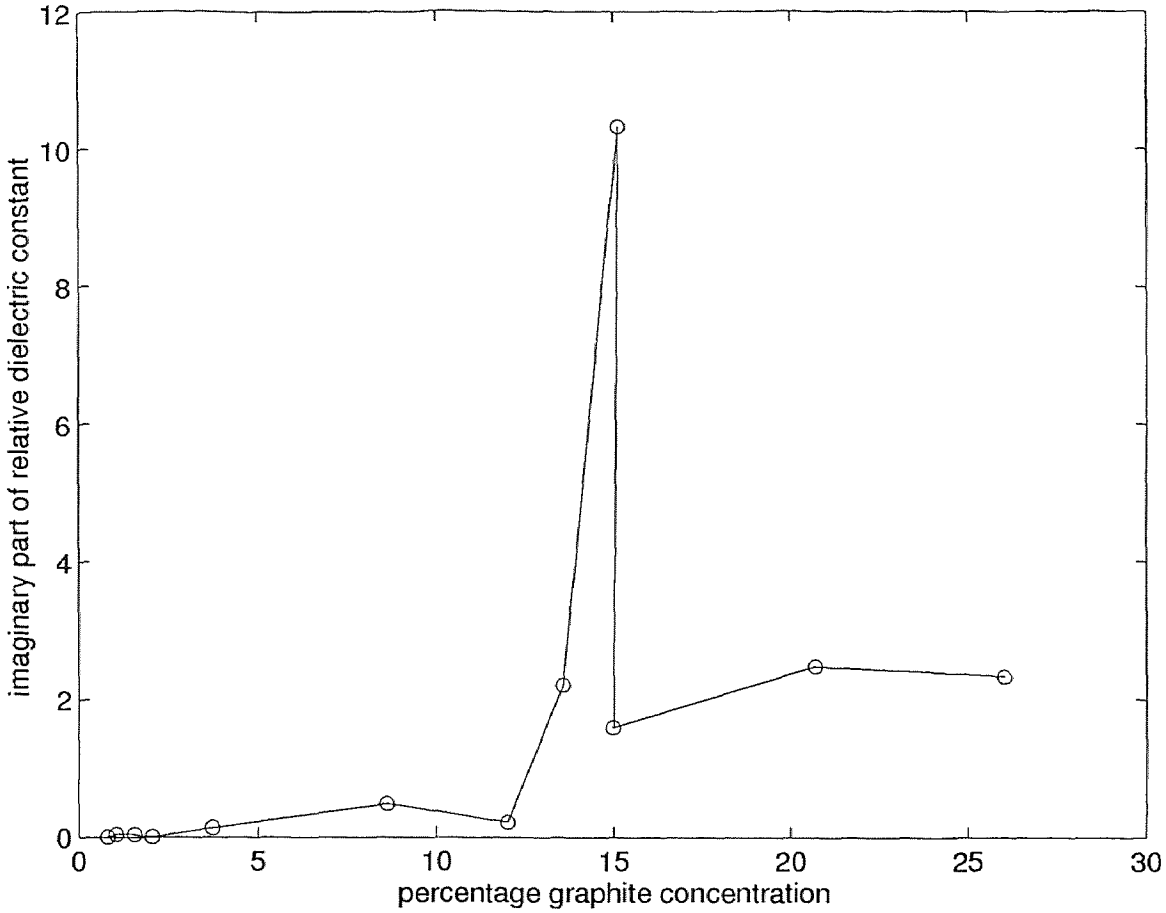

Figure 2.3 Variation of the imaginary part of dielectric constant of the graphite-pmma composites (at 1kHz) as a function of the weight percent of graphite in the composites.

2.2.2 Graphite - PMMA composites tested at 10kHz

The variation of the real part of dielectric constant versus the weight percent of graphite in graphite-PMMA mixtures (at 10kHz) is shown in figure 2.5. It is clearly seen that the the real part of the dielectric constant reaches its peak value at around 15 % for both measurement frequencies eliminating the possibility of the occurrence of the peak due to any circuit resonance. The variation of the imaginary part of dielectric constant of the graphite-pmma composites (at 10kHz) as a function of the weight percent of graphite in the composites is shown in figure 2.6. The

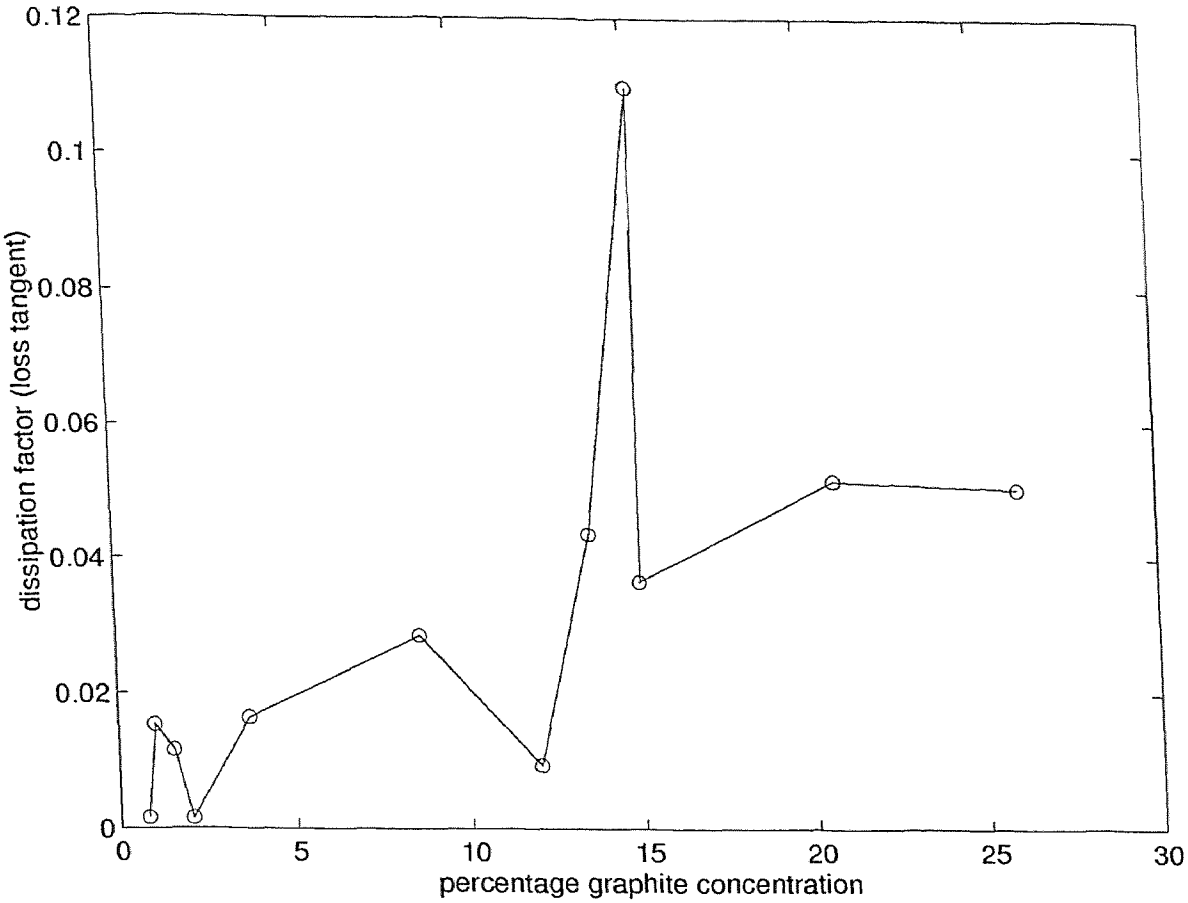

Figure 2.4 Variation of dissipation factor of the graphite-pmma composites (at 1kHz) as a function of the weight percent of graphite in the composites.

variation of the dissipation factor of the graphite-pmma composites (at 10kHz) as a function of the weight percent of graphite in the composites is shown in figure 2.7.

2.2.3 PVDF-PMMA composites

The plots of the dielectric constant and dissipation factor at 1 kHz are given in Appendix A. It is seen that the real part of dielectric constant increases with the increase in the PVDF concentration and so does the imaginary part. The real

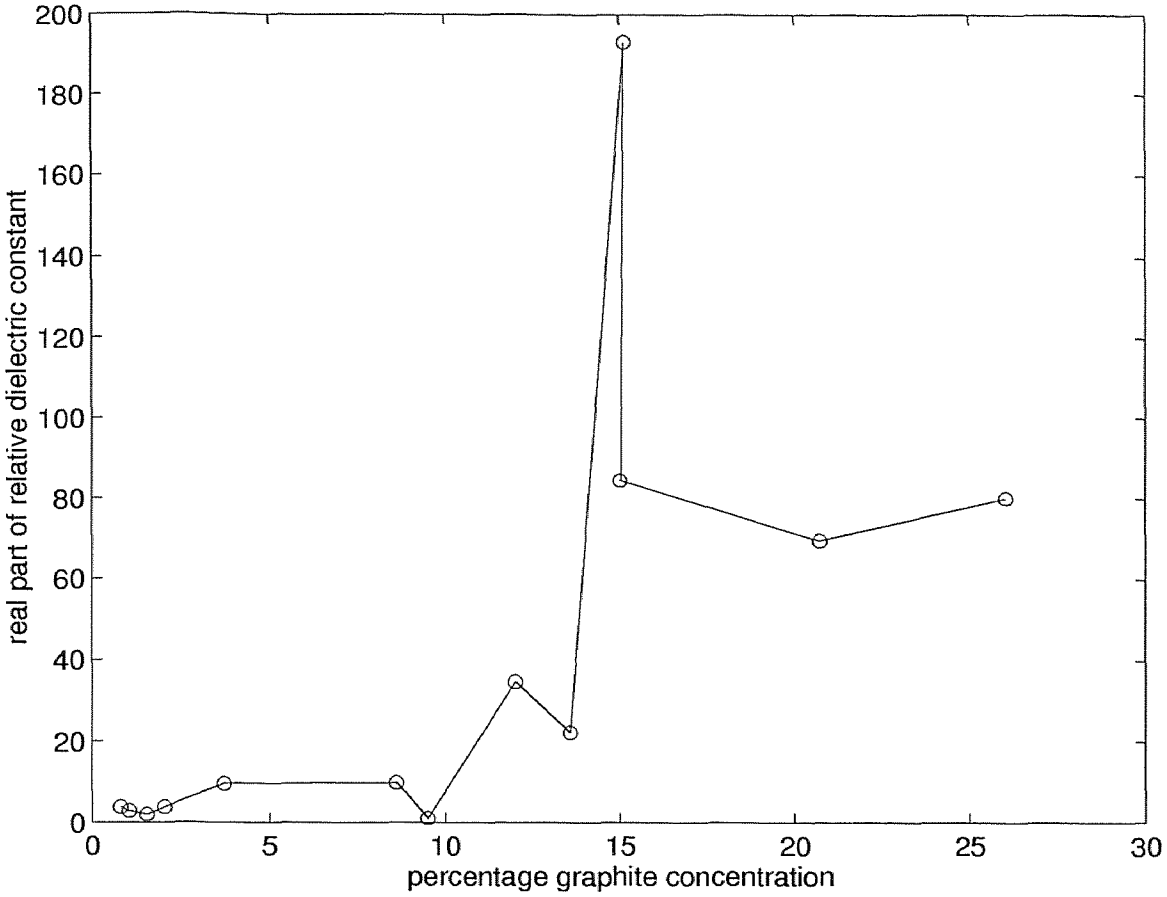

Figure 2.5 Variation of the real part of dielectric constant of the graphite-pmma composites (at 10kHz) as a function of the weight percent of graphite in the composites.

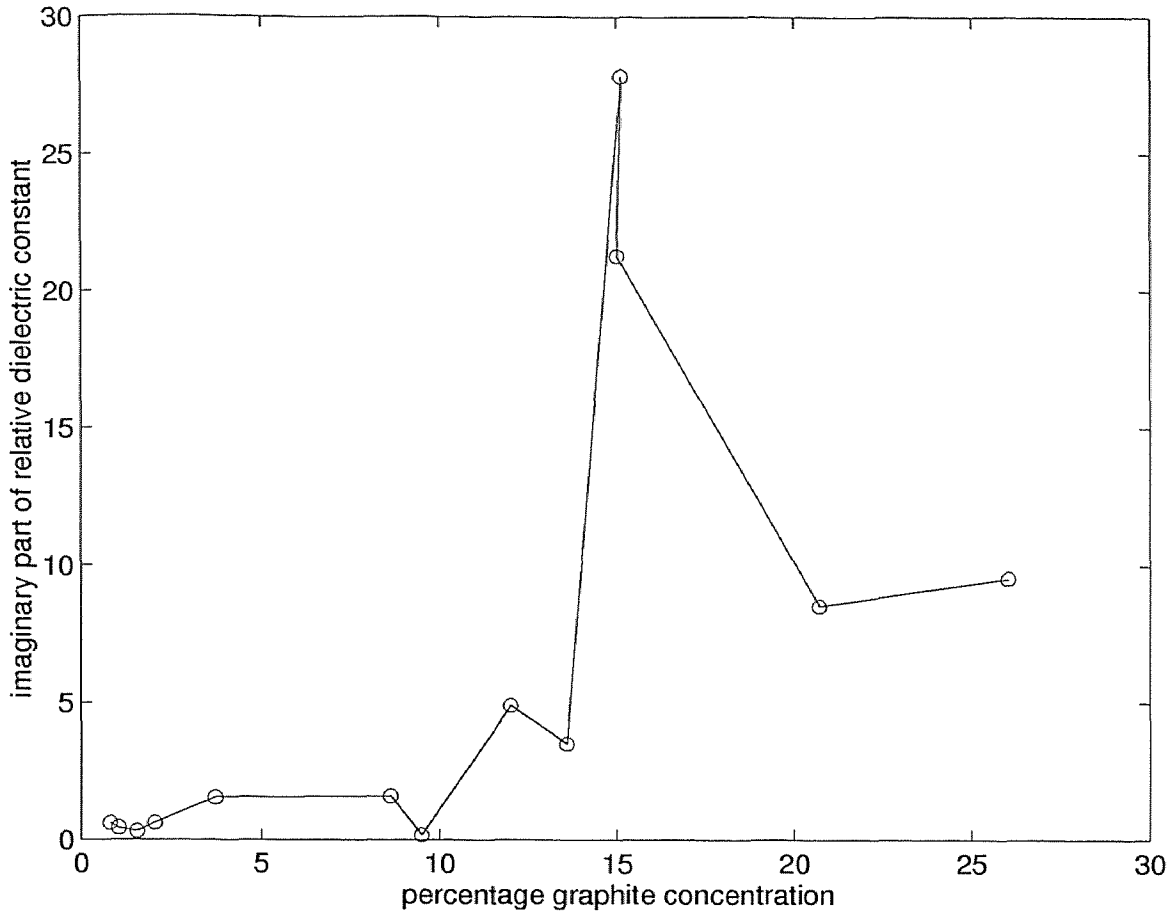

Figure 2.6 Variation of the imaginary part of dielectric constant of the graphite-pmma composites (at 10kHz) as a function of the weight percent of graphite in the composites.

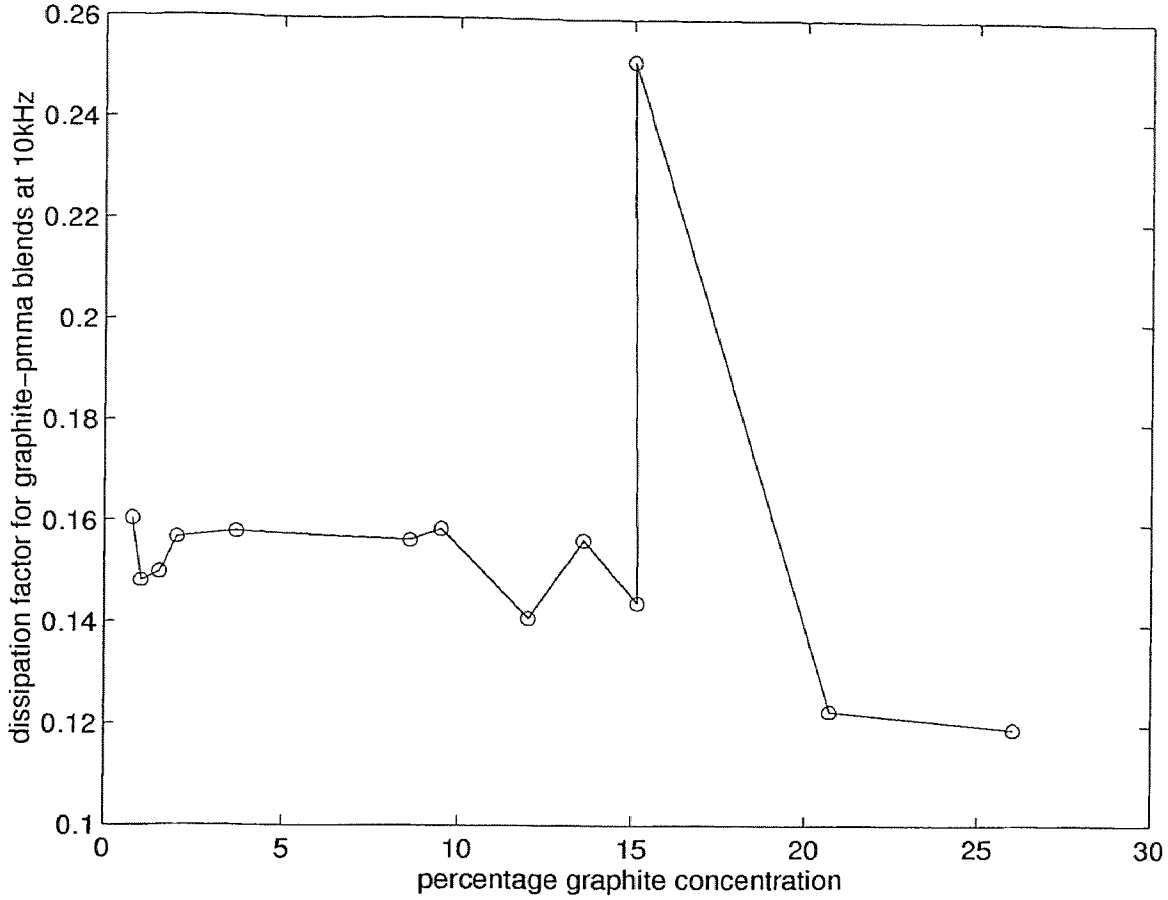

Figure 2.7 Variation of dissipation factor of the graphite-pmma composites (at 10kHz) as a function of the weight percent of graphite in the composites.

part does not exhibit the same nature as observed in the case of graphite-pmma composites. The imaginary part, however, falls down after a certain concentration.

CHAPTER 3

HIGH FREQUENCY MEASUREMENT OF DIELECTRIC CONSTANT USING A SLOTTED RECTANGULAR WAVEGUIDE

3.1 Theory of measurement

The high frequency measurements using the rectangular waveguide were done using the setup shown in figure 3.1 The dielectric constant may be calculated from the

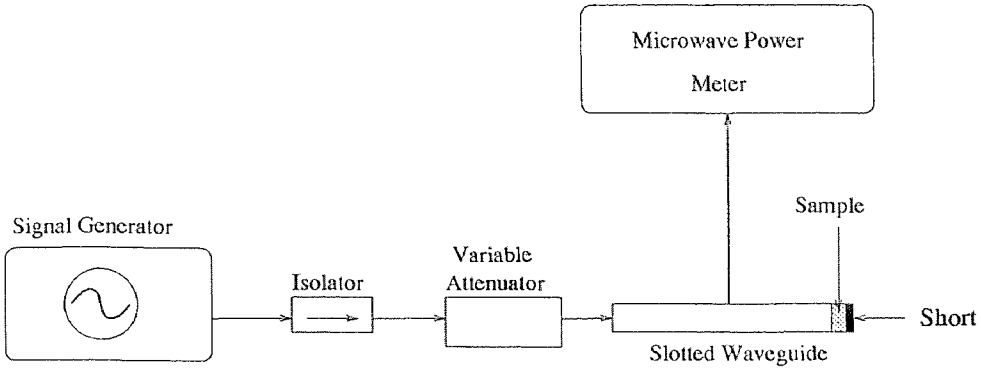

Figure 3.1 Rectangular waveguide setup for measuring the dielectric constant of a material

knowledge of the reflected wave amplitudes with and without the dielectric in the guide and the positions of the minimum (or maximum) amplitudes of the voltage standing wave in the guide. The experiments using the rectangular waveguide were done at 10.7 GHz. The basic theory used in calculating the complex dielectric constant using the rectangular waveguide method is outlined below [13] [1].

The complex dielectric constant is given by equation 2.7 and is repeated here for convenience,

$$\epsilon = \epsilon' - j\epsilon'' \tag{3.1}$$

The electromagnetic wavelengths in an infinite dielectric filled region and a free-space region are related as

$$\lambda_c = \lambda_o/\sqrt{\epsilon} \tag{3.2}$$

where λ_ϵ is the wavelength in the dielectric; λ_o is the free space wavelength. The complex propagation constant in the dielectric is given by γ_ϵ,

$$\gamma_\epsilon = 2\pi/\lambda_\epsilon \tag{3.3}$$

The complex propagation constant in the dielectric filled region of the rectangular waveguide is given, assuming the lowest propagation mode, as $\gamma_{\epsilon g}$,

$$\gamma_{\epsilon g} = \jmath\sqrt{\gamma_\epsilon^2 - (\pi/a)^2} \tag{3.4}$$

where, a is the rectangular waveguide cavity width. The characteristic impedance of the dielectric filled waveguide is given by $Z_{\epsilon g}$

$$Z_{\epsilon g} = \jmath\beta_o Z_o/\gamma_{\epsilon g} \tag{3.5}$$

where, β_o is the free space propagation constant (real quantity); Z_o is the intrinsic impedance of free space.

The input impedance seen looking into the dielectric sample (of length d) in the rectangular waveguide backed by a short (metal plate) is given by Z_d:

$$Z_d = Z_{\epsilon g}[Z_s - Z_{\epsilon g} tanh(\gamma_{\epsilon g} d)]/[Z_{\epsilon g} - Z_s tanh(\gamma_{\epsilon g} d)] \tag{3.6}$$

where Z_s is the input impedance of the metal plate alone.

The impedance seen looking at any point in the waveguide at a distance s towards the generator from the load is given by the following equation:

$$Z(s) = Z_g(1 + re^{\jmath(\theta_p - 2\beta_s)})/(1 - re^{\jmath(\theta_p - 2\beta_s)}) \tag{3.7}$$

where, r = load reflection coefficient and is computed as:

$$r = (SWR - 1)/(SWR + 1) \tag{3.8}$$

where, SWR = standing wave ratio in the waveguide and is found as:

$$SWR = V_{max}/V_{min} = (P_{max}/P_{min})^{1/2} \tag{3.9}$$

where, V_{max} and V_{min} respectively are the maximum and minimum voltages along the waveguide and P_{max} and P_{min} are maximum and minimum powers measured at the points where the maximum and minimum voltages occur. θ_p is the constant phase part of the reflection coefficient in the waveguide and is given by:

$$\theta_p = -\pi + 2\beta s_{1,min} \tag{3.10}$$

The input impedance seen looking from the $s_{1,min}$ point towards the load is given by evaluation of equation 3.7 at $s = s_{1,min}$ and using the above given expression for θ_p:

$$Z_{s_{1,min}} = Z_g(1+re^{j(-\pi+2\beta s_{1,min}-2\beta s_{1,min})})/(1-re^{j(-\pi+2\beta s_{1,min}-2\beta s_{1,min})}) = Z_g(1-r)/(1+r) \tag{3.11}$$

The input impedance seen looking towards the load from the first voltage minimum point is given by either side of the following equality:

$$Z_g[Z_d - jZ_g tan(\beta_g s_{1,min}/j)]/[Z_g - jZ_d tan(\beta_g s_{1,min})] = Z_g[1-r]/[1+r] \tag{3.12}$$

where, $s_{1,min}$ is the distance (towards the source) of the first voltage minimum next to the air-dielectric interface in the guide. Z_g is the characteristic impedance of the free space filled guide and is calculated as follows:

$$Z_g = j\beta_o Z_o/\beta_g \tag{3.13}$$

where, $\beta_g$is the propagation constant in the air-filled waveguide and is found as follows (β_g is assumed only due to dispersion, the guide being practically lossless):

$$\beta_g = (\beta_c^2 - \beta_o^2)^{1/2} \tag{3.14}$$

where β_c is the cutoff propagation constant in the air-filled waveguide and is given by:

$$\beta_c = \pi/a \tag{3.15}$$

Note that Z_g in equation 3.12 is common on both sides and so would cancel out.

Some caution is required in using the above method. In addition to extracting power from the line, the penetration of the sampling probe into the slotted section gives rise to reflections from the probe itself. These reflections travel back toward the generator. If the generator is mismatched, the reflections are re-reflected. When probe is moved under these conditions, the phase of the reflection is changed and error results. However, reflections from the generator are a second order effect, important only when one is measuring a low SWR (2 or less) [17]. In this case a moderately good match between the generator and the load is desirable. In these measurements a solid state frequency generator was used together with an isolator so most of the reflections were avoided.

3.1.1 Determining $s_{1,min}$

A metal block of the same size as the dielectric block to be tested is inserted at the load end of the waveguide, and a convenient position of the voltage standing wave minimum is noted (see figure 3.2). The block to be tested is then inserted (with the metal block removed, of course) and the corresponding shift (towards the generator) in this minimum position is calculated by subtracting the formerly observed position from the newly observed minimum position of the voltage standing wave [13]. This shift gives the value of $s_{1,min}$.

3.2 Experimental results

The real part of the dielectric constant as calculated from the above technique is shown in figure 3.3. The imaginary part of the dielectric constant as calculated from the above technique is shown in figure 3.4.

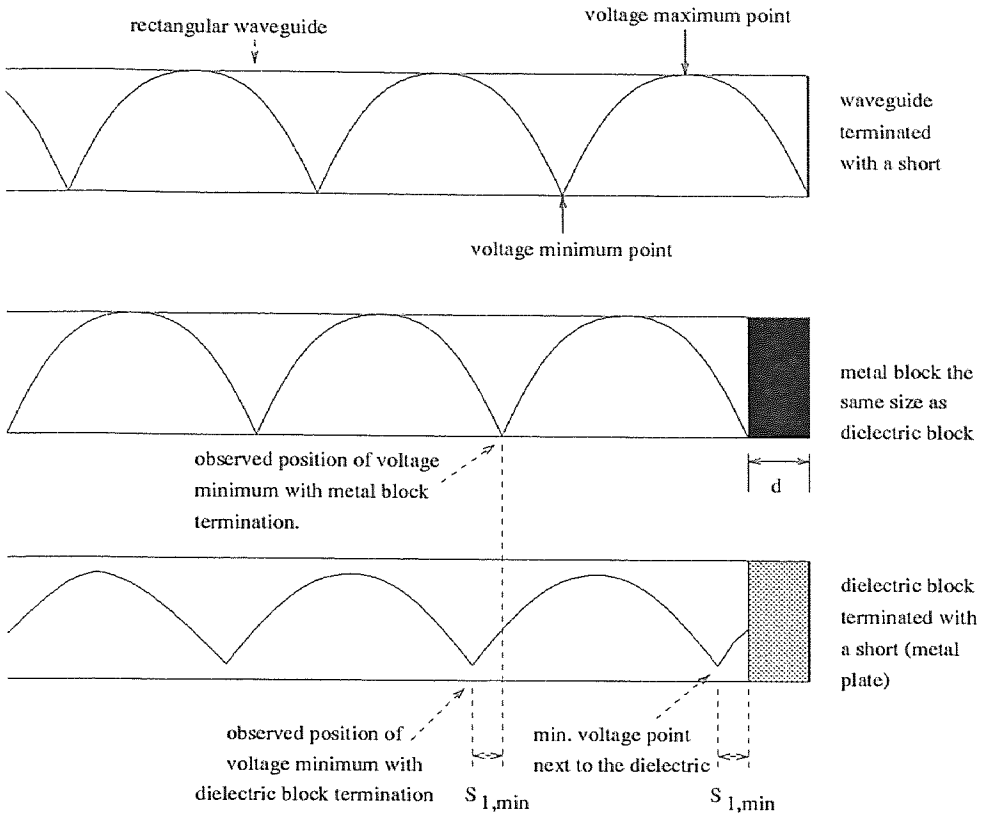

Figure 3.2 Determining the position of voltage minimum immediately next to the air-dielectric interface

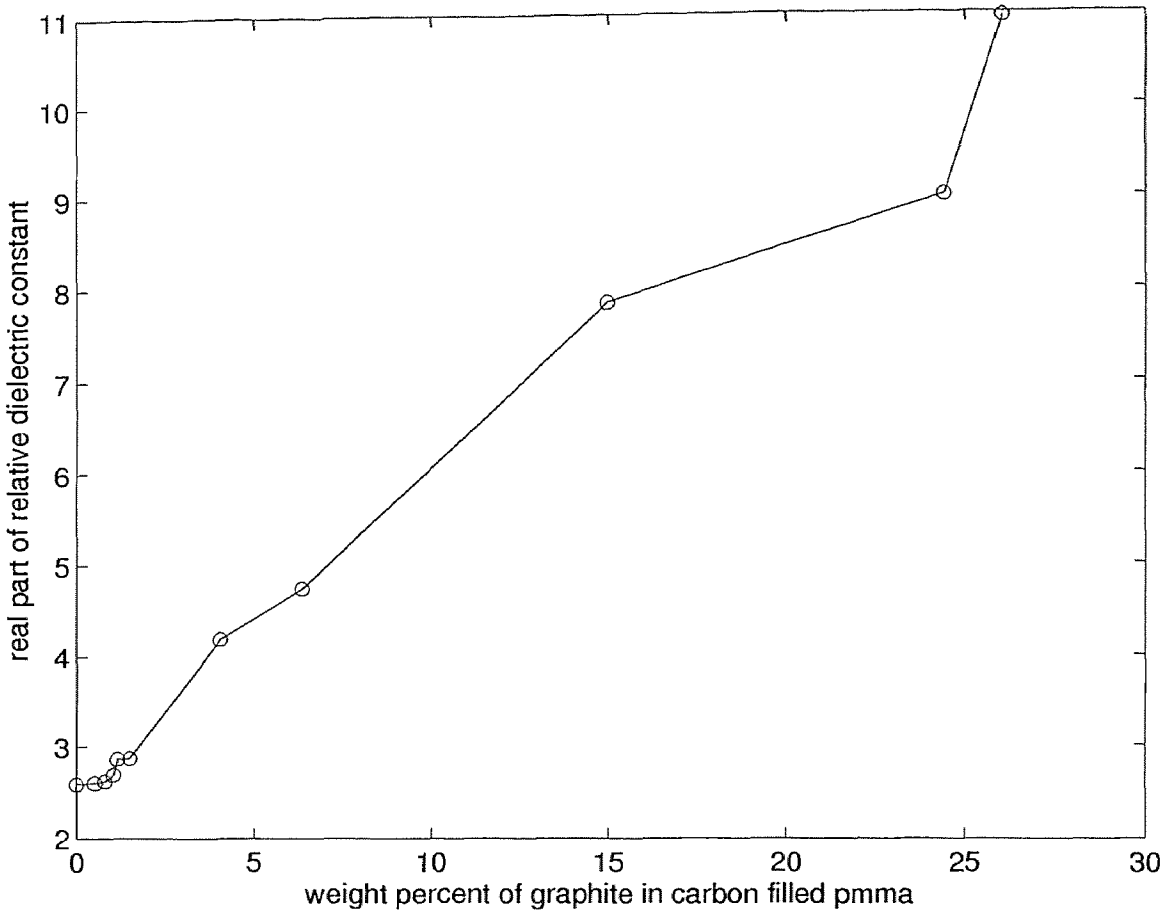

Figure 3.3 Real part of the dielectric constant plotted against the concentration of graphite in the PMMA-Graphite samples.

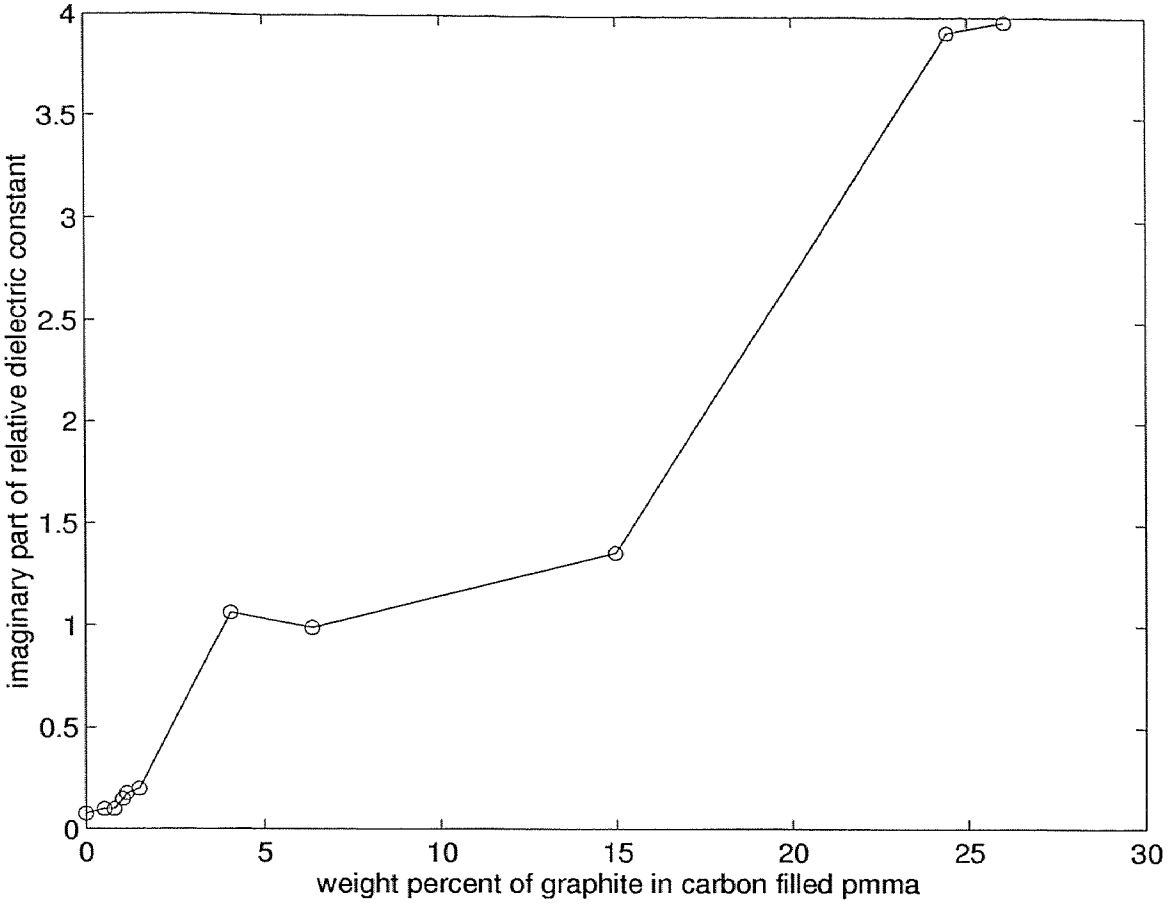

Figure 3.4 Imaginary part of the dielectric constant plotted against the concentration of graphite in the PMMA-Graphite samples.

CHAPTER 4

HIGH FREQUENCY MEASUREMENT OF DIELECTRIC CONSTANT USING S-PARAMETER PRINCIPLES AND A VECTOR NETWORK ANALYZER

4.1 Theory of measurement

The measurements were made with the sample material installed in a 50-ohm (Z_o) air line. This 7 mm diameter airline served as the measurement fixture (sample holder). The dielectric sample is machined into a bead to slide into the coaxial sample holder shown in figure 4.1. The measuring instrument was a HP 8720C

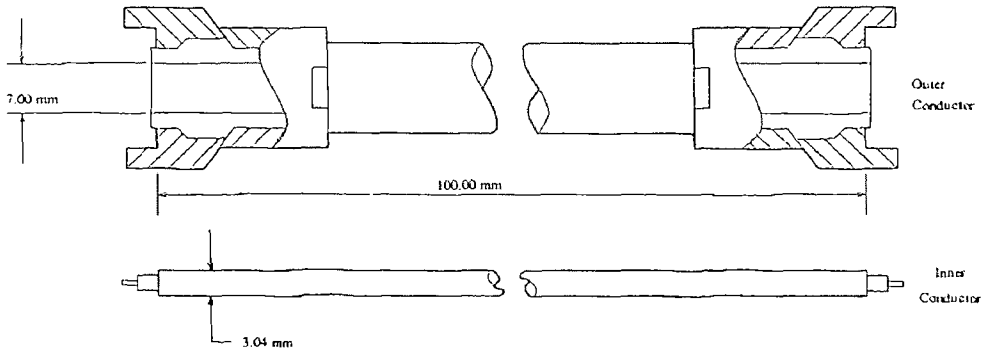

Figure 4.1 Coaxial sample holder (10 cm APC-7 Beadless Air-Line)

network analyzer. The measurement setup is shown in figure 4.2. The theory used in calculating the complex dielectric constant by the s-parameter method is explained below [16] [15] [18]. For a two port analysis, the air line filled with the dielectric is shown with the various currents and voltages in figure 4.3 A two port network is generally represented as shown in figure 4.4. In general, the S-parameter equations for a 2-port network are defined by the following two equations:

$$V_1^- = S_{11}V_1^+ + S_{12}V_2^+ \tag{4.1}$$

$$V_2^- = S_{21}V_1^+ + S_{22}V_2^+ \tag{4.2}$$

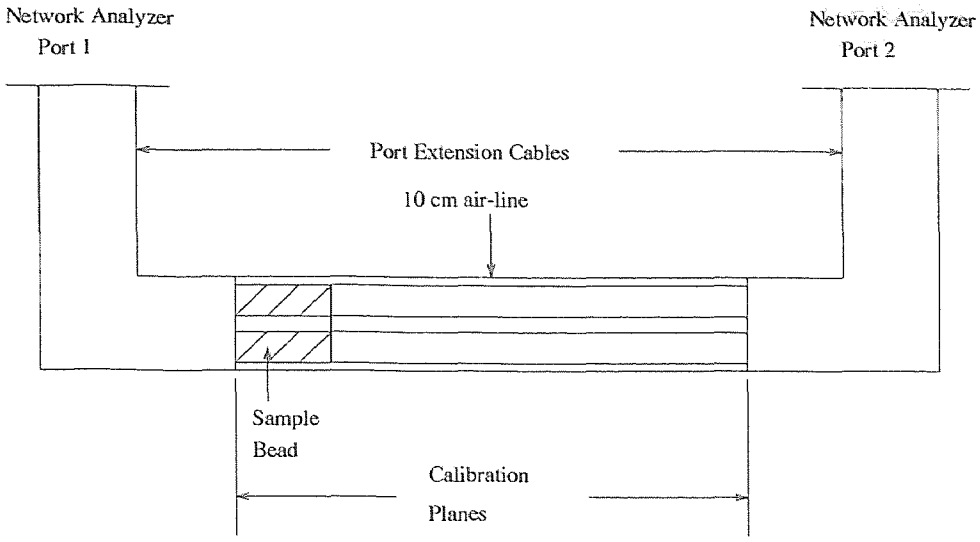

Figure 4.2 Coaxial measurement setup for the measurement of dielectric constant

The reflection coefficient at port 1 with the port 2 perfectly matched is found as:

$$S_{11} = V_1^- / V_1^+ \big|_{V_2^+=0} \tag{4.3}$$

The forward transmission coefficient from port 1 to port 2 with the port 2 perfectly matched is found as:

$$S_{21} = V_2^- / V_1^+ \big|_{V_2^+=0} \tag{4.4}$$

It is to be noted that the S-parameters measured in this method represent the whole air-line with the dielectric bead in it and it is thus necessary to account for the phase introduced by the extra part of the 50 Ω airline in the s-parameters to get the s-parameters of the bead in the air-line. Since the sample is kept at the start of the air-line, there is no extra phase introduced by the air-line in s_{11}. The correct S_{21} of the bead in the air-line is obtained by adjusting the following phase value in the measured S_{21} results:

$360 \times f \times (L - d)/c$ degrees

where,

f = the measurement frequency;

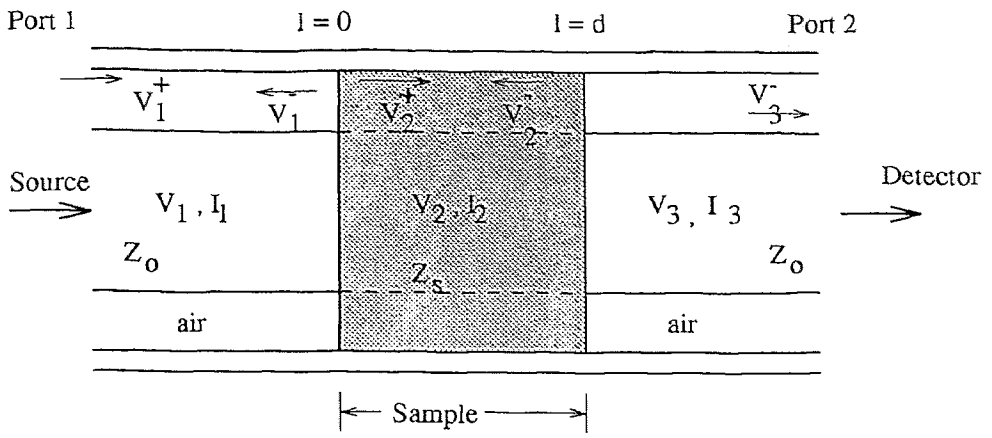

Figure 4.3 2-port representation of the air-line

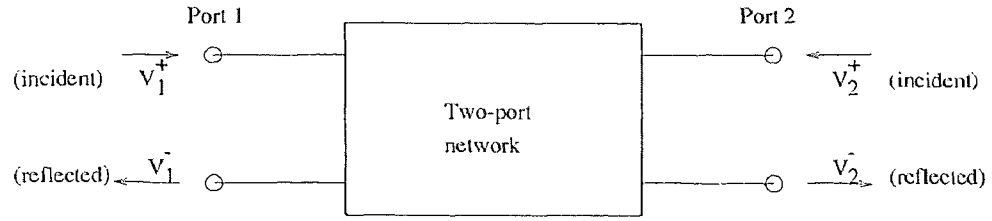

Figure 4.4 General representation of a two port network showing the incident and reflected waves at each port

L = length of the air-line;

d = length of the sample;

c = velocity of light in free space.

There are three distinct regions in the air line measurement setup. First is the region between port 1 and the dielectric. The second is the region inside the dielectric. The third is the region between the dielectric and port 2. The phase reference plane of the waves in each region starts from the beginning of that region. The forward and reverse travelling waves in regions 1, 2 and 3 are given respectively as:

$$V_1^+ exp^{-j\beta_o(l)} \qquad l \leq 0 \ (region1) \qquad (4.5)$$

$$V_1^- exp^{\jmath\beta_o(l)} \qquad l \leq 0\ (region1) \tag{4.6}$$

$$V_2^+ exp^{-\jmath\gamma l} \qquad 0 \leq l \leq d\ (region2) \tag{4.7}$$

$$V_2^- exp^{\jmath\gamma l} \qquad 0 \leq l \leq d\ (region2) \tag{4.8}$$

$$V_3^- e^{-\jmath\beta_o(l-d)} \qquad l \geq d\ (region3) \tag{4.9}$$

$$V_3^+ = 0 \qquad l \geq d\ (region3) \tag{4.10}$$

Here,

d = length of the dielectric sample;

γ = complex propagation factor in the dielectric;

βo = propagation constant in free space.

The continuity of voltages at the air-dielectric interface at $l = 0$ yields the following equity:

$$V_1^+ + V_1^- = V_2^+ + V_2^- \tag{4.11}$$

The continuity of currents at the first air dielectric interface (l=0) yields:

$$(1/Z_o)(V_1^+ - V_1^-) = (1/Z_s)(V_2^+ - V_2^-) \tag{4.12}$$

The continuity of voltages at the air-dielectric interface of region 2 and region 3 is given by:

$$V_2^+ exp^{-\jmath\gamma d} + V_2^- exp^{\jmath\gamma d} = V_3^- \tag{4.13}$$

In writing this equation it has been assumed that there is no reflected wave into the air-line due to perfect match at the end of region 3 ($V_3^+ = 0$) The continuity of currents at the air-dielectric interface of region 2 and region 3 is given by:

$$(1/Z_s)(V_2^+ exp^{-\jmath\gamma d} - V_2^- exp^{\jmath\gamma d}) = (1/Zo)(V_3^-) \tag{4.14}$$

For our system, the equations 4.1 get modified to the following:

$$V_1^- = S_{11} V_1^+ \tag{4.15}$$

$$V_2^- = S_{21} V_1^+ \tag{4.16}$$

Combining equations 4.13 and 4.14 we get: $V_2^+ e^{-\gamma d} + V_2^- e^{\gamma d} = (Z_o/Z_s)(V_2^+ e^{-\gamma d} - V_2^- e^{\gamma d})$ Substituting $e^{-\gamma d}$ as the transmission factor , T, through the dielectric, i.e.,

$$T = e^{-\gamma d} \tag{4.17}$$

$$V_2^+ T + V_2^-/T = Z_o/Z_s(V_2^+ T - V_2^-/T) \tag{4.18}$$

Putting equation 4.15 in equations 4.11 and 4.12 we get:

$$V_1^+ + S_{11} V_1^+ = V_2^+ + V_2^- \tag{4.19}$$

$$V_1^+ - S_{11} V_1^+ = (Z_o/Z_s)(V_2^+ - V_2^-) \tag{4.20}$$

Combining the above two equations we get:

$$V_1^+ = (V_2^+ + V_2^-)/(1 + S_{11}) = (Z_o/Z_s)(V_2^+ - V_2^-)/(1 - S_{11}) \tag{4.21}$$

Combining common voltage terms in equation 4.18 we obtain:

$TV_2^+(1 - Z_o/Z_s) = (-V_2^-/T)(1 + Z_o/Z_s)$

from which we obtain:

$$-V_2^-/(T^2 V_2^+) = (Z_s - Z_o)/(Z_s + Z_o) = \Gamma \tag{4.22}$$

where, Γ is the reflection coefficient at the air-dielectric interface when the dielectric is of infinite length. Rearranging equation 4.21 we obtain:

$$Z_s/Z_o = ((1 + S_{11})/(1 - S_{11}))(V_2^+ - V_2^-)/(V_2^+ + V_2^-) \tag{4.23}$$

Subtracting 1 from both sides from the above equation we get:

$(Z_s - Z_o)/Z_o = ((1 + S_{11})(V_2^+ - V_2^-) - (1 - S_{11})(V_2^+ + V_2^-))/(1 - S_{11})(V_2^+ + V_2^-)$

from which we obtain:

$$(Z_s - Z_o)/Z_o = 2(S_{11} V_2^+ - V_2^-)/(1 - S_{11})(V_2^+ + V_2^-) \tag{4.24}$$

Adding 1 to both sides of 4.23 we get:

$$(Z_s + Z_o)/Z_o = ((1 + S_{11})(V_2^+ - V_2^-) + (1 - S_{11})(V_2^+ + V_2^-))/(1 - S_{11})(V_2^+ + V_2^-)$$

from which we obtain:

$$(Z_s + Z_o)/Z_o = 2(V_2^+ - S11V_2^-)/(1 - S_{11})(V_2^+ + V_2^-) \tag{4.25}$$

Divide equation 4.24 by equation 4.25 to get:

$$(Z_s - Z_o)/(Z_s + Z_o) = \Gamma = (S_{11}V_2^+ - V_2^-)/(V_2^+ - S_{11}V_2^-) \tag{4.26}$$

Dividing R.H.S. of equation refeqn:f by V_2^+, we obtain:

$$\Gamma = (S_{11} - V_2^-/V_2^+)/(1 - S_{11}V_2^-/V_2^+) \tag{4.27}$$

From equation 4.22 we get:

$$-V_2^-/V_2^+ = T^2\Gamma \tag{4.28}$$

Putting equation 4.28 into equation 4.27 we obtain:

$$\Gamma = (S_{11} + T^2\Gamma)/(1 + S_{11}T^2\Gamma) \tag{4.29}$$

$$\Rightarrow \Gamma + S_{11}T^2\Gamma^2 = S_{11} + T^2\Gamma \tag{4.30}$$

$$\Rightarrow S_{11}(T^2\Gamma - 1) = (T^2 - 1)\Gamma \tag{4.31}$$

$$\Rightarrow S_{11} = ((T^2 - 1)\Gamma)/(T^2\Gamma^2 - 1) \tag{4.32}$$

Putting equation 4.15 in equation 4.11 and equation 4.16 in equation 4.13 we get:

$$V_1^+(1 + S_{11}) = V_2^+ + V_2^- \tag{4.33}$$

$$V_2^+T + V_2^-/T = S_{21}V_1^+ \tag{4.34}$$

Eliminating V_1^+ from the above two equations we get:

$$(V_2^+ + V_2^-)/(1 + S_{11}) = (V_2^+T + V_2^-/T)/S_{21} \tag{4.35}$$

Dividing both sides of the above equation by V_2^+ and using equation 4.22 and equation 4.32 to get:

$$(1 - \Gamma T^2)/(1 + (1 - T^2)\Gamma/(1 - T^2\Gamma^2) = T(1 - \Gamma)/S_{21} \tag{4.36}$$

$$\Rightarrow S_{21} = T(1 - \Gamma)\{1 - \Gamma T^2 + \Gamma(1 - \Gamma T^2)\}/(1 - T^2\Gamma^2)(1 - \Gamma T^2) \tag{4.37}$$

$$\Rightarrow S_{21} = T(1 - \Gamma)(1 - \Gamma T^2)(1 + \Gamma)/(1 - T^2\Gamma^2)(1 - \Gamma T^2) \tag{4.38}$$

$$\Rightarrow S_{21} = T(1 - \Gamma^2)/(1 - T^2\Gamma^2) \tag{4.39}$$

The term Γ (the reflection coefficient at the air-dielectric interface when the length of the dielectric is infinite) can be found as:

$$\Gamma = K \pm (K^2 - 1)^{1/2} \tag{4.40}$$

where,

$$K = (\{S_{11}^2 - S_{21}^2\} + 1)/2S_{11} \tag{4.41}$$

The appropriate sign in equation 4.40 should be used so as to keep the value $|\Gamma| < 1$. The transmission through the dielectric, T can be found as [16]:

$$T = (\{S_{11}^2 + S_{21}^2\} - \Gamma)/(1 - \{S_{11} + S_{21}\}\Gamma) \tag{4.42}$$

The complex propagation factor, γ, through the dielectric is given by the following equation:

$$\gamma = (\omega/c)(\mu_r \epsilon_r)^{1/2} \tag{4.43}$$

where,

$\omega = 2 \times \pi \times f$ (f is the measurement frequency);

$c =$ velocity of light in free space;

ϵ_r = complex relative dielectric constant (relative electric permittivity) of the material;

$\mu_r =$ complex relative magnetic permeability of the material.

The transmission through the dielectric is given by equation 4.17 which, again, is written in terms of relative permittivity and relative permeability as:

$$T = e^{\{-j(\omega/c)(\mu_r\epsilon_r)^{1/2}d\}} \tag{4.44}$$

From equation 4.22 and equation 4.44 we can write the ratio and the product of the relative permittivity and the permeability as follows:

$$\mu_r/\epsilon_r = \{(1+\Gamma)/(1-\Gamma)\}^2 = x \tag{4.45}$$

$$\mu_r\epsilon_r = -\{(c/(\omega d))\ln(1/T)\}^2 = y \tag{4.46}$$

The term $\ln(1/T)$, in general , is written as:

$$\ln(1/T) = a + j(b + 2\pi n) \tag{4.47}$$

Here, a and b are real and $n = 0, 1, 2, 3...$, is the integral part of (d/λ_g).

A non-zero value of n is to be used when the length of the sample is larger than the wavelength in the sample. The value of n is not accounted for automatically, but has to be determined by the user because the phase of the propagation factor does not change when the length of the material is increased by the multiple of a wavelength. However, the delay through the material is a function of the total length of the sample material and this delay can be measured and used to determined the correct value of n. The correct value of n is determined when the difference between the computed value of the group delay for the n^{th} solution of equation 4.47 and the measured value of group delay is nearly equal to zero. The group delay at each frequency is computed for each solution of ϵ_r and μ_r by the following equation:

$$\tau_{gn} = d \cdot (d/df\{\{(\epsilon_r\mu_r)^{1/2}/\lambda_o\}_n\}) \tag{4.48}$$

Assuming that the changes in $\epsilon_r and \mu_r$ are negligible over small increments of frequency, equation 4.48 reduces to:

$$\tau_{gn} = d\{\mu_r\epsilon_r\}_n^{1/2}/c \tag{4.49}$$

The correct root $n = k$ is found when:

$$\tau_{gn} - \tau_g \simeq 0 \tag{4.50}$$

where,

τ_g is the measured value of group delay.

The complex relative permittivity can now be computed from Equation 4.46 and Equation 4.45 as: $\epsilon_r = (x/y)^{1/2}$

4.2 Experimental Results

This section depicts the values of the complex dielectric constant and dissipation factor of the various composites studied in this thesis.

4.2.1 Low graphite concentration composites

The graphite concentration was low (between 1 to 2 %) in these samples. The real part of dielectric constant for 1.147 % graphite in graphite-pmma mixture is plotted in figure 4.5. The real part of the dielectric constant is observed to be close to 2.8. The real part of the dielectric constant for pure PMMA at these frequencies is 2.6 [14]. The imaginary part is observed to be close to zero indicating that there is little loss for low graphite concentrations. The zero crossing of the imaginary part is due to system noise and mismatch (the imaginary part does not become negative as this would indicate gain). The imaginary part of dielectric constant for 1.147 % graphite in graphite-pmma mixture is plotted in figure 4.6. The loss for 1.147 % graphite in graphite-pmma mixture is plotted in figure 4.7. The real part of dielectric constant for 2 % graphite in graphite-pmma mixture is plotted in figure 4.8. It is observed that a slightly higher concentration of graphite raises the real part of the dielectric constant to values around 3.25. The imaginary part is higher than the 1.14 % case indicating a higher loss material. The values of dielectric constant

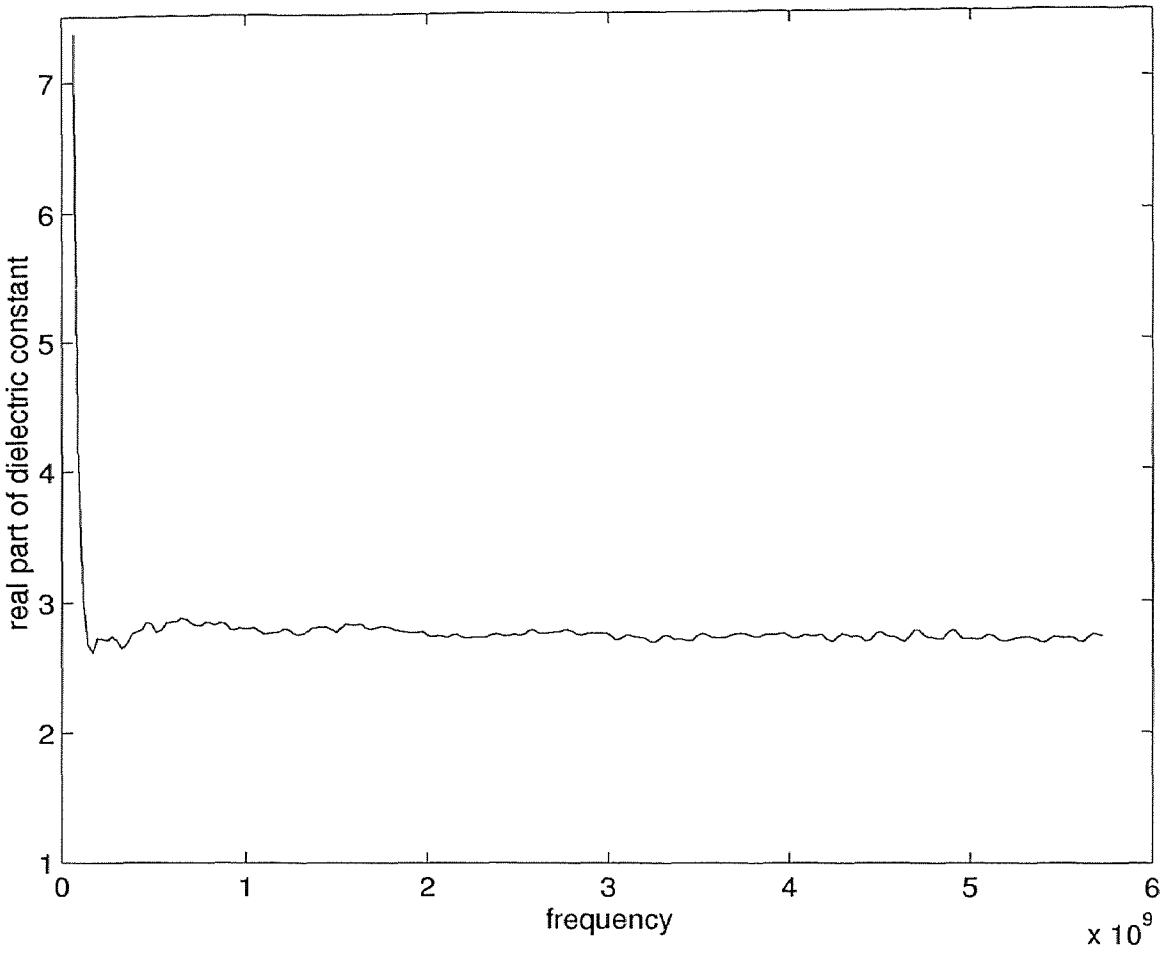

Figure 4.5 Real part of dielectric constant versus the frequency for graphite loaded PMMA in which the graphite concentration was 1.147 % by weight.

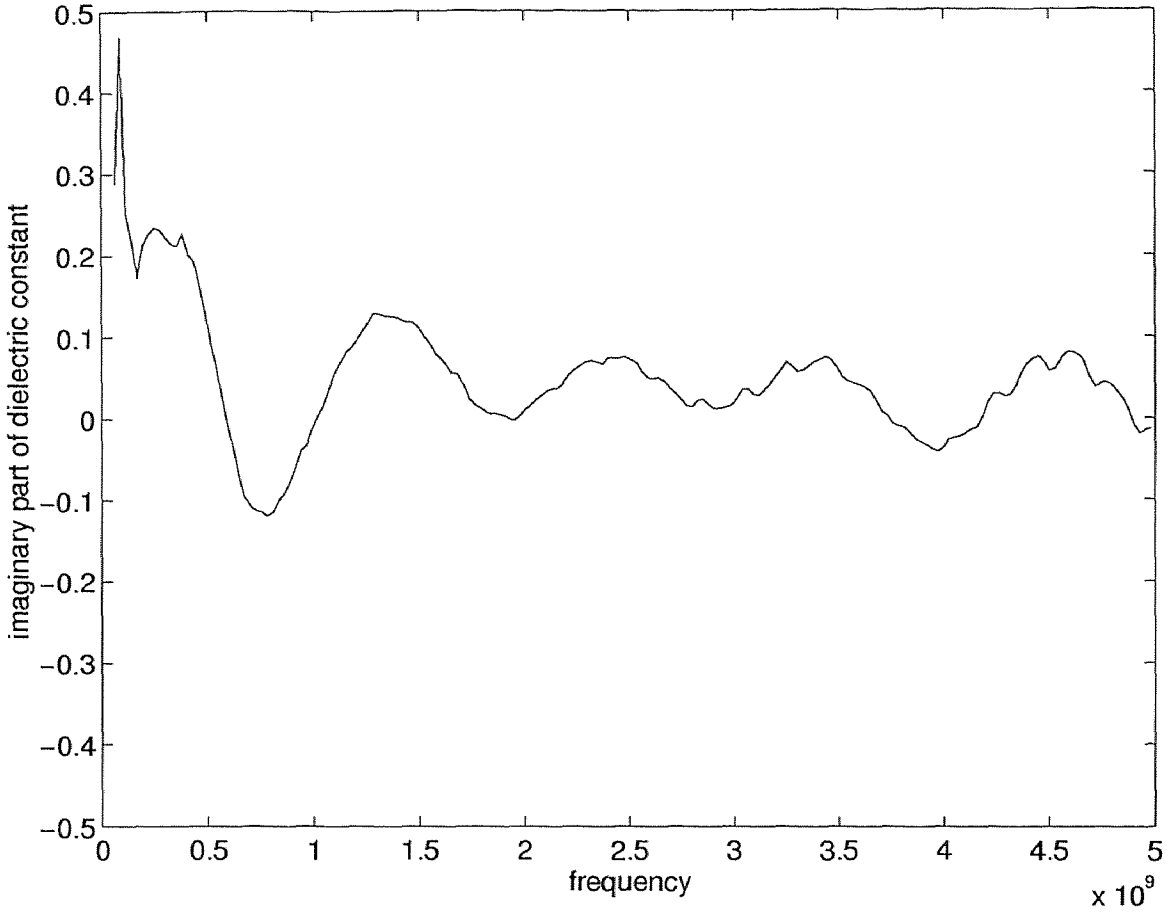

Figure 4.6 Imaginary part of dielectric constant versus the frequency for graphite loaded PMMA in which the graphite concentration was 1.147 % by weight.

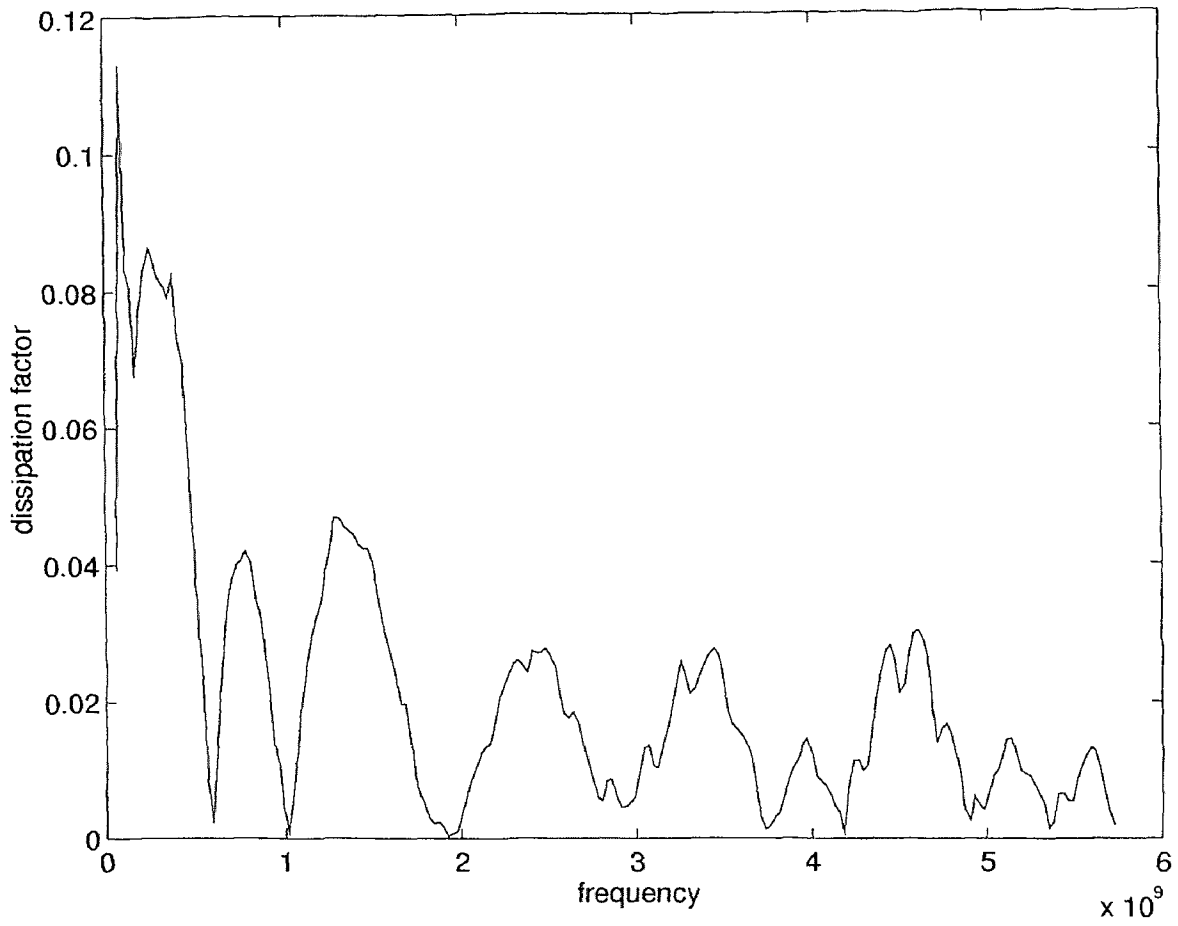

Figure 4.7 Dissipation factor versus the frequency for graphite loaded PMMA in which the graphite concentration was 1.147 % by weight.

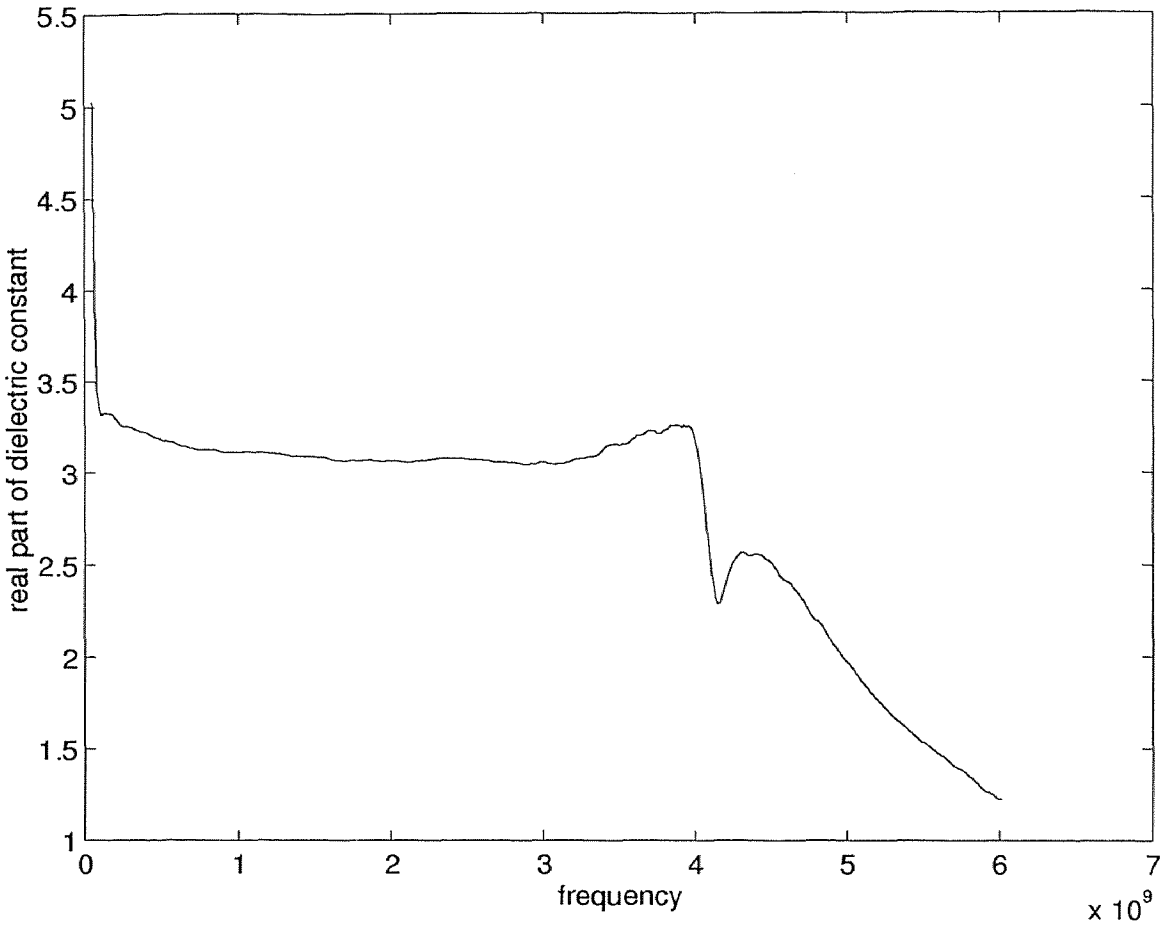

Figure 4.8 Real part of dielectric constant versus the frequency for graphite loaded PMMA in which the graphite concentration was 2 % by weight.

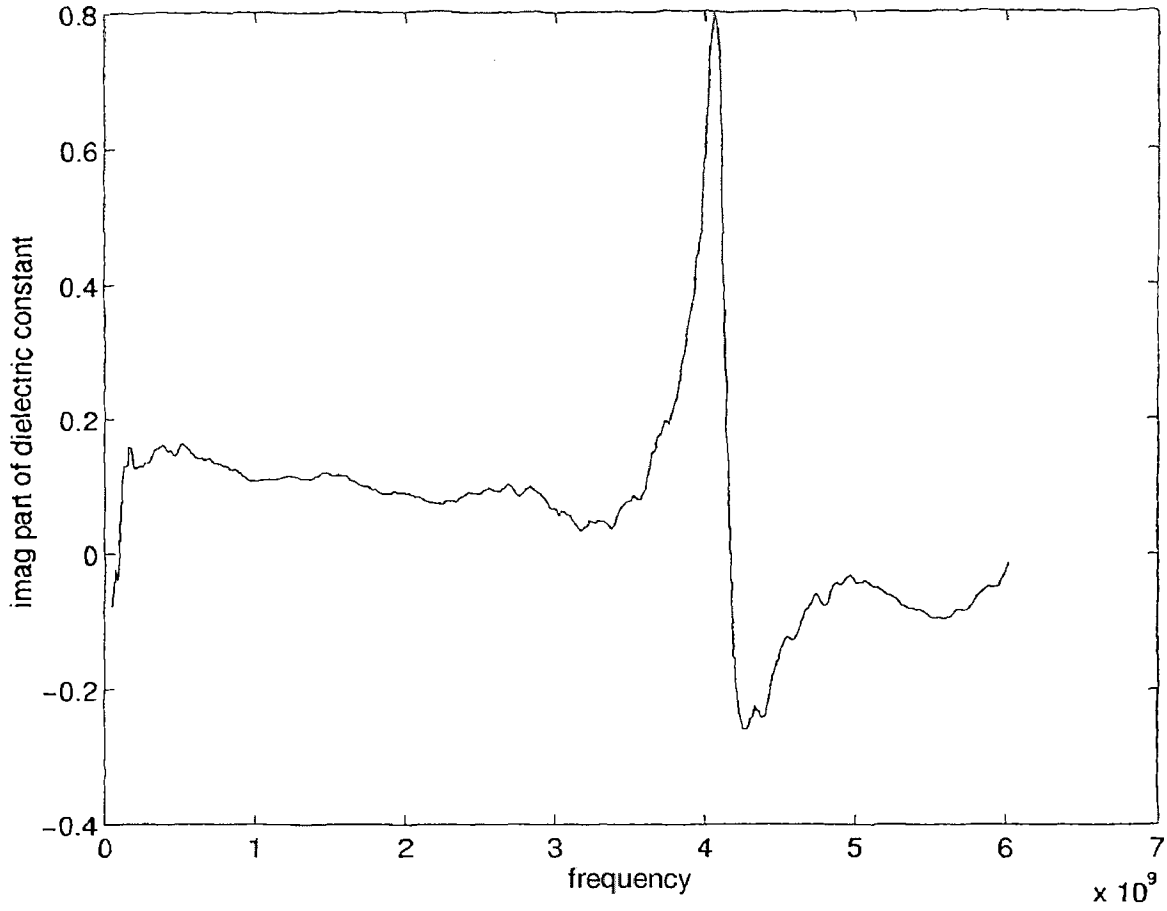

Figure 4.9 Imaginary part of dielectric constant versus the frequency for graphite loaded PMMA in which the graphite concentration was 2 % by weight.

after the point the imaginary part changes sign should be disregarded as they are erroneous because of the multimode nature of the air-line beyond these frequencies.

The imaginary part of dielectric constant for 2 % graphite in graphite-pmma mixture is plotted in figure 4.9. The loss for 2 % graphite in graphite-pmma mixture is plotted in figure 4.10.

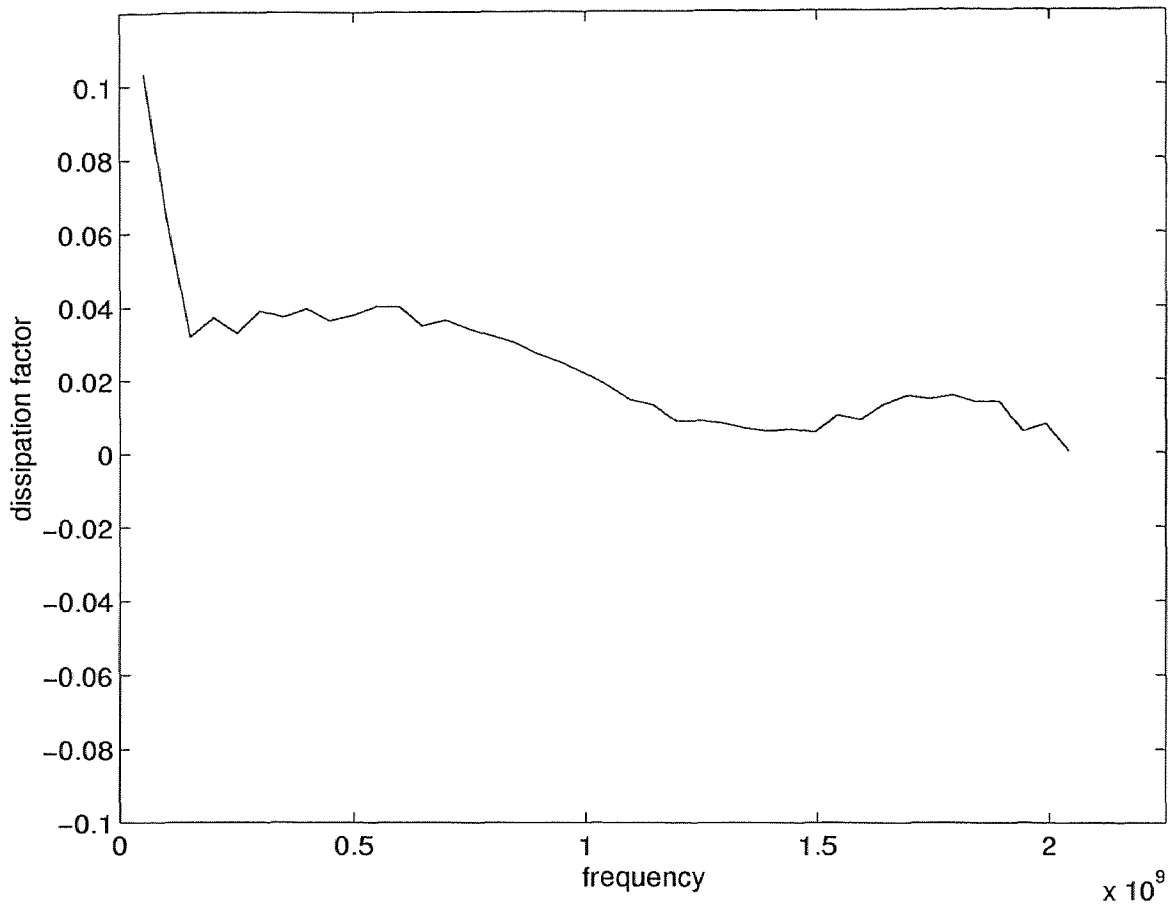

Figure 4.10 Dissipation factor versus the frequency for graphite loaded PMMA in which the graphite concentration was 2 % by weight.

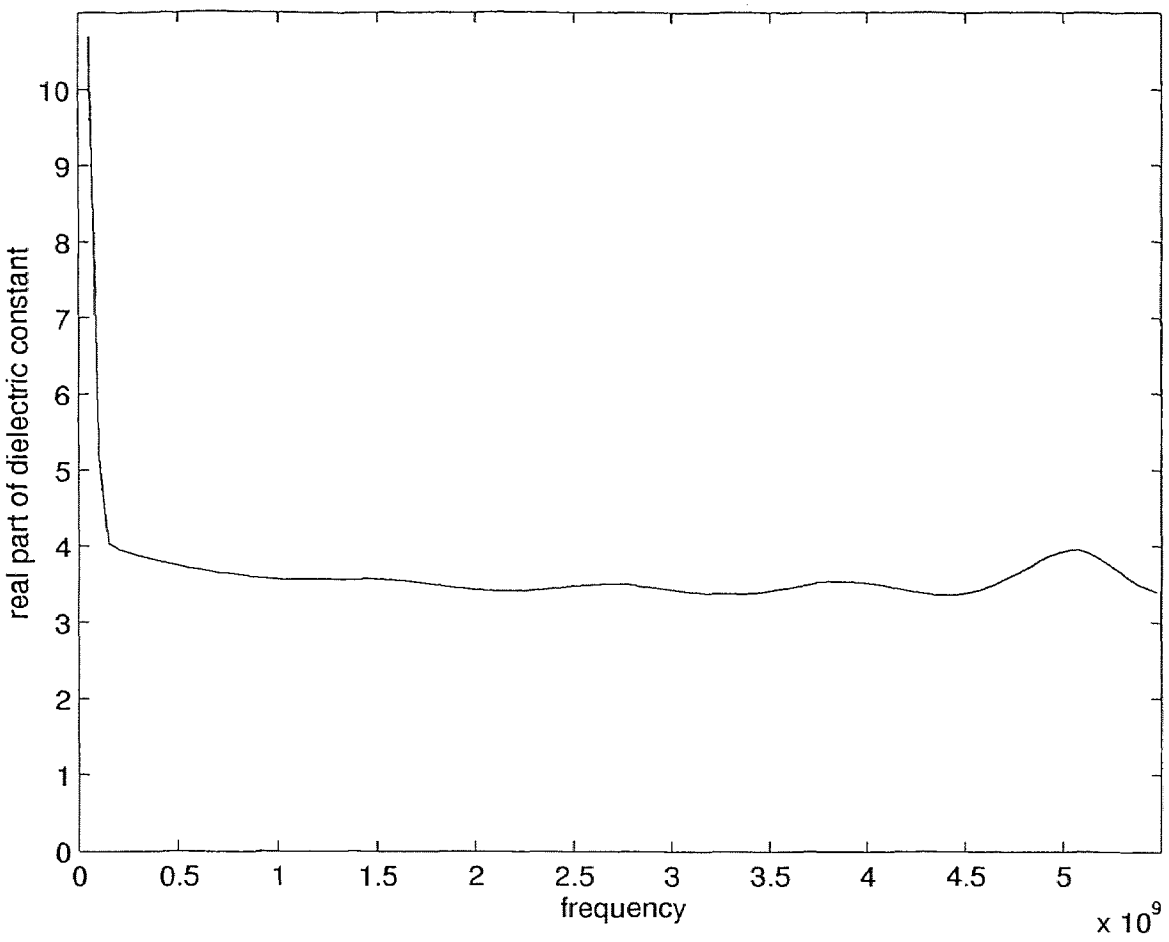

Figure 4.11 Real part of dielectric constant versus the frequency for fine graphite loaded PMMA in which the graphite concentration was 1.147 % by weight.

4.2.2 Fine graphite-PMMA blend

A sample of 1.14 % fine graphite (1 micron size particles) in PMMA matrix was tested for dielectric constant in order to determine the dependency of loss on particle size. The resulting graphs follow. The real part of dielectric constant for 1.14 % fine graphite in graphite-pmma mixture is plotted in figure 4.11. It is observed that for the same low concentration (1.14 %) of fine graphite (1 micron) particles, the dielectric constant is greater than its coarse (30 micron) counterpart. The imaginary part of the dielectric constant is seen to be higher too. This may be expected as there are more number of particles per unit volume in the fine graphite case and so the

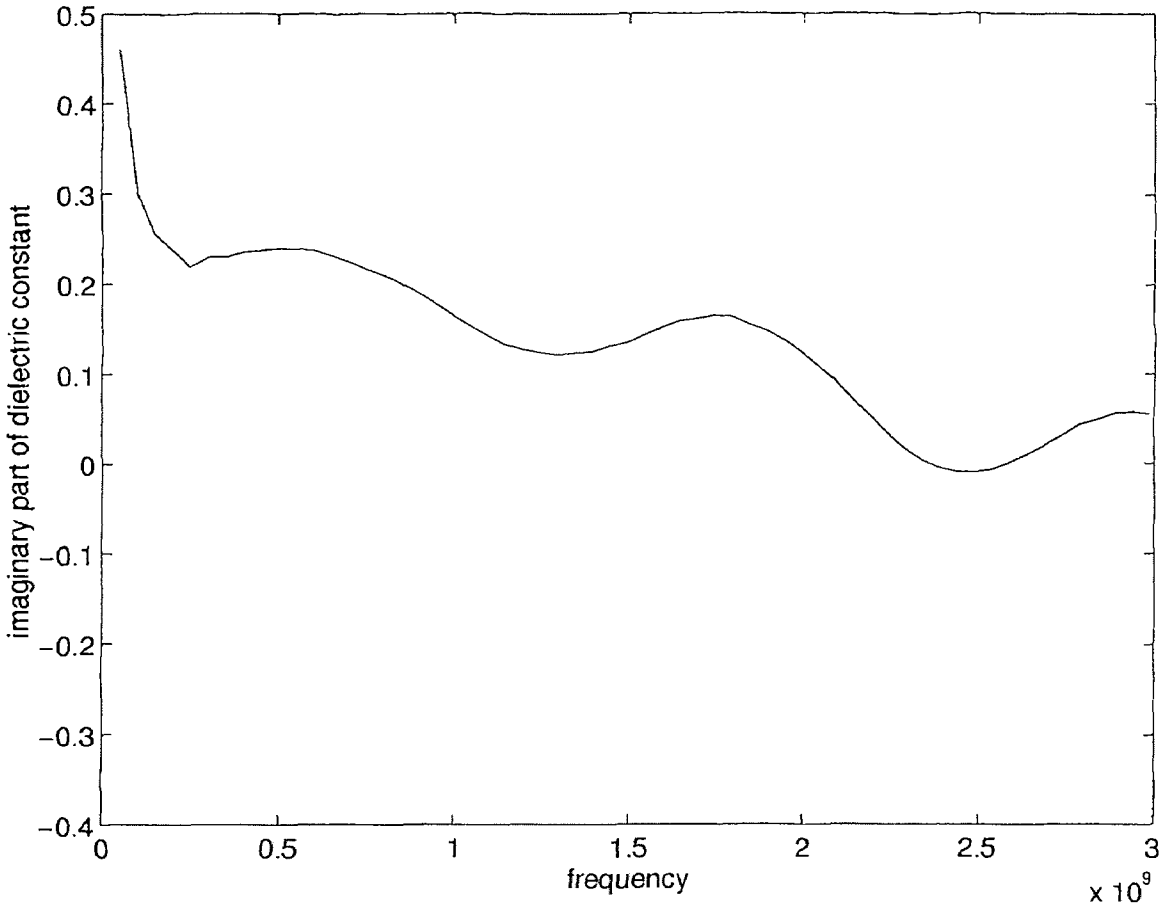

Figure 4.12 Imaginary part of dielectric constant versus the frequency for fine graphite loaded PMMA in which the graphite concentration was 1.14 % by weight.

number of dipoles present are increased. The imaginary part of dielectric constant for 1.14 % fine graphite in graphite-pmma mixture is plotted in figure 4.12. The dissipation factor for 1.14 % fine graphite in graphite-pmma mixture is plotted in figure 4.13.

4.2.3 High graphite concentration samples

The graphite concentration was kept from 20 to 26 % in these samples. The real part of dielectric constant for 20.71 % graphite in graphite-pmma mixture is plotted in figure 4.14. The imaginary part of dielectric constant for 20.71 % graphite in

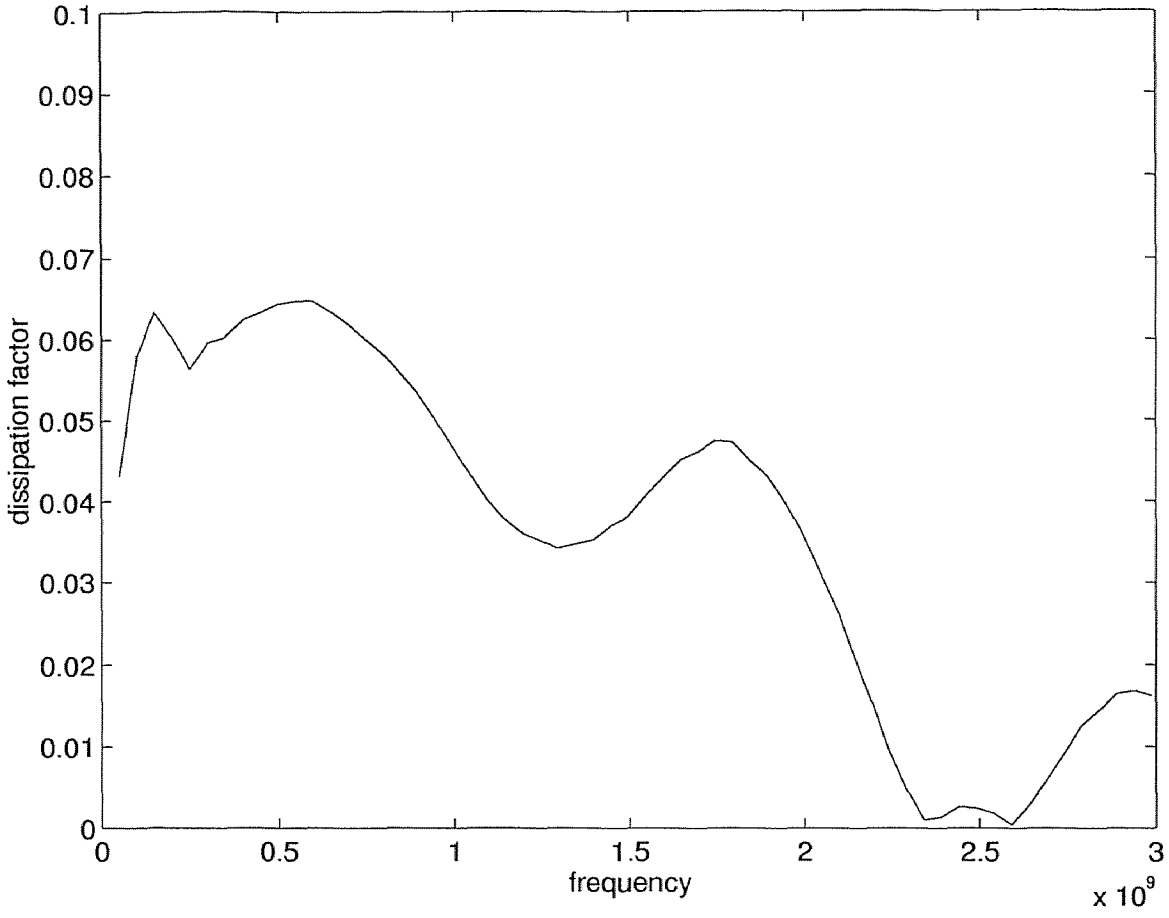

Figure 4.13 Imaginary part of dielectric constant versus the frequency for fine graphite loaded PMMA in which the graphite concentration was 1.147 % by weight.

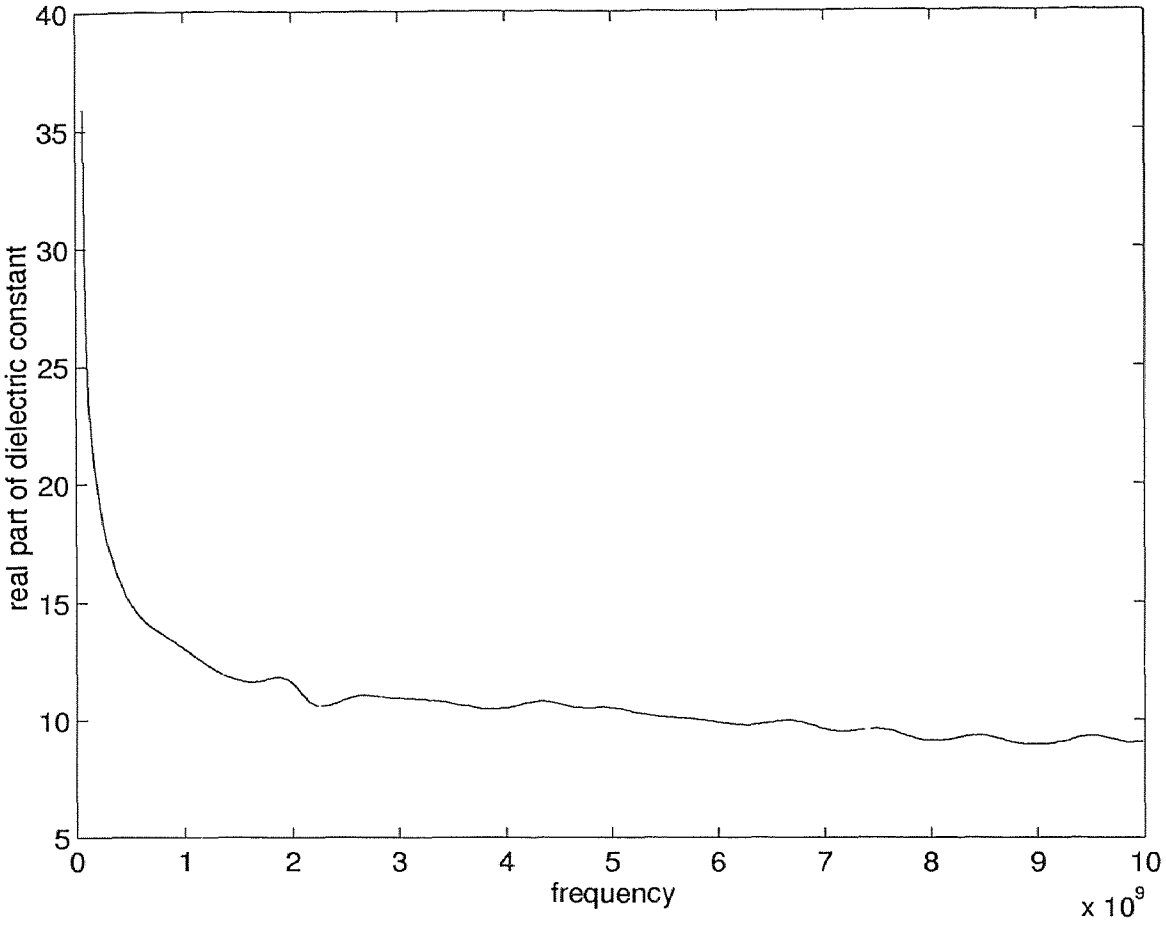

Figure 4.14 Real part of dielectric constant versus the frequency for graphite loaded PMMA in which the graphite concentration was 20.71 % by weight.

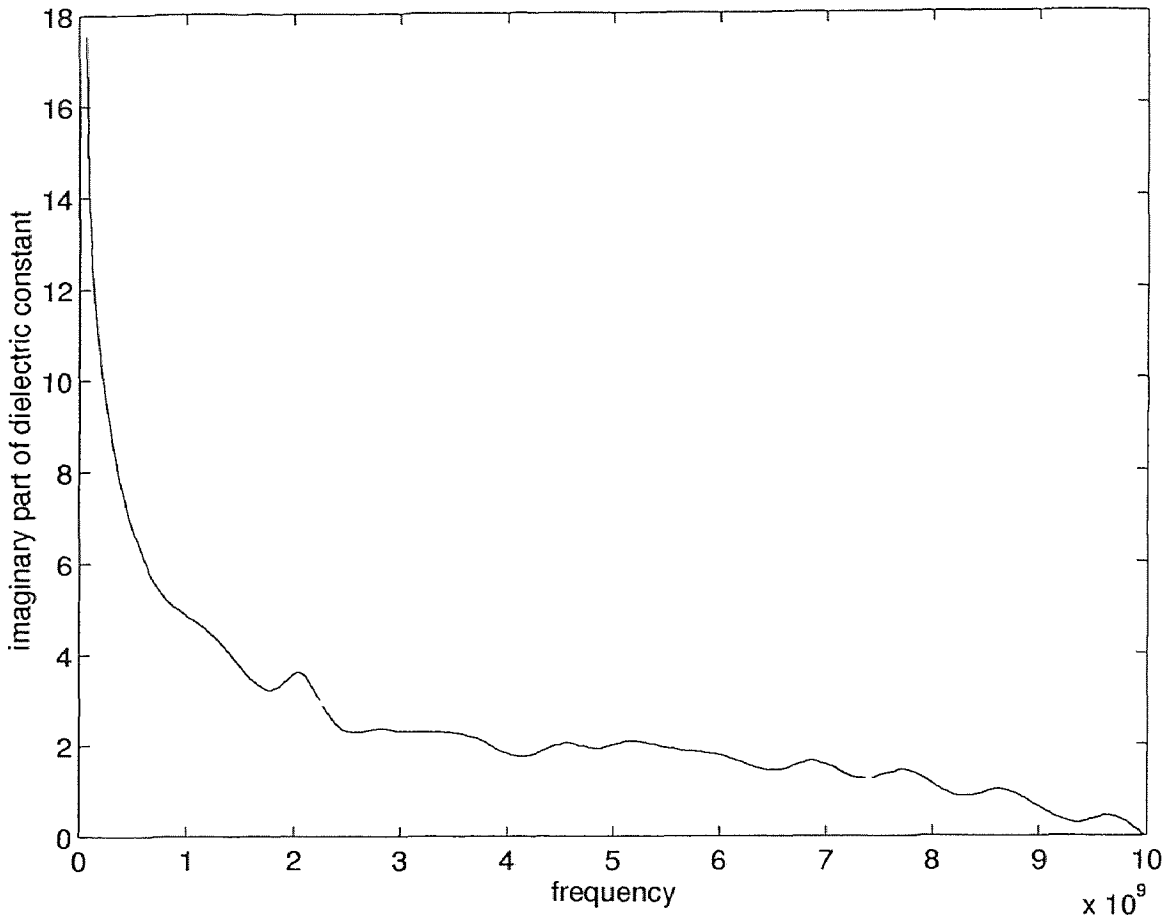

Figure 4.15 Imaginary part of dielectric constant versus the frequency for graphite loaded PMMA in which the graphite concentration was 20.71 % by weight.

graphite-pmma mixture is plotted in figure 4.15. The dissipation factor for 20.71 % graphite is plotted in figure 4.16. The real part of dielectric constant for 24.41 % graphite in graphite-pmma mixture is plotted in figure 4.17. The imaginary part of dielectric constant is plotted in figure 4.18. The dissipation factor is plotted in figure 4.19. A dispersion (dielectric relaxation) is observed because of transition from full orientational polarization at low frequencies to negligible orientational polarization at high frequencies. The real part of the dielectric constant decreases because the dipole polarization decreases with increasing frequency for reasons explained in section 1.2 and can also be seen by equation 1.1. The relative

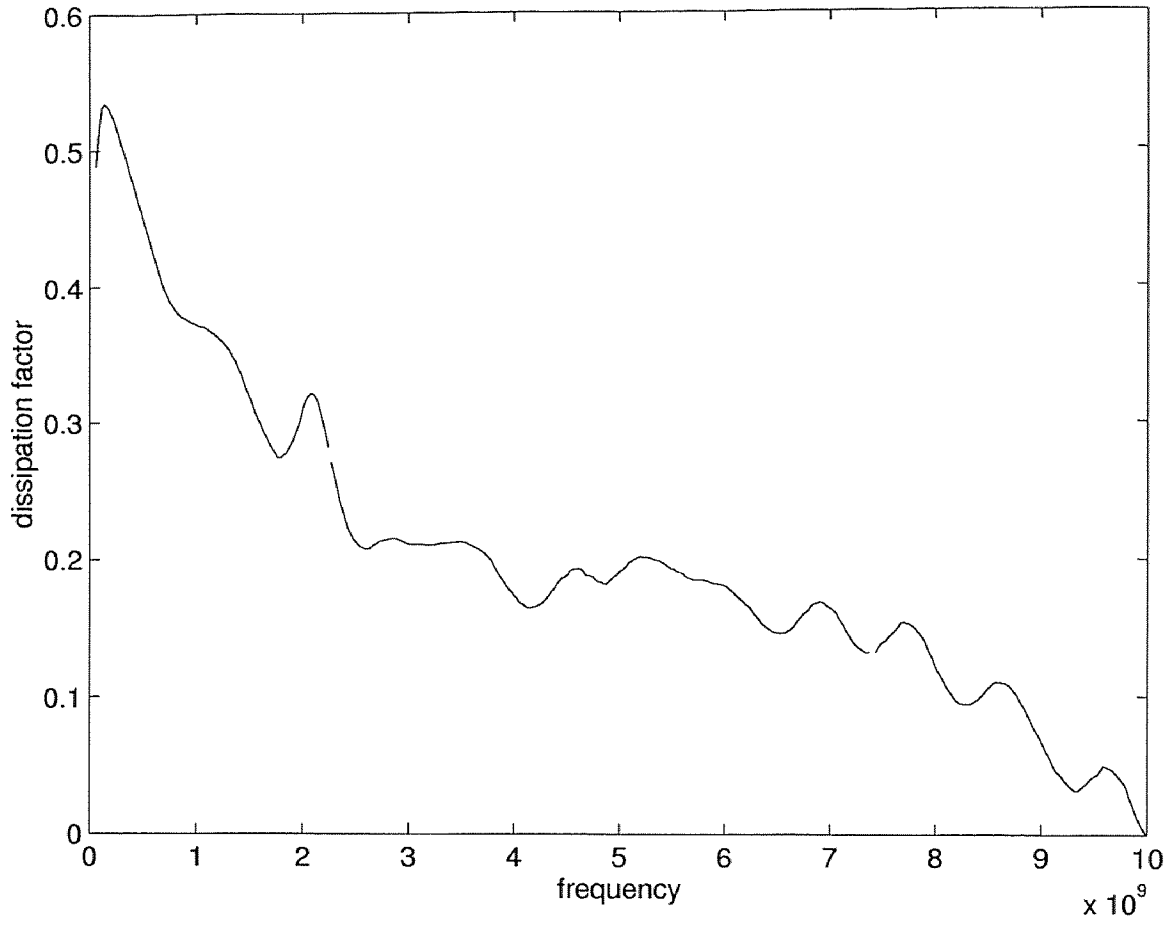

Figure 4.16 Dissipation factor versus the frequency for graphite loaded PMMA in which the graphite concentration was 20.71 % by weight.

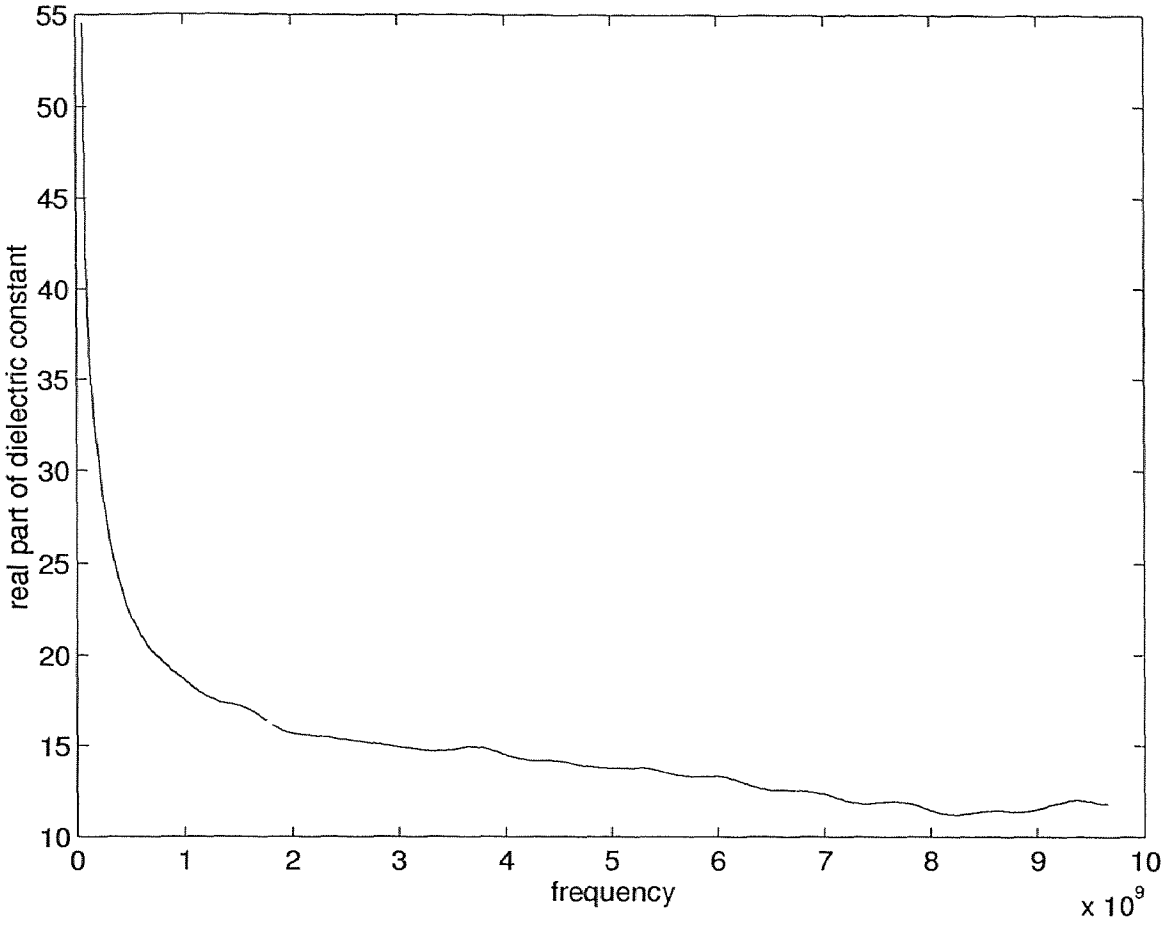

Figure 4.17 Real part of dielectric constant versus the frequency for graphite loaded PMMA in which the graphite concentration was 24.41 % by weight.

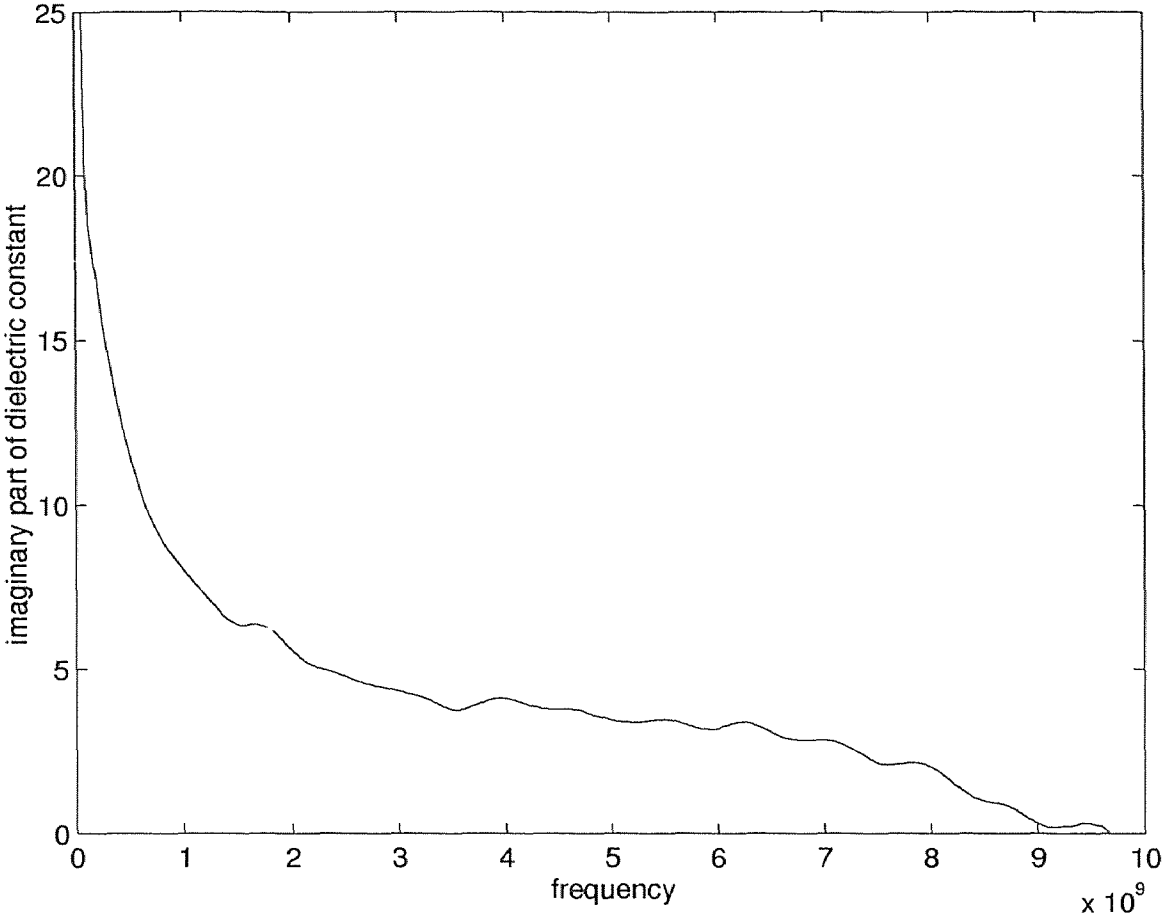

Figure 4.18 Imaginary part of dielectric constant versus the frequency for graphite loaded PMMA in which the graphite concentration was 24.41 % by weight.

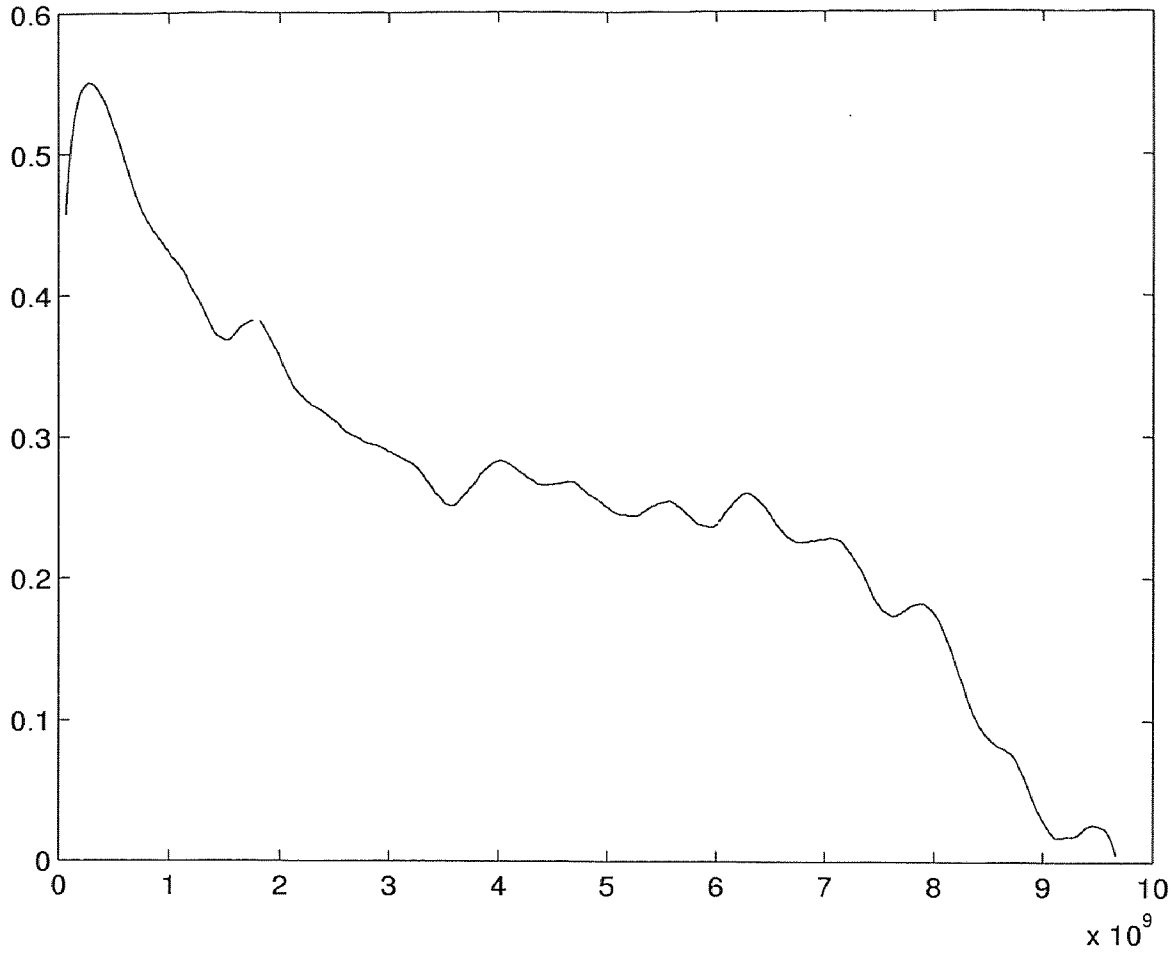

Figure 4.19 Dissipation factor versus the frequency for graphite loaded PMMA in which the graphite concentration was 24.41 % by weight.

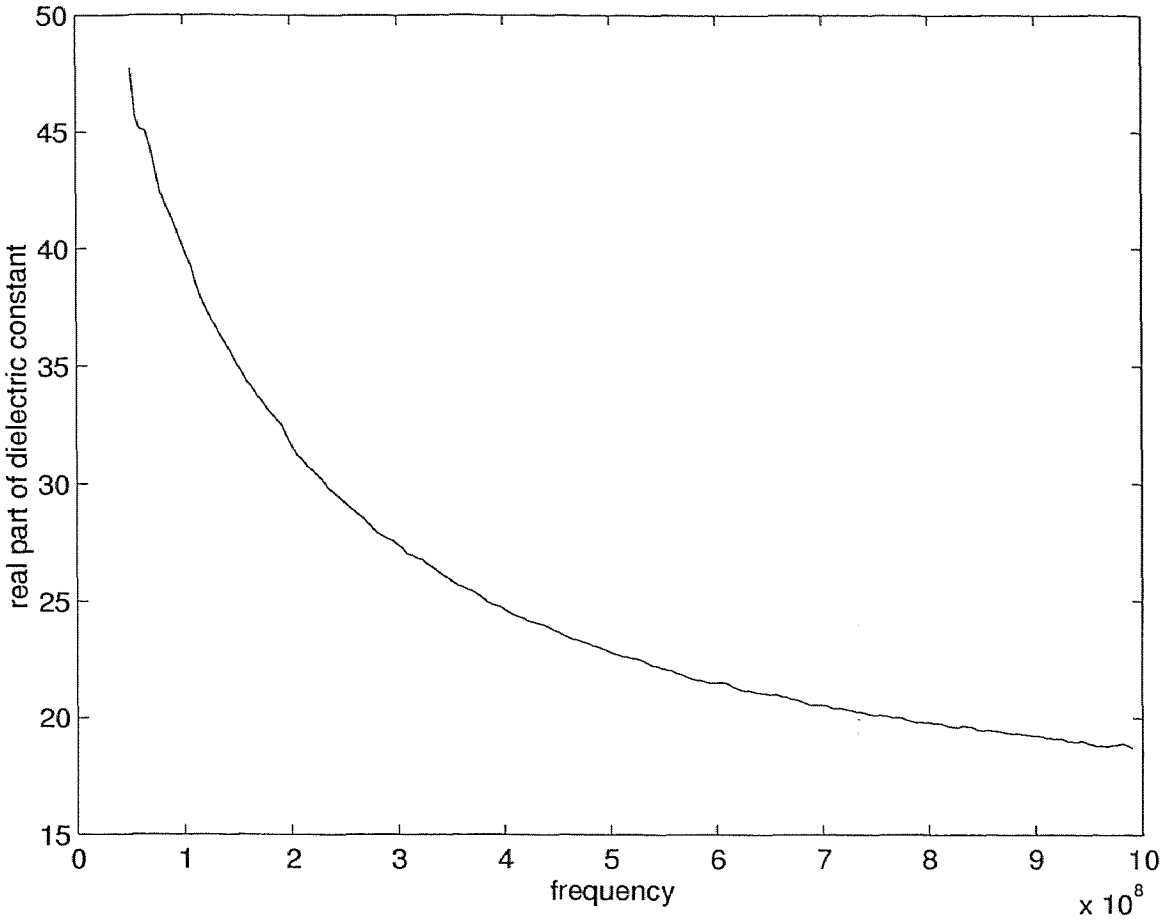

Figure 4.20 Real part of dielectric constant in the lower frequency region versus the frequency for graphite loaded PMMA in which the graphite concentration was 24.41 % by weight.

dielectric constant for low frequencies measured for this particular concentration was around 50 (real) as seen in figure 2.2; the imaginary part being close to zero as seen in figure 2.3.

To verify the validity of the plots at the lower end of the frequency range (50 MHz to 1 GHz) additional measurements were done in this region. The plots indeed conform to each other. It is noted that the real part of the dielectric constant has the same value around 55 at 50 MHz and falls to a value around 18 at 1 GHz. The real part of the dielectric constant in this low band is shown in figure 4.20. The

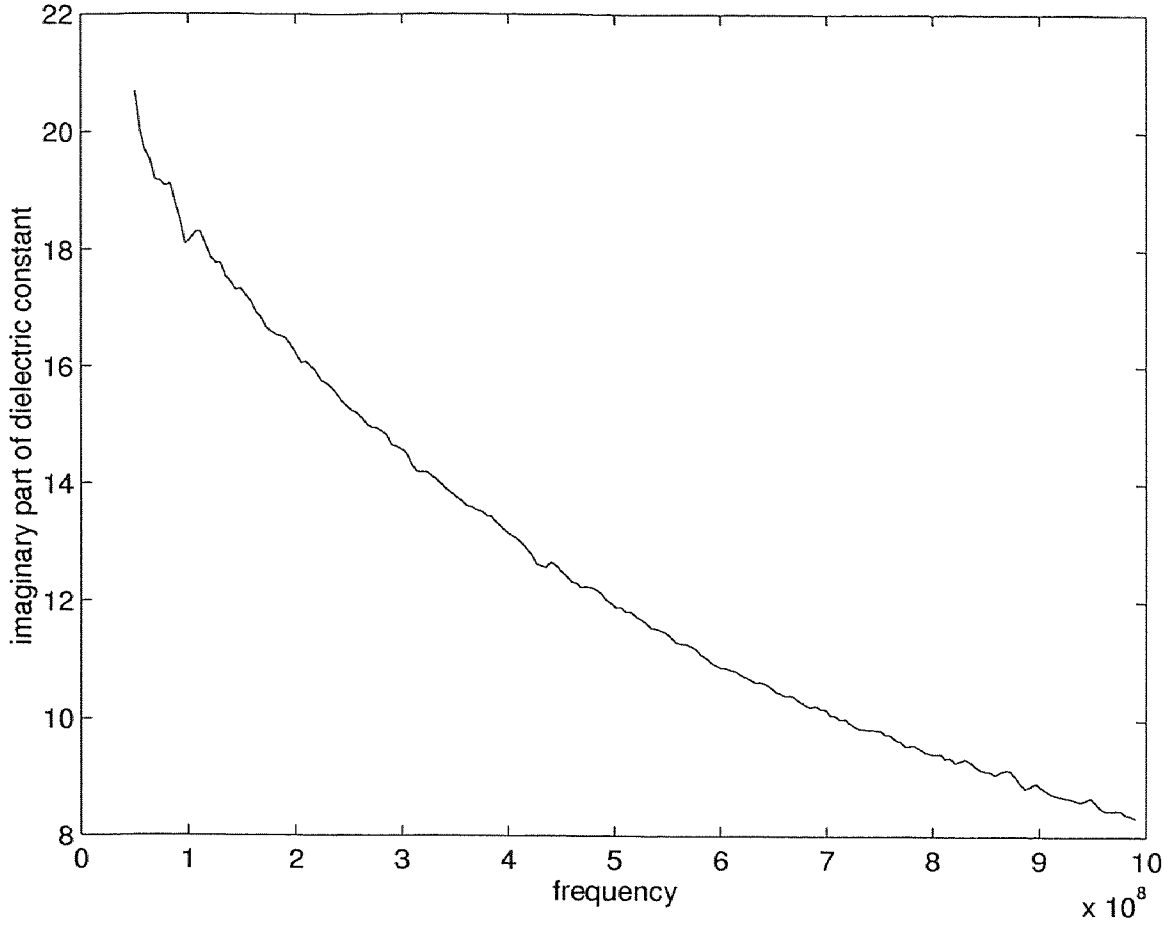

Figure 4.21 Imaginary part of dielectric constant versus the frequency for graphite loaded PMMA in which the graphite concentration was 24.41 % by weight.

imaginary part of the dielectric constant in the lower frequency range is shown in figure 4.21.

The dielectric constant plots for highest graphite concentration follow. These measurements, however, were done only up to 10.7 GHz. The real part of dielectric constant for 26 % graphite in graphite-pmma mixture is plotted in figure 4.22. The imaginary part of dielectric constant for 26 % graphite in graphite-pmma mixture is plotted in figure 4.23. The dissipation factor for 26 % graphite in graphite-pmma mixture is plotted in figure 4.24.

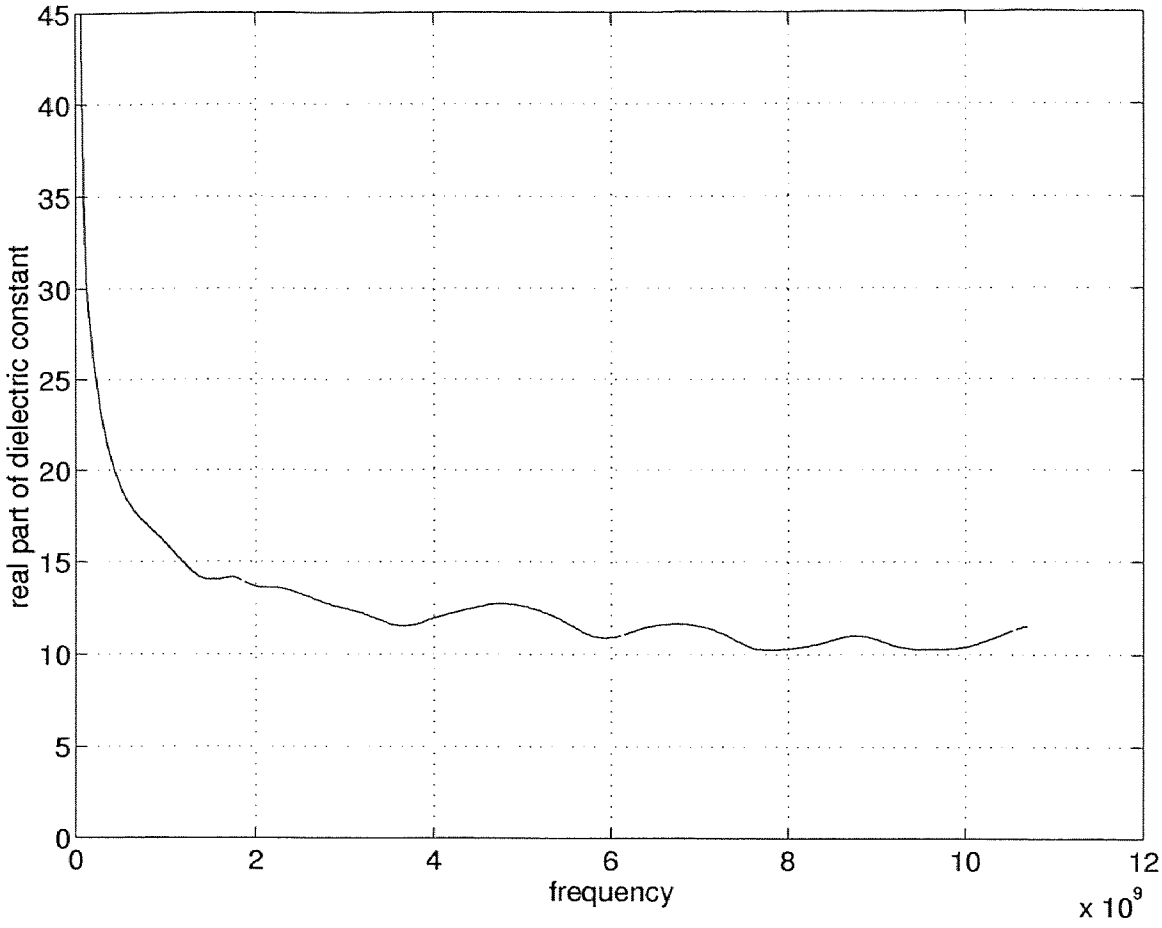

Figure 4.22 Real part of dielectric constant versus the frequency for graphite loaded PMMA in which the graphite concentration was 26 % by weight.

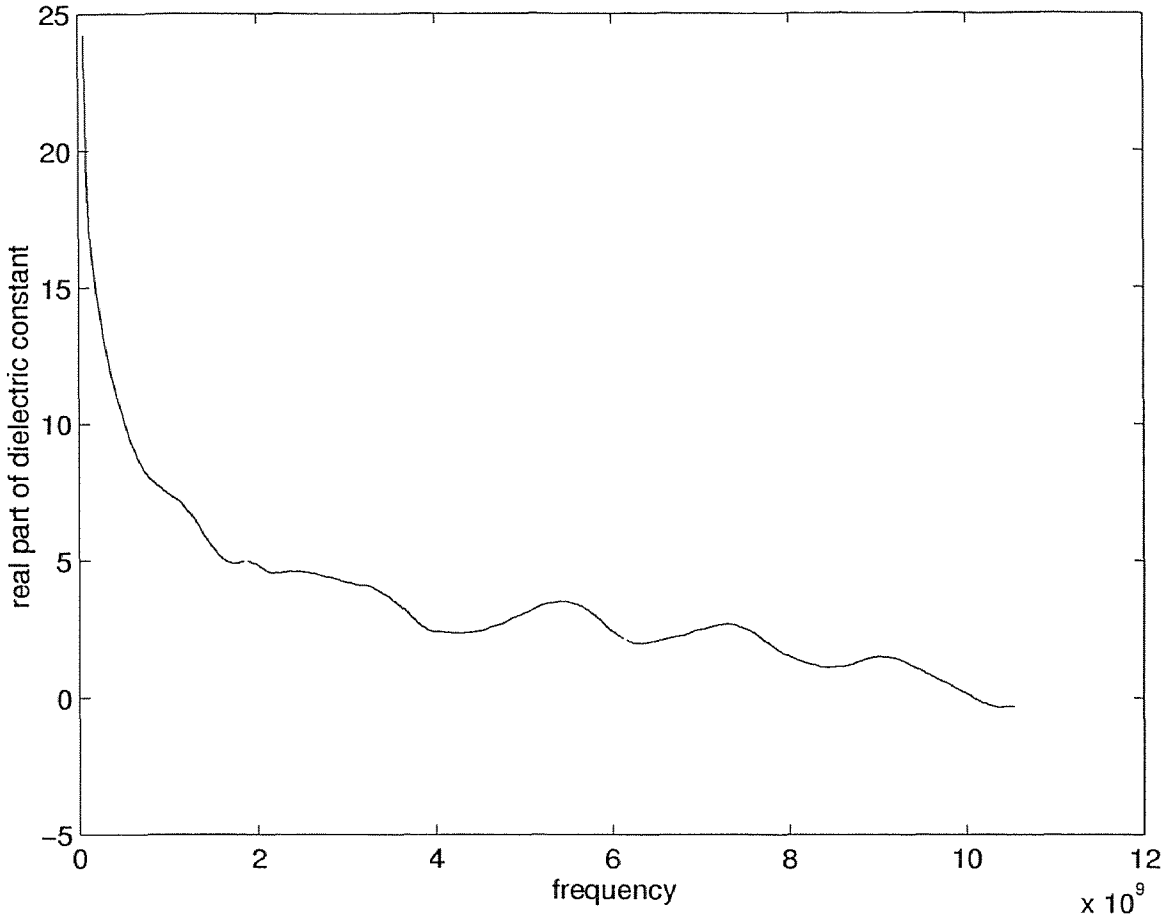

Figure 4.23 Imaginary part of dielectric constant versus the frequency for graphite loaded PMMA in which the graphite concentration was 26 % by weight.

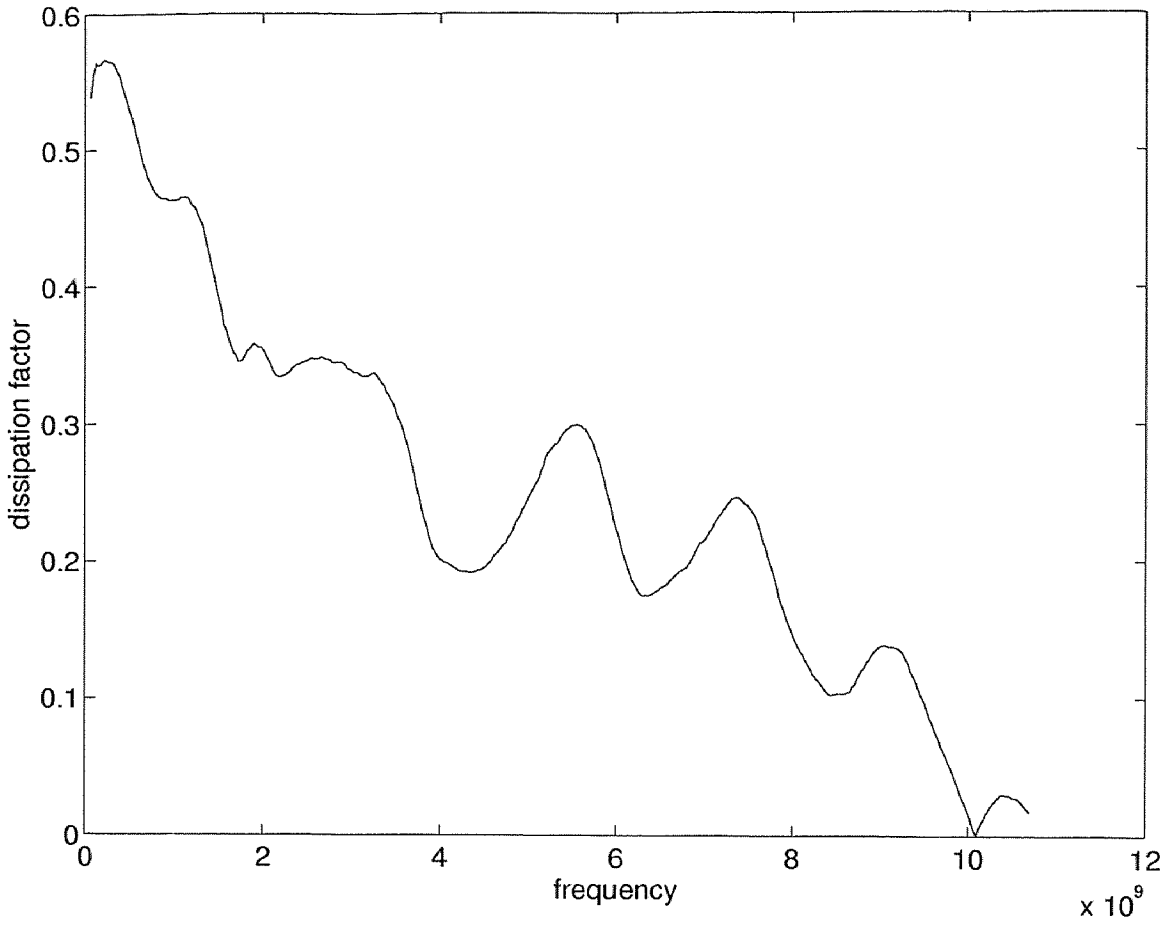

Figure 4.24 Dissipation factor versus the frequency for graphite loaded PMMA in which the graphite concentration was 26 % by weight.

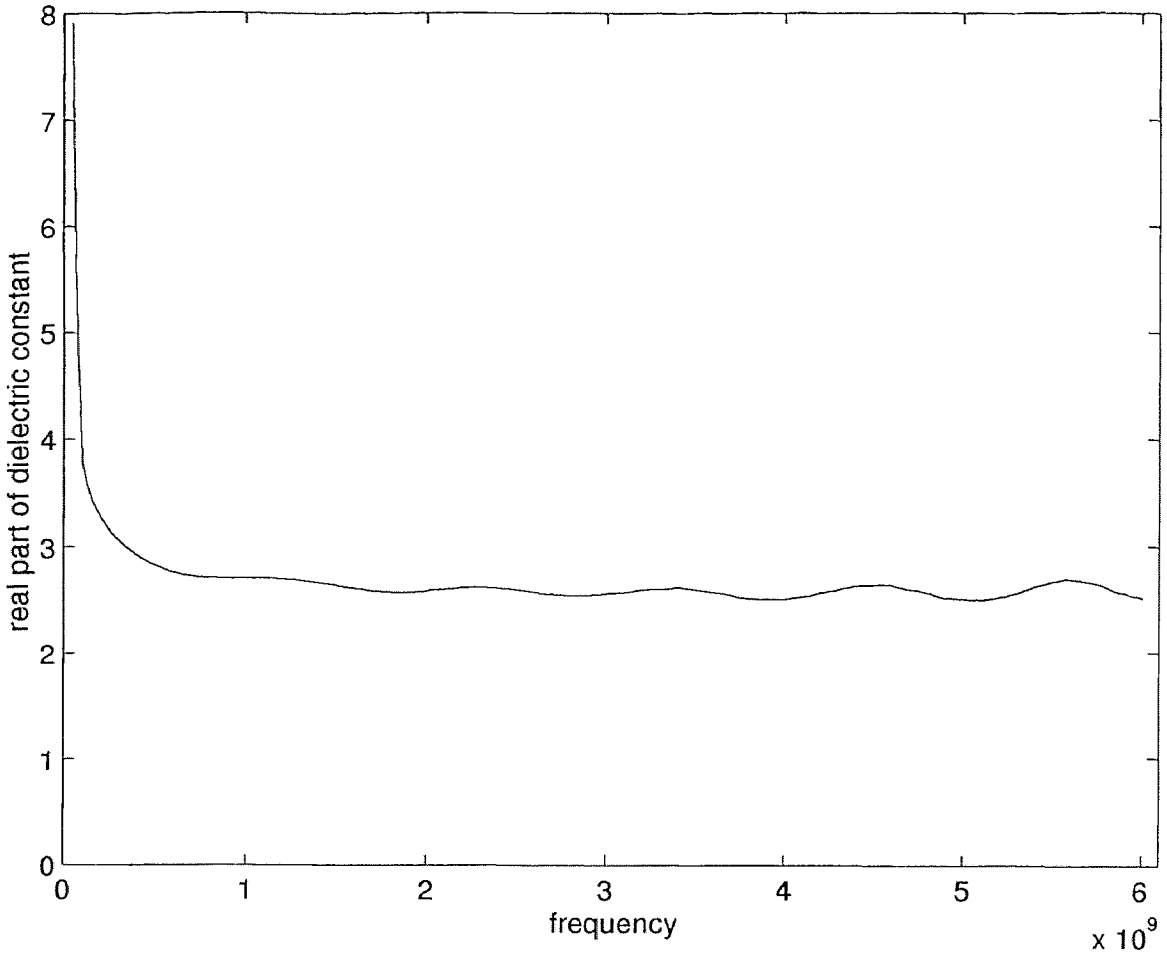

Figure 4.25 Real part of dielectric constant versus the frequency for PVDF loaded PMMA in which the PVDF concentration was 16.15 % by weight.

4.2.4 PVDF-PMMA composites

The real part of the dielectric constant for 16.15 % PVDF in PVDF-PMMA mixture is plotted in figure 4.25.

4.2.5 PVDF-PMMA composites

The real part of dielectric constant for 16.15 % PVDF in PVDF-PMMA mixture is plotted in figure 4.25. The imaginary part of the complex dielectric constant for 16.15 % PVDF in PVDF-PMMA mixture is plotted in figure 4.26. The dissi-

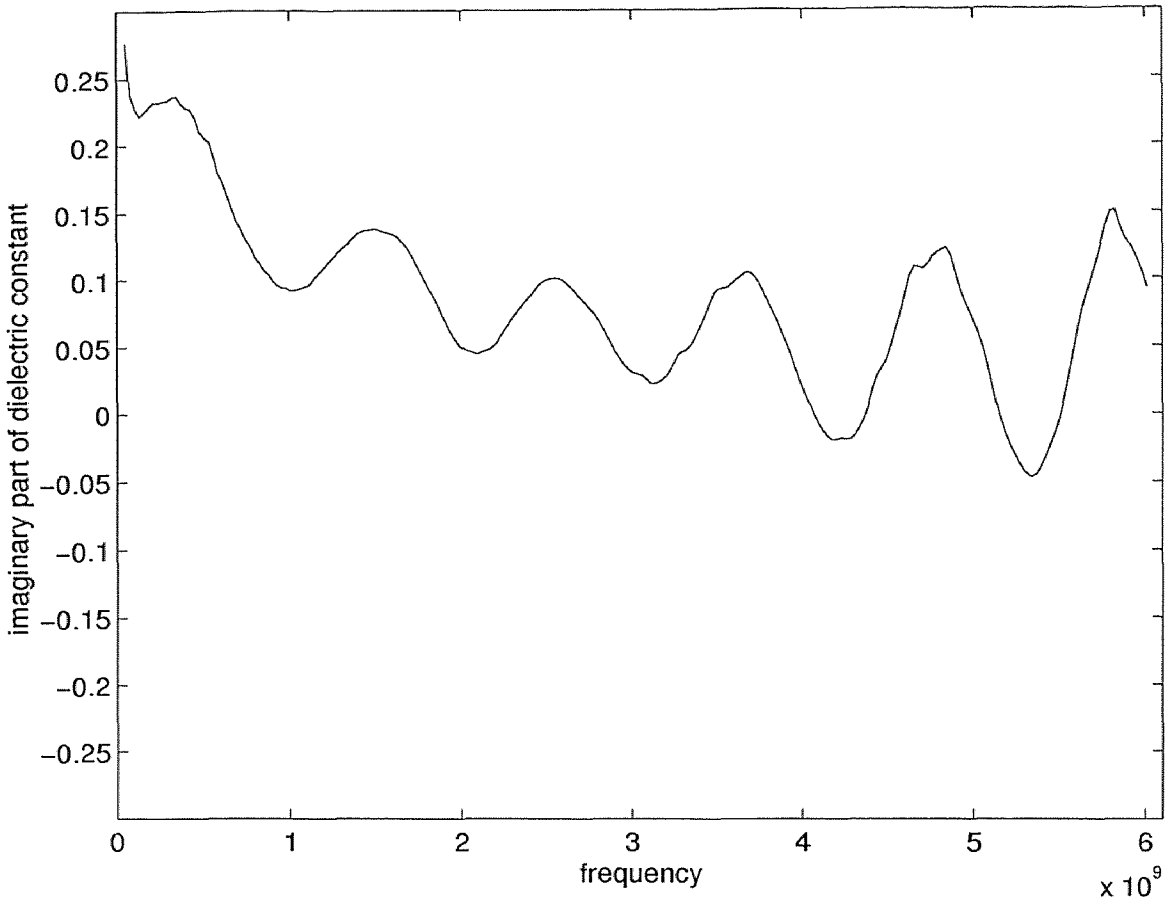

Figure 4.26 Imaginary part of dielectric constant versus the frequency for PVDF loaded PMMA in which the PVDF concentration was 16.15 % by weight.

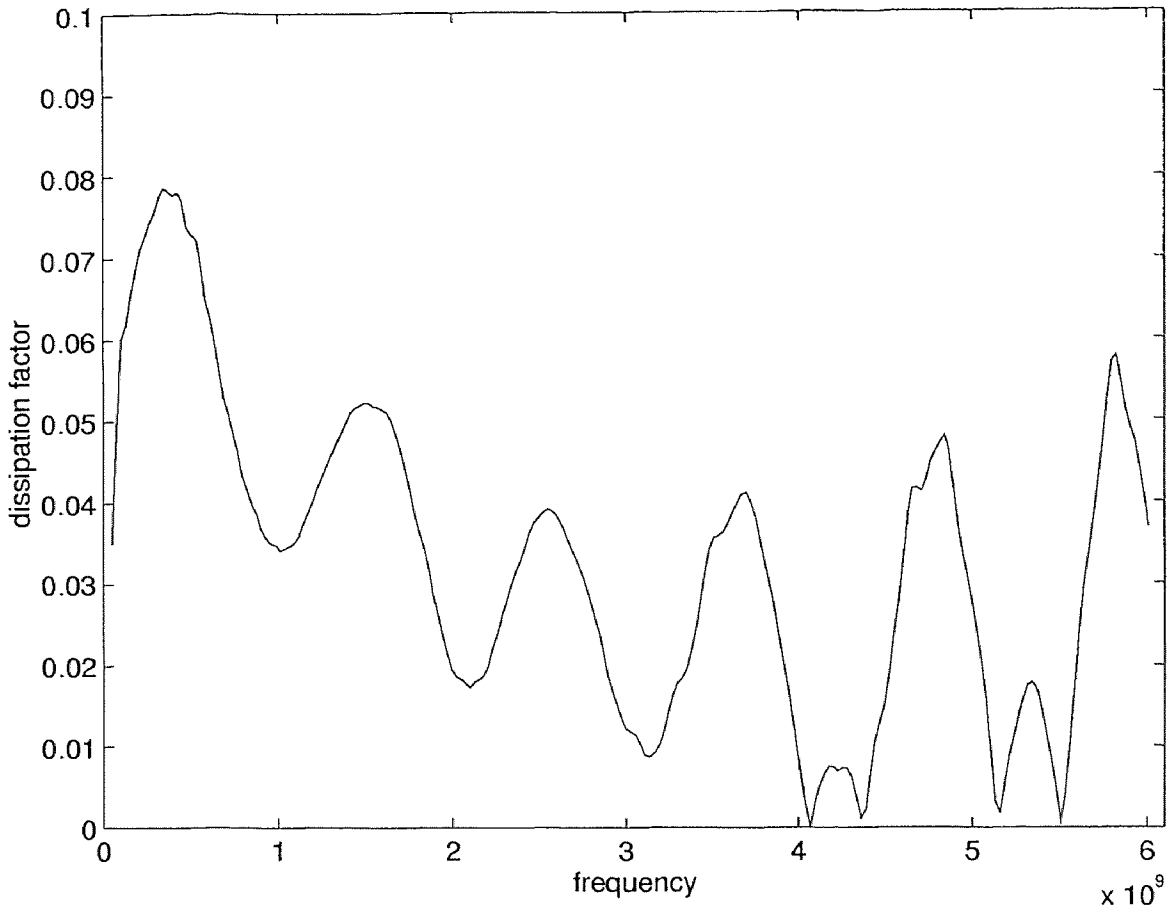

Figure 4.27 Dissipation factor versus the frequency for PVDF loaded PMMA in which the PVDF concentration was 16.15 % by weight.

pation factor for 16.15 % PVDF in PVDF-PMMA mixture is plotted in figure 4.27. The real part of the complex dielectric constant for 19.6 % PVDF in PVDF-PMMA mixture is plotted in figure 4.28. The imaginary part of the complex dielectric constant for 19.6 % PVDF in PVDF-PMMA mixture is plotted in figure 4.29. The dissipation factor for 19.6 % PVDF in PVDF-PMMA mixture is plotted versus frequency in figure 4.30.

For the rest of the dielectric constant plots for 26.7 % PVDF and 33.78 % PVDF the reader should refer to Appendix B.

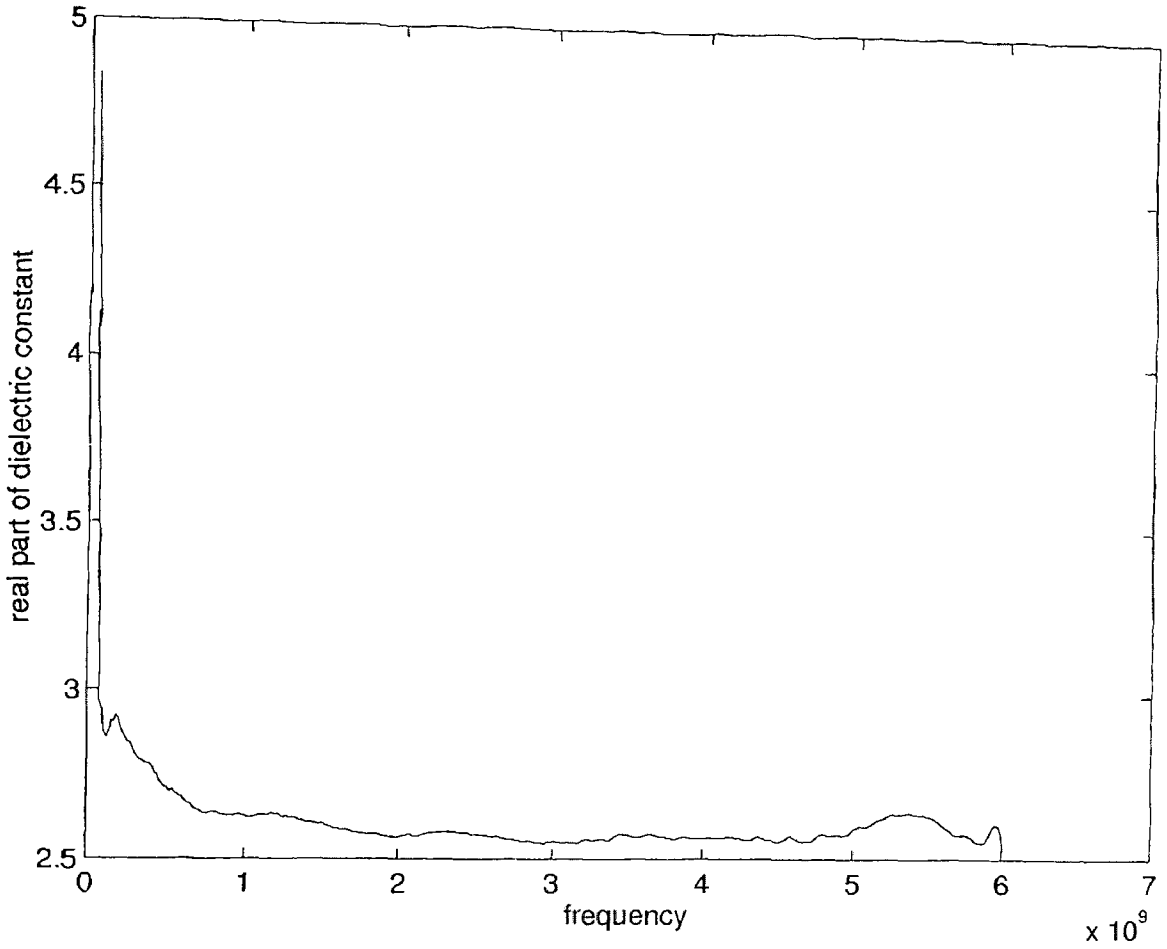

Figure 4.28 Real part of dielectric constant versus the frequency for PVDF loaded PMMA in which the PVDF concentration was 19.6 % by weight.

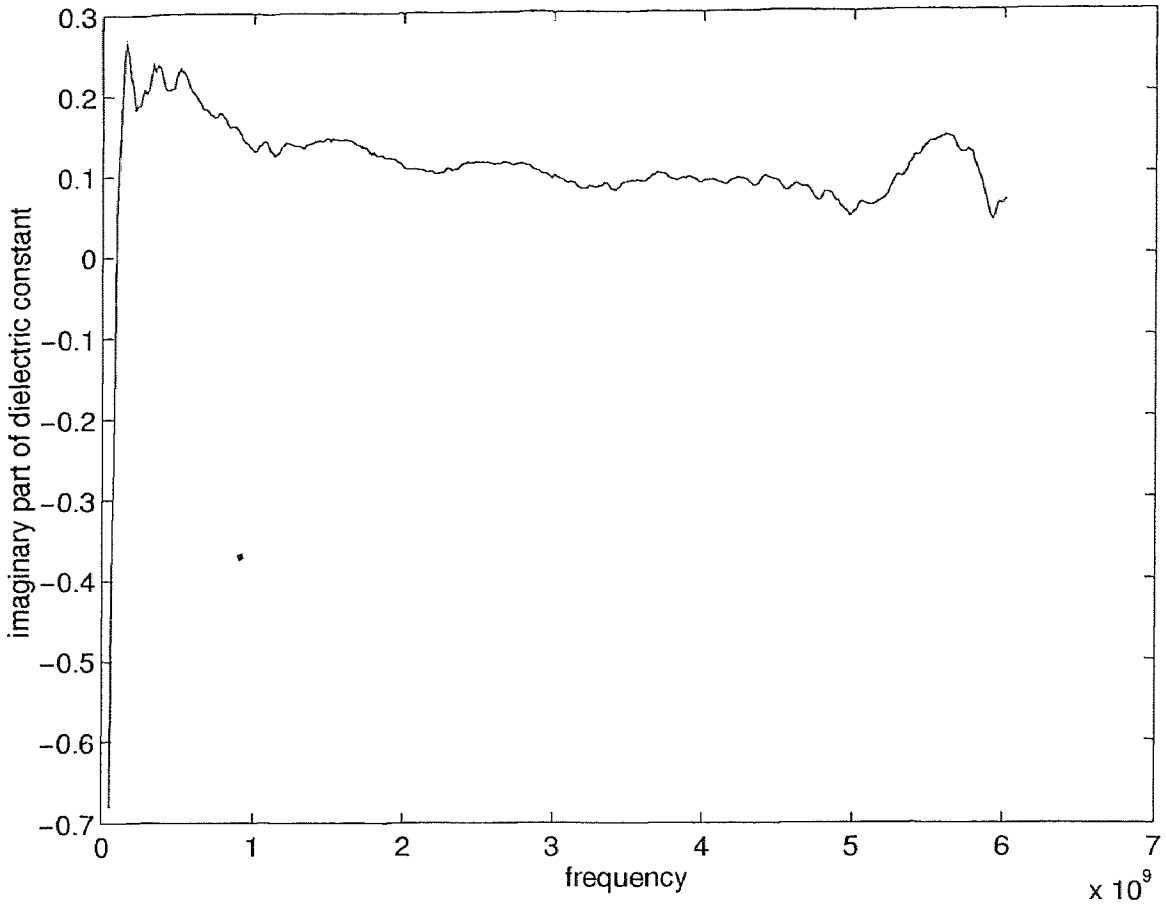

Figure 4.29 Imaginary part of dielectric constant versus the frequency for PVDF loaded PMMA in which the PVDF concentration was 19.6 % by weight.

4.2.6 PVDF-graphite-PMMA composites

The dielectric constant plots for the PVDF-graphite-pmma composites are given in Appendix B. The graphite concentration was varied in the blend with the PVDF concentration held constant at 5 % for each sample. The dielectric constant has been determined for 0.9 %, 9.5 %, 17 % and 20.5 % graphite in the blend.

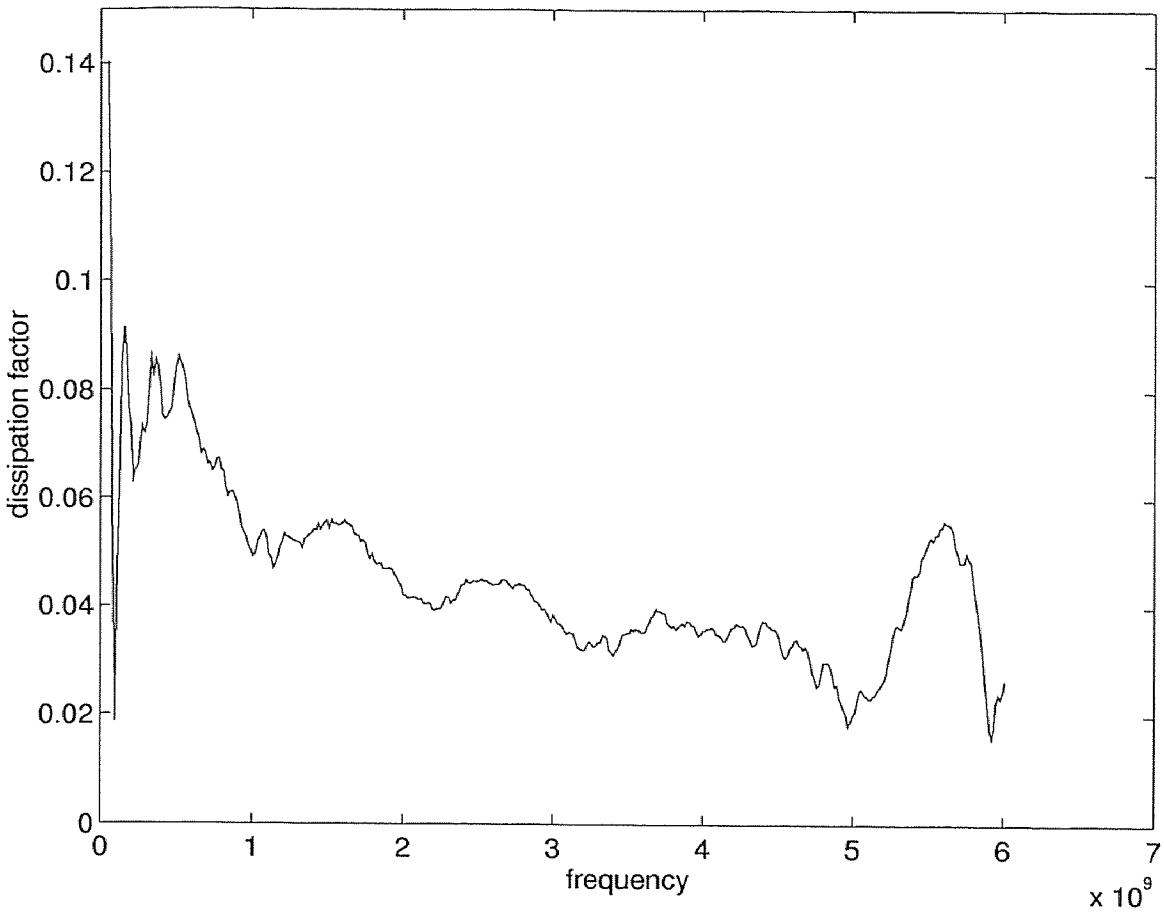

Figure 4.30 Dissipation factor versus the frequency for PVDF loaded PMMA in which the PVDF concentration was 19.6 % by weight.

CHAPTER 5

DISCUSSION

5.1 Low frequency measurements

It is observed that the dielectric constant of graphite PMMA reaches its peak at a certain critical concentration (percolation point at about 15 % graphite concentration). The peak point in the dielectric constant was observed at the same graphite concentration point for two different measurement frequencies (1kHz and 10 kHz) which eliminates the possibility of any circuit resonance since such a resonance would occur at a particular frequency only for a certain graphite concentration (or equivalently, certain circuit element values). A similar kind of measurement was made by Narkis [11] at 10 MHz. They assumed that the dielectric concentration would keep on increasing with the increasing graphite concentration. However, their conclusion was based on the overloading of their measuring instrument (a HP Q-meter). Overloading of the measuring system was observed here too but was prevented by introducing a tape at one end of the carbon-graphite films and taking the tape impedance into account. Hence, it is believed that the measurement in the present study is more accurate. Moreover, because the phase is also measured, the imaginary part of the dielectric constant is also determined. Note that the imaginary part is determined from the real part of the dielectric constant and the dissipation factor.

5.2 Comments on low concentration graphite loaded PMMA

It is seen that the real part is flat to around frequencies up to 5 GHz. At this point the real part starts to fall down and an oscillation is observed in the imaginary part. This can be attributed to the higher order modes starting to propagate beyond 5 GHz depending upon the loading of graphite/PVDF in PMMA. It is known that

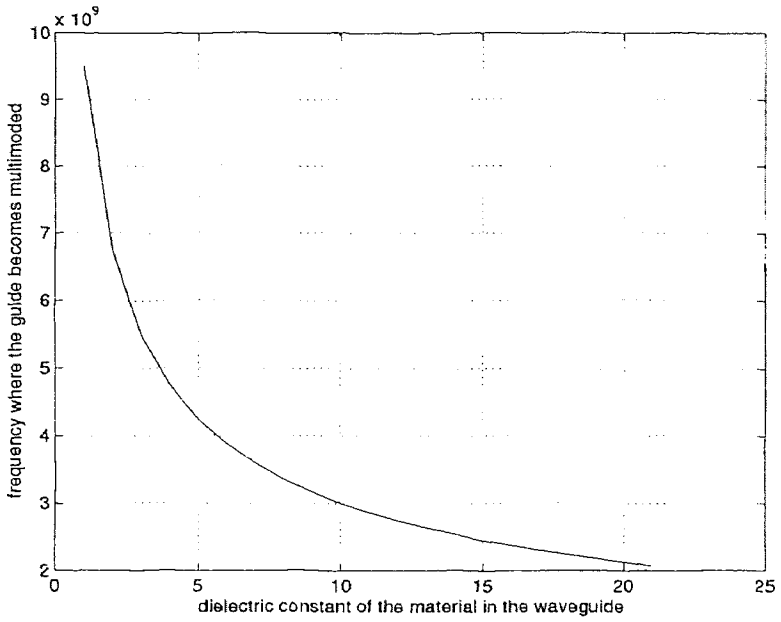

Figure 5.1 The variation of the on-set of TE_{11} mode with the real part of the dielectric constant

the frequency at which the TE_{11} mode starts to propagate in a coaxial line is given by [23]:

$$f_c = ck_c/(2\pi(\epsilon_r)^{1/2})$$

where, c is the velocity of light in free space;

k_c is given by $k_c a$ which is the normalized cutoff frequency;

$k_c a = 2/(1 + b/a)$ and a and b respectively being the inner and outer conductor dimensions;

ϵ_r = real part of the dielectric constant.

The frequency at which the TE_{11} mode starts to propagate is plotted as a function of the (real part) dielectric constant in figure 5.1. Deleterious results were observed at higher frequencies due to multimode behavior of the guide. Figures B.14, B.15and B.16 show the effect higher order modes.

5.3 Comments on behavior of high concentration graphite samples

In the high graphite concentration case it is observed that there is no anomaly in the imaginary part of the dielectric constant over a relatively large bandwidth. This may be explained as follows: The high concentration graphite samples are too lossy to let the higher order modes propagate, thus only the fundamental mode is sustained. The peaking at 18 GHz may be due to the fact that the connectors no more act as 50 Ω lines and exhibit a lot of parasitics at such a high frequency.

5.4 Behavior of PVDF-PMMA blends

The PVDF-PMMA blends all show a real part close to that of PMMA ($\epsilon_{real,PMMA} = 2.6$). There is an increase in the dielectric constant as the concentration of PVDF is increased. However, the increase is relatively lesser than that found when graphite is added to PMMA. It is probably because graphite is conducting whereas PVDF is a dielectric.

5.5 Behavior of PVDF-Graphite-PMMA blends

A PMMA-PVDF-graphite dielectric constant curve was plotted up to 20 GHz to for 9.5 % graphite. It can be seen that the imaginary part of the dielectric constant shows an anomaly at around 8 GHz. This is due to the fact that the waveguide becomes multimoded at that frequency. Otherwise, the real part of dielectric constant shows a rather gradual decreasing change.

CHAPTER 6

CONCLUSIONS

The dielectric behavior of three kinds of artificial dielectrics has been characterized at both microwave and low frequencies. It is observed that the dielectric constant can be controlled by controlling the concentration of the conductive particles in the dielectric. The properties can also be controlled by controlling the size of the dispersed particles. This can be concluded from the comparison between the fine graphite and the coarse graphite particle samples. In general, with the rise in frequency, the effective dielectric constant decreases.

The air-line method was useful only up to around 6 GHz for the low graphite concentration samples as the air-line would become multimoded thereafter. For higher concentration samples of graphite the air-line method could be used up to 10 GHz as the higher order modes were not supported up to this frequency due to the lossy nature of the dielectric.

APPENDIX A

FIGURES OF CHAPTER 2

The plots of dielectric constant and dissipation factor of PVDF-PMMA composites at 1 kHz are shown here. The variation of the real part of dielectric constant versus the weight percent of PVDF in PVDF-PMMA mixtures (at 1kHz) is shown in figure A.1.

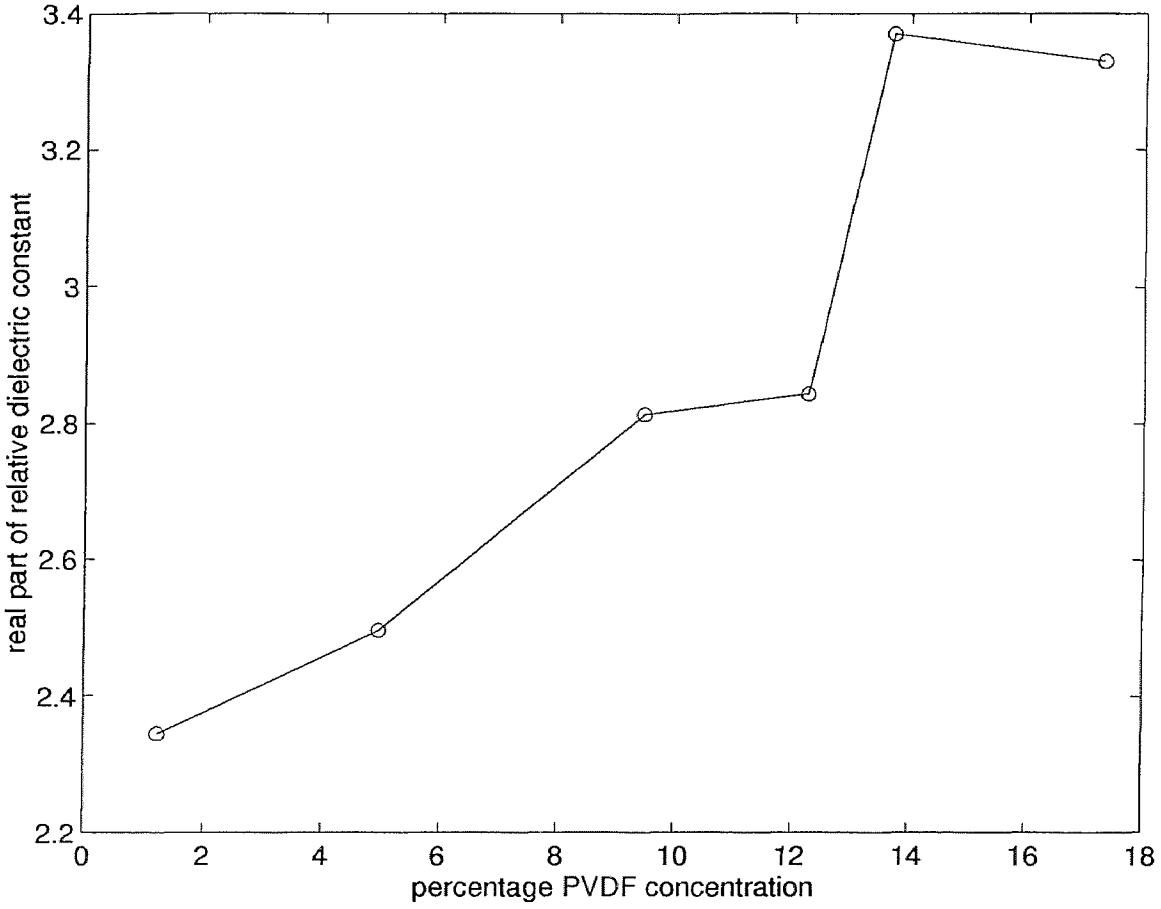

Figure A.1 Variation of the real part of dielectric constant of the PVDF-PMMA composites (at 1kHz) as a function of the weight percent of PVDF in the composites.

The variation of the imaginary part of dielectric constant of the PVDF-PMMA composites (at 1kHz) as a function of the weight percent of PVDF in the composites is shown in figure A.2.

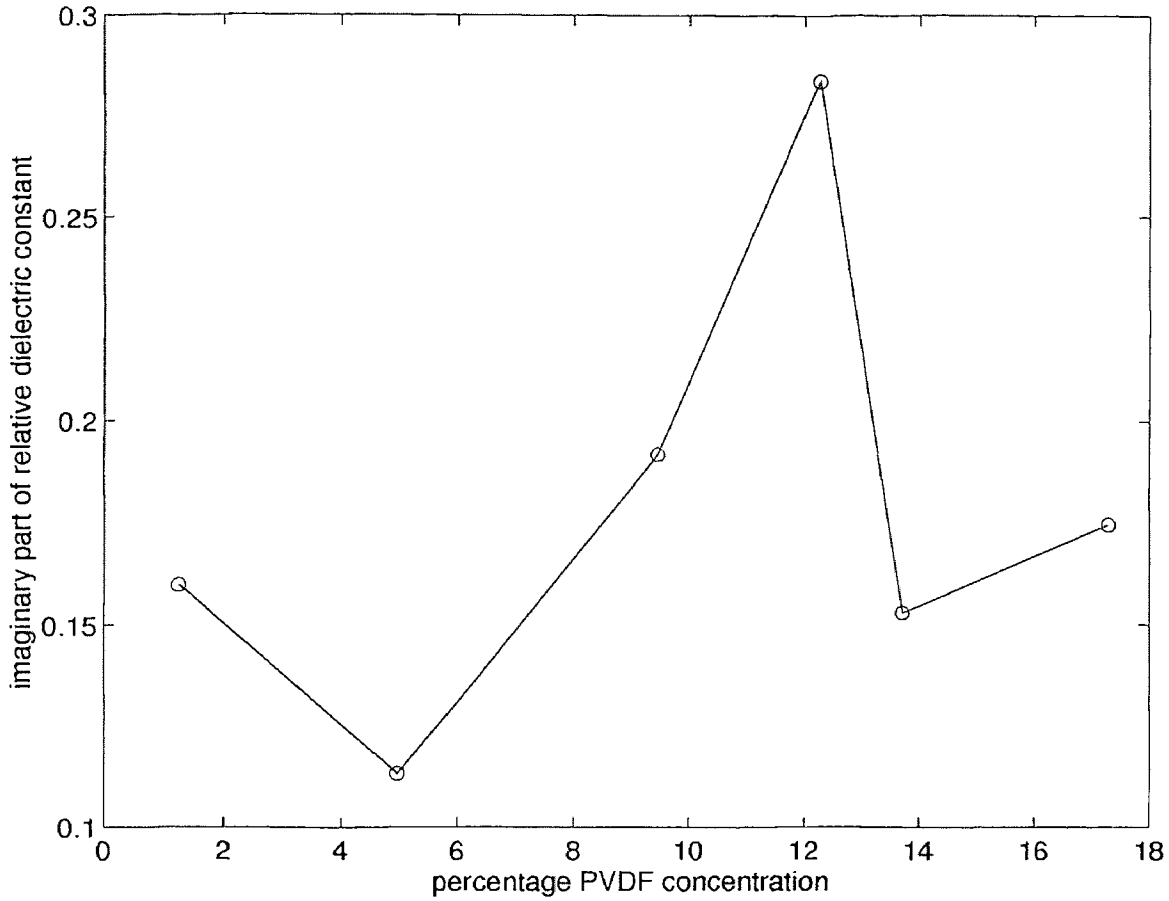

Figure A.2 Variation of the imaginary part of dielectric constant of the PVDF-PMMA composites (at 1kHz) as a function of the weight percent of PVDF in the composites.

The variation of the dissipation factor (loss tangent) in the PVDF-PMMA composites (at 1kHz) as a function of the weight percent of PVDF in the composites is shown in figure A.3.

The real part and the imaginary part of the dielectric constant as well as the dissipation factor are plotted all together for comparison in figure A.4.

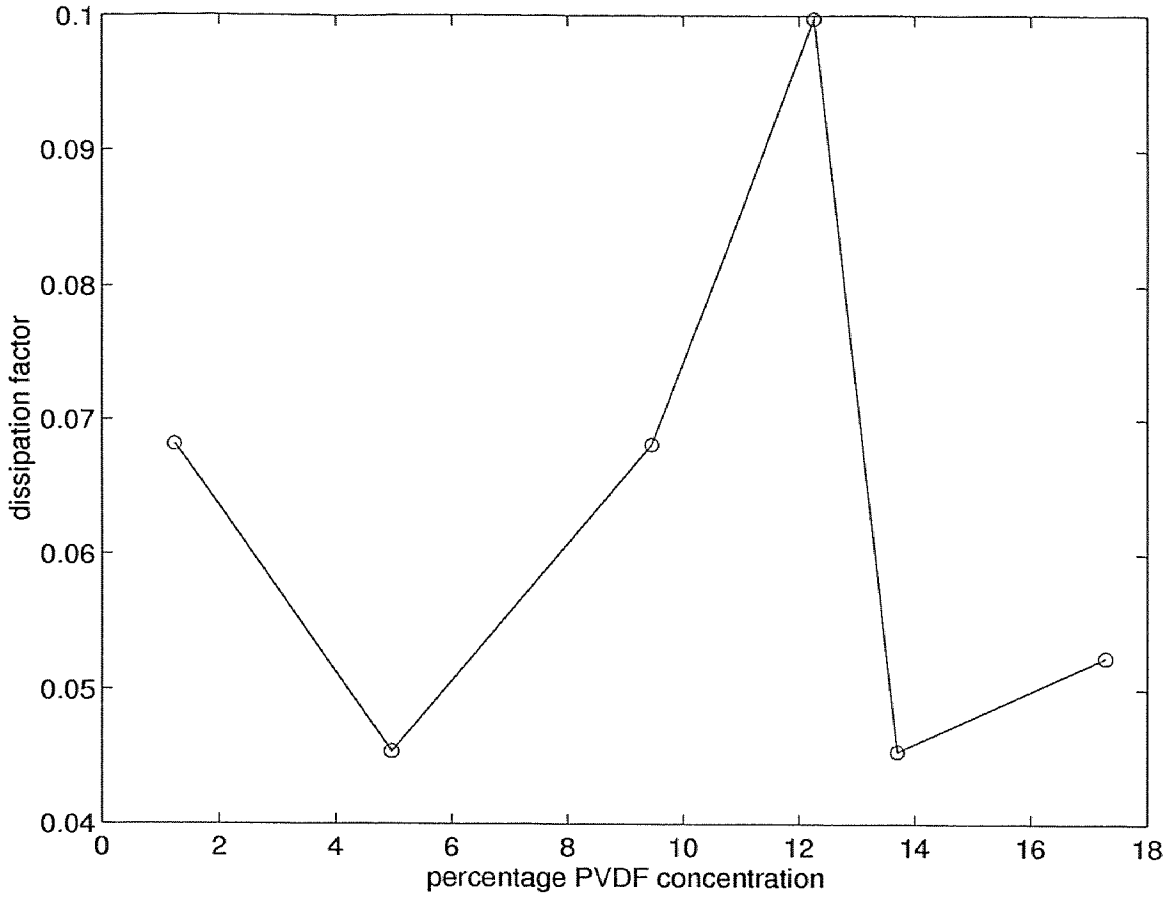

Figure A.3 Variation of dissipation factor of the PVDF-PMMA composites (at 1kHz) as a function of the weight percent of PVDF in the composites.

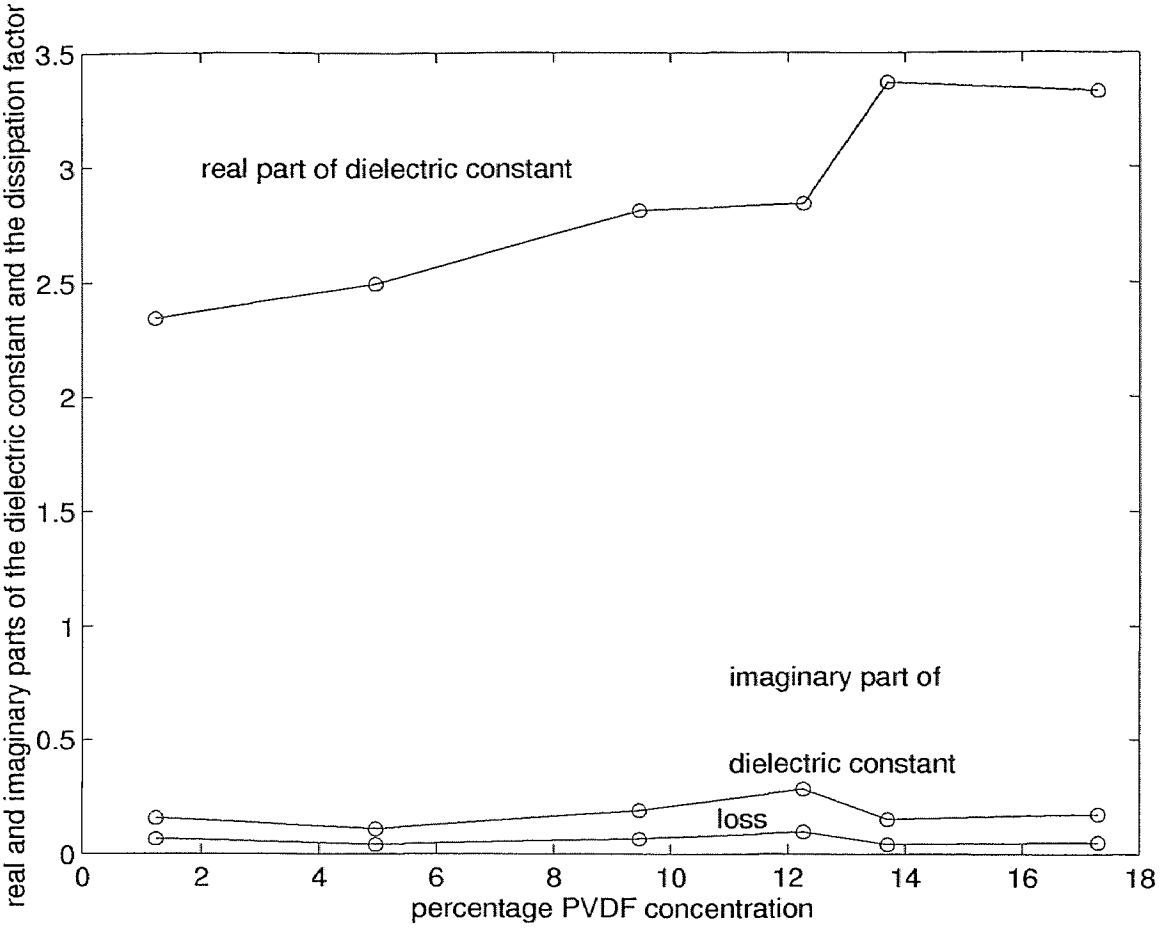

Figure A.4 Variation of the real and imaginary parts of dielectric constant of the PVDF-PMMA composites (at 1kHz) as well as the loss (dissipation) factor as a function of the weight percent of PVDF in the composites.

APPENDIX B

FIGURES OF CHAPTER 4

B.1 Dielectric constant curves for Teflon and PMMA

The dielectric constant was determined for standard materials of known dielectric constant such as Teflon and PMMA in the frequency range of interest. This was done to actually verify the validity and accuracy of the air-line method of determination of dielectric constant in the frequency range of interest. The real part of the dielectric constant of Teflon and PMMA in the centimeter wavelength range is 2.0 and 2.6 respectively [14]. These are practically lossless materials and it seen that the air-line method gives reasonably accurate results in both cases.

The real part of the complex dielectric constant for Teflon is graphed in figure B.1. The imaginary part of the complex dielectric constant for Teflon is graphed in figure B.2. The real part of the complex dielectric constant for PMMA is graphed in figure B.3. The imaginary part of the complex dielectric constant for PMMA is graphed in figure B.4.

B.2 Figures for PVDF-PMMA composites

The real part of the complex dielectric constant for 26.7 % PVDF in PVDF-PMMA mixture is plotted in figure B.5. The imaginary part of the complex dielectric constant for 26.7 % PVDF in PVDF-PMMA mixture is plotted in figure B.6. The dissipation factor for 26.7 % PVDF in PVDF-PMMA mixture is plotted versus frequency in figure B.7. The real part of the complex dielectric constant for 33.78 % PVDF in PVDF-PMMA mixture is plotted in figure B.8. The imaginary part of the complex dielectric constant for 33.78 % PVDF in PVDF-PMMA mixture is plotted in figure B.9. The dissipation factor for 33.78 % PVDF in PVDF-PMMA

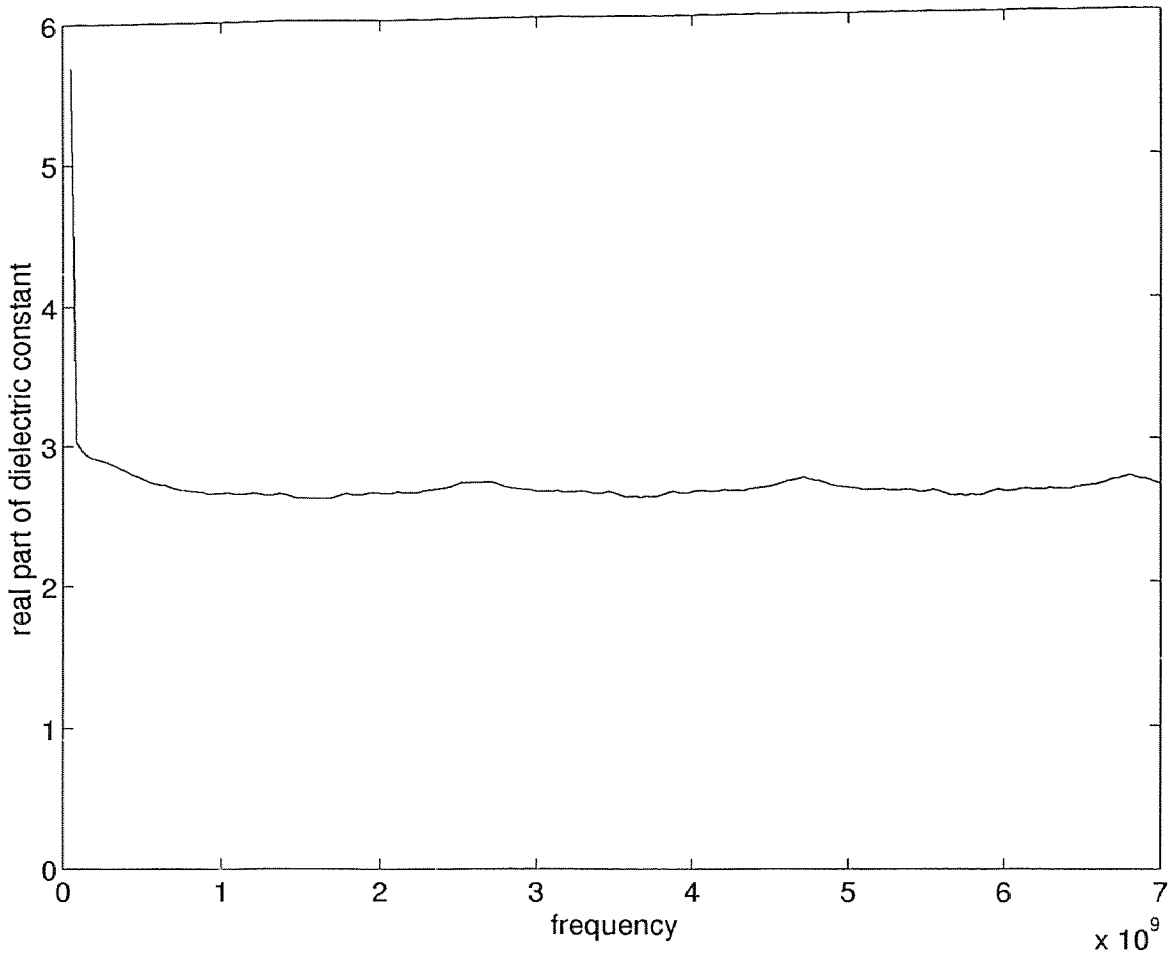

Figure B.1 Real part of dielectric constant versus the frequency for Teflon

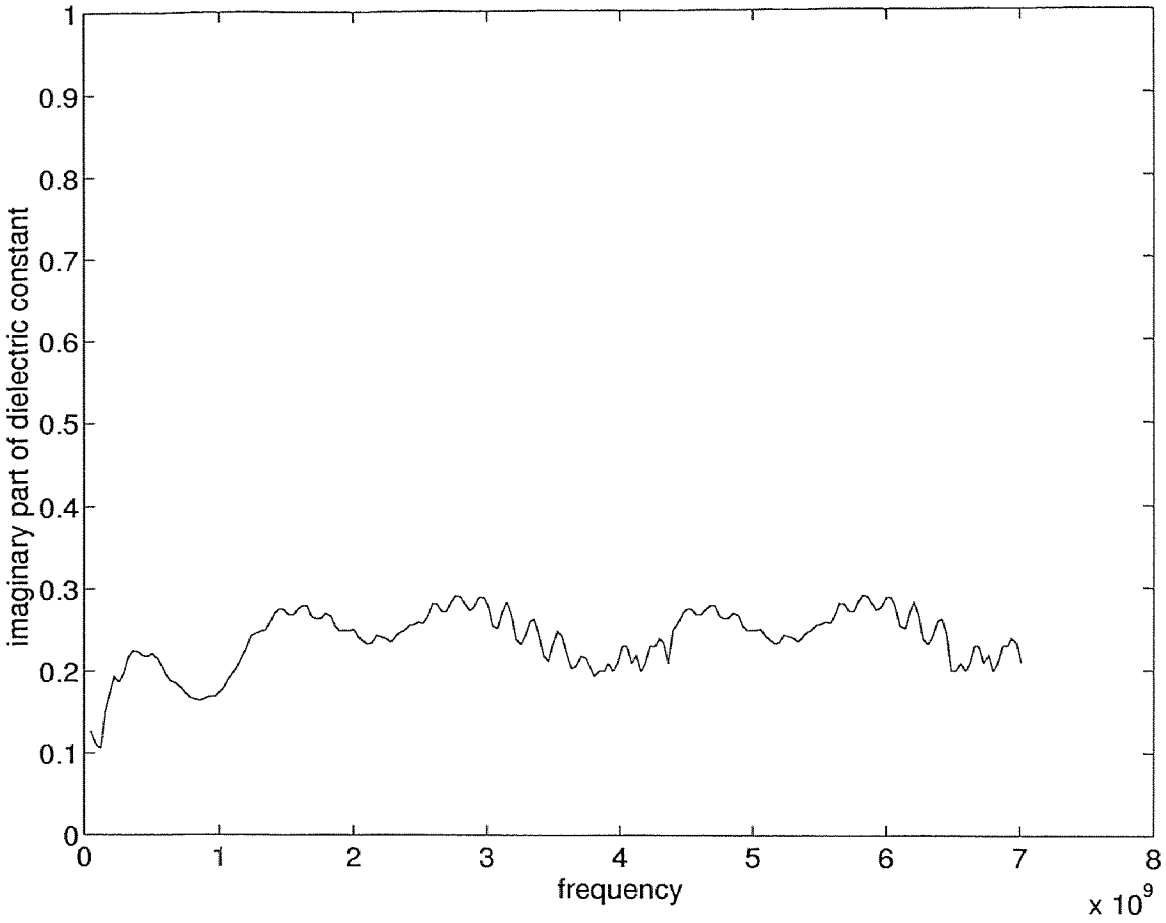

Figure B.2 Imaginary part of dielectric constant versus the frequency for Teflon.

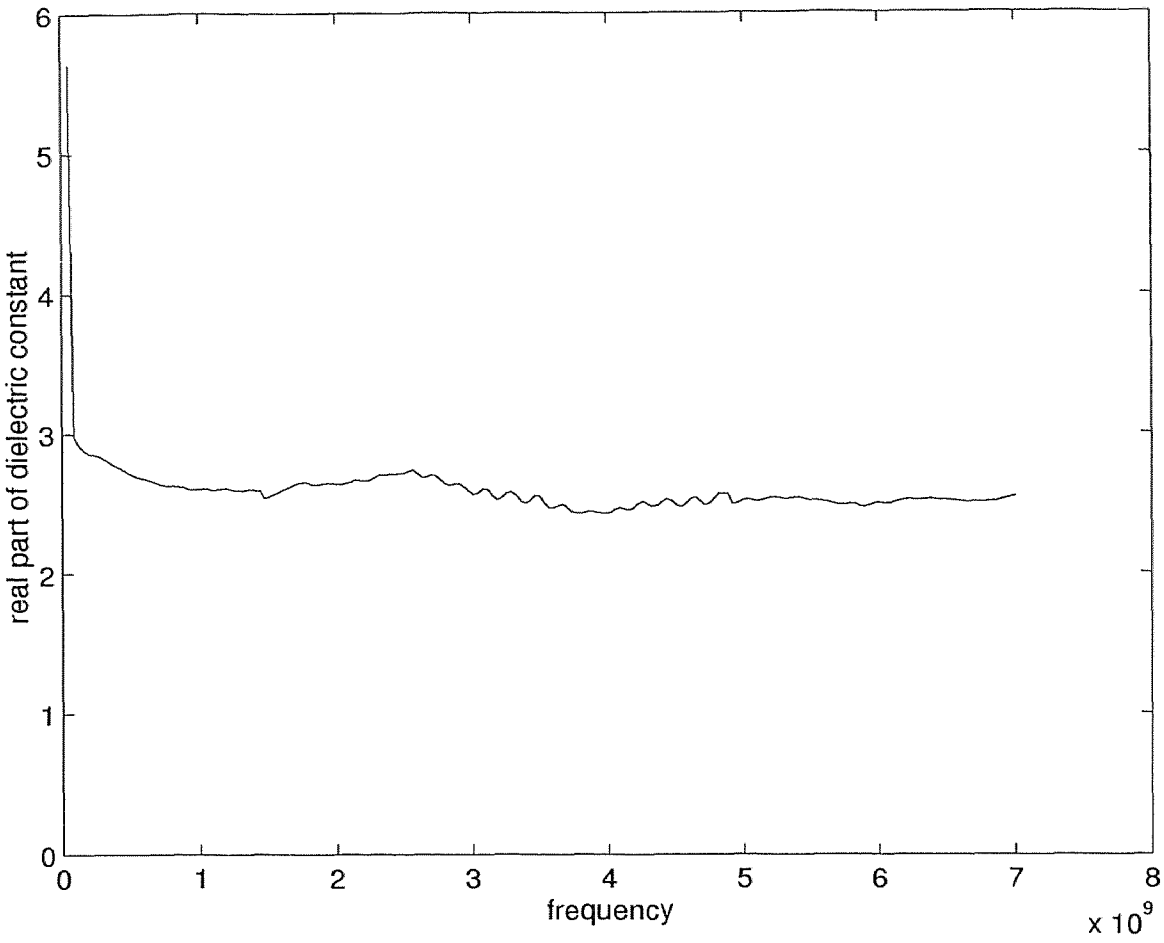

Figure B.3 Real part of dielectric constant versus the frequency for PMMA.

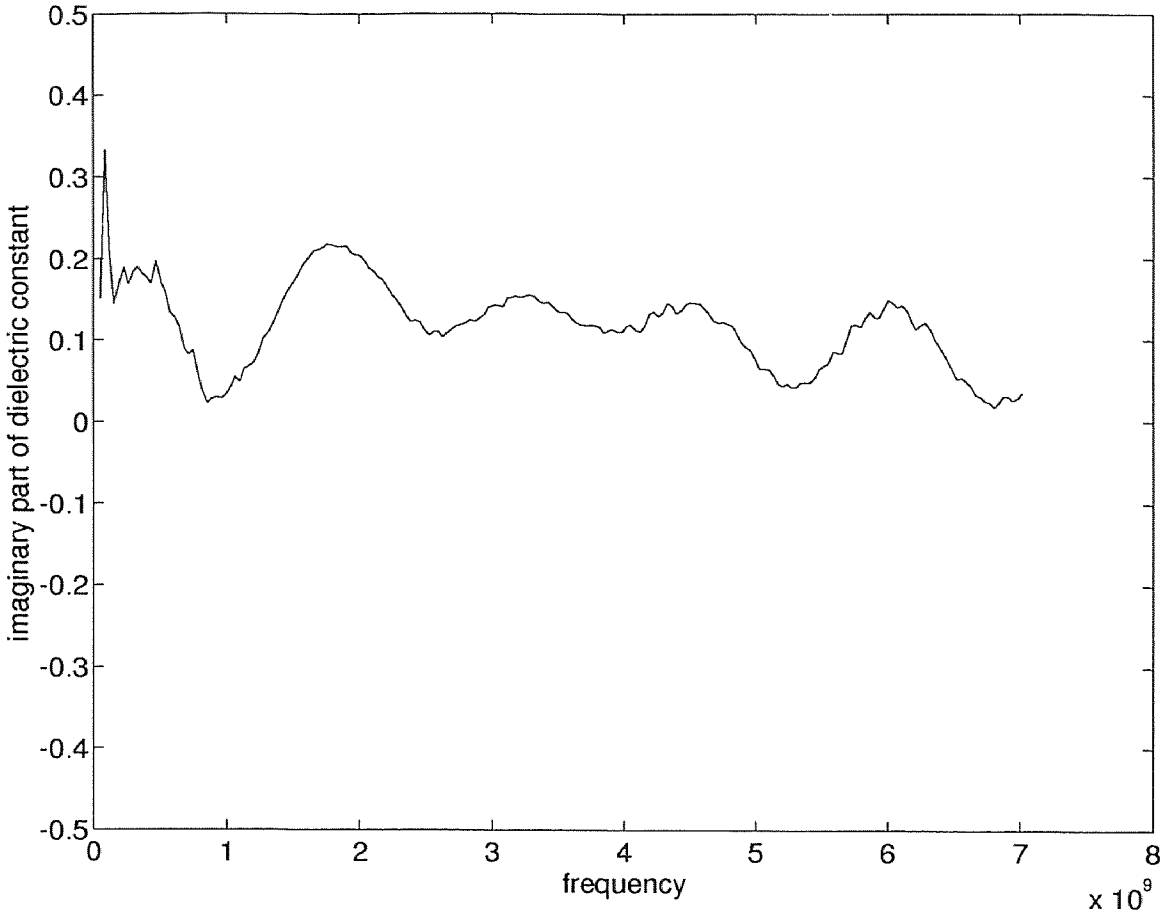

Figure B.4 Imaginary part of dielectric constant versus the frequency for PMMA.

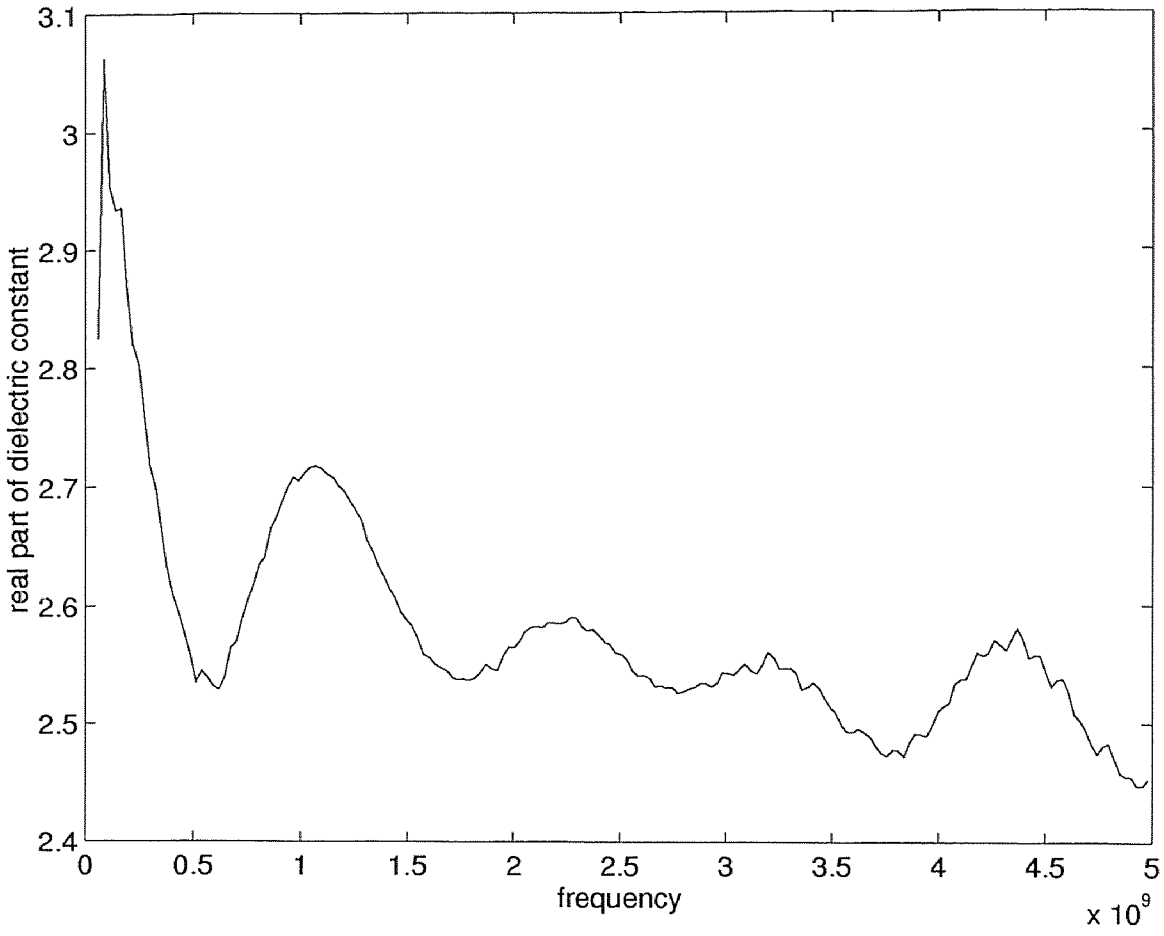

Figure B.5 Real part of dielectric constant versus the frequency for PVDF loaded PMMA in which the PVDF concentration was 26.7 % by weight.

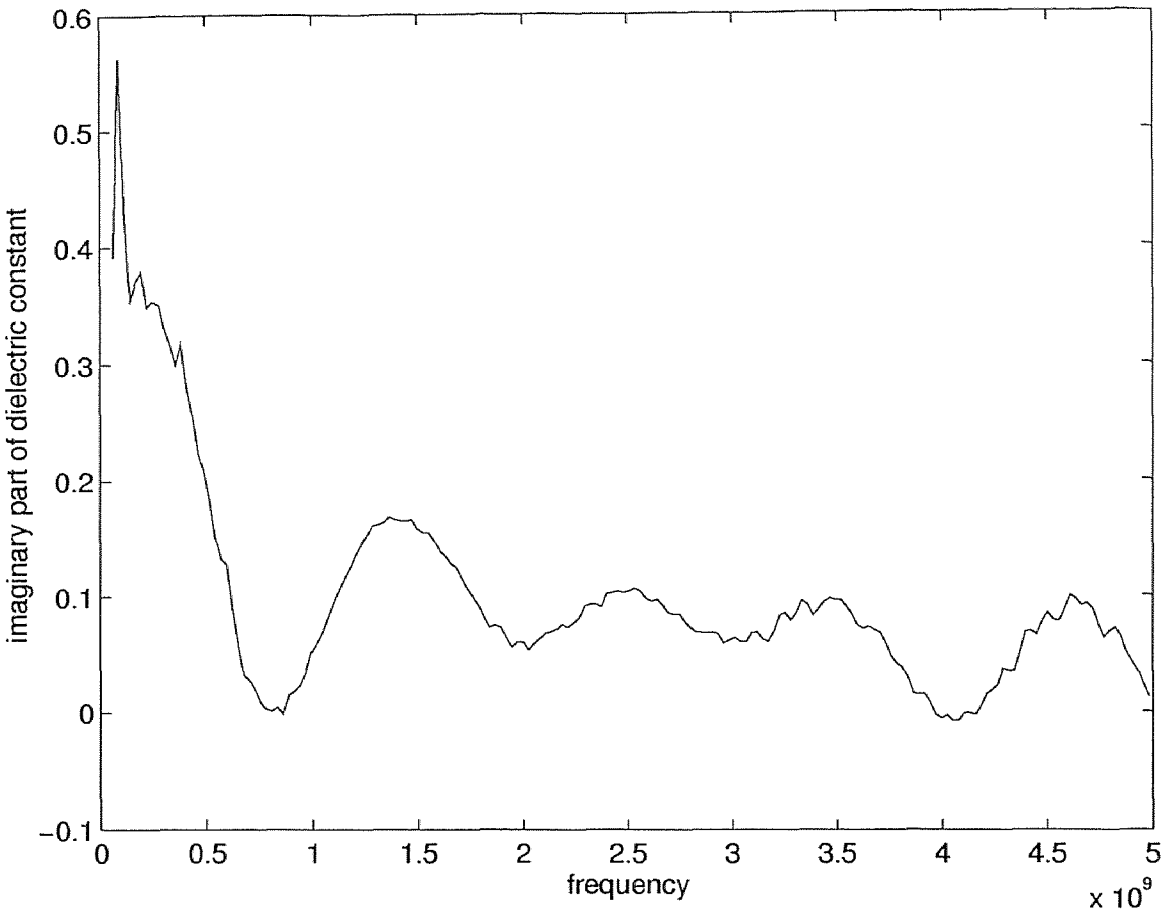

Figure B.6 Imaginary part of dielectric constant versus the frequency for PVDF loaded PMMA in which the PVDF concentration was 26.7 % by weight.

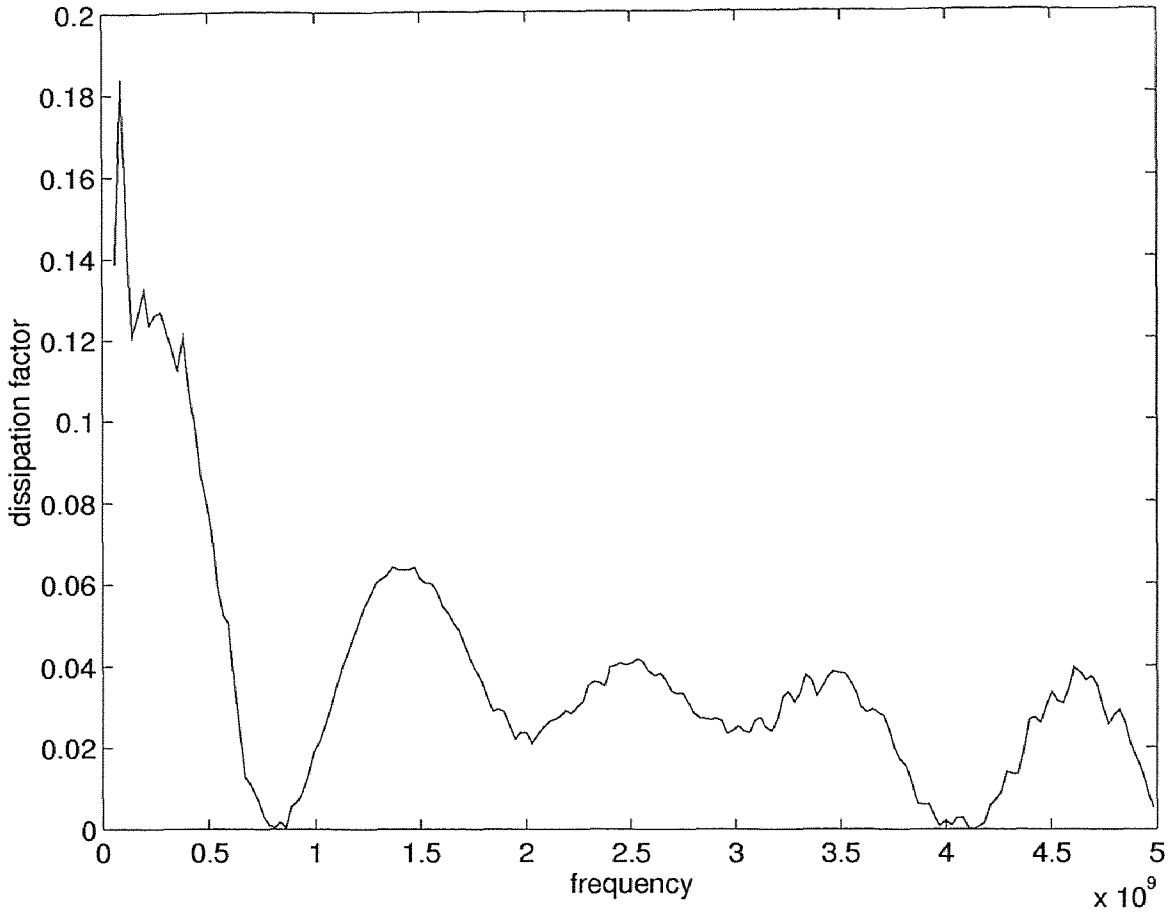

Figure B.7 Dissipation factor versus the frequency for PVDF loaded PMMA in which the PVDF concentration was 26.7 % by weight.

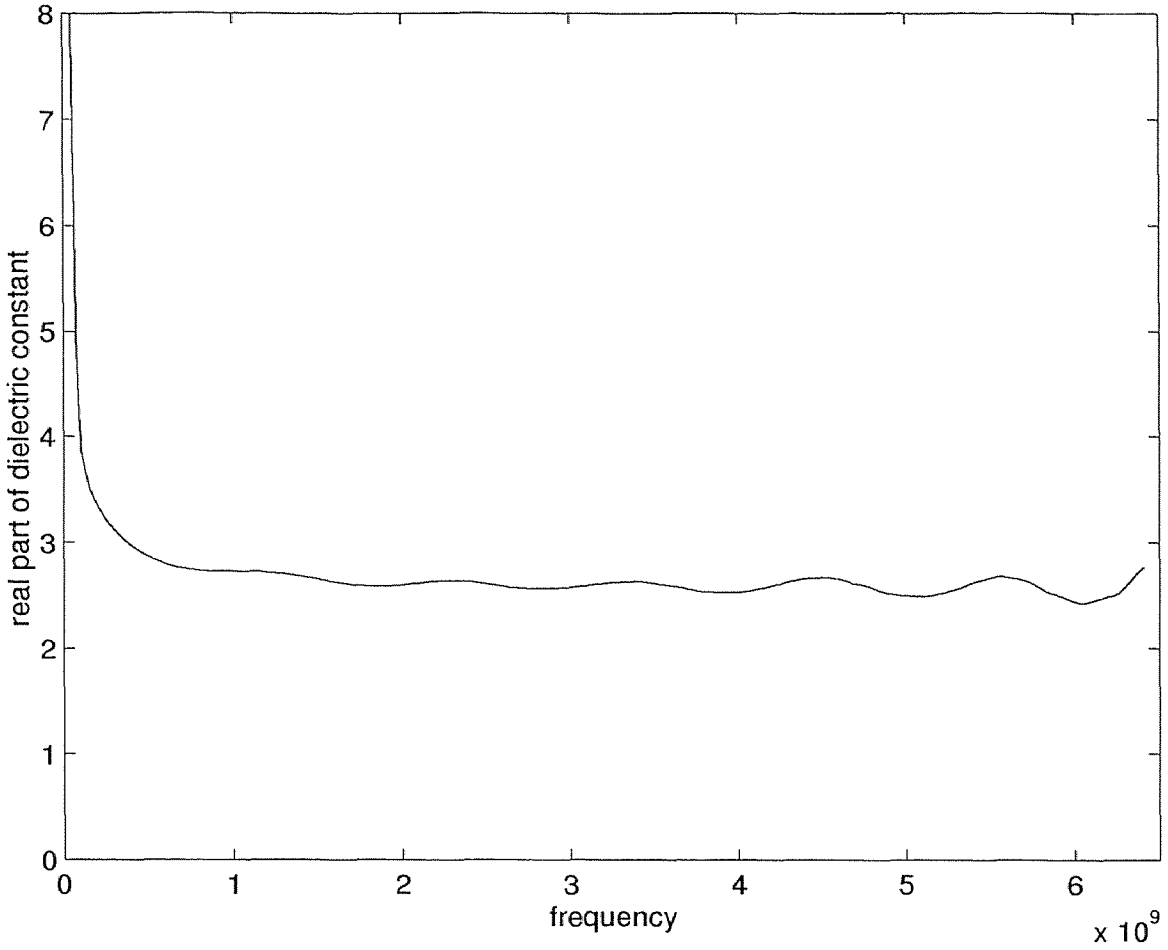

Figure B.8 Real part of dielectric constant versus the frequency for PVDF loaded PMMA in which the PVDF concentration was 33.78% by weight.

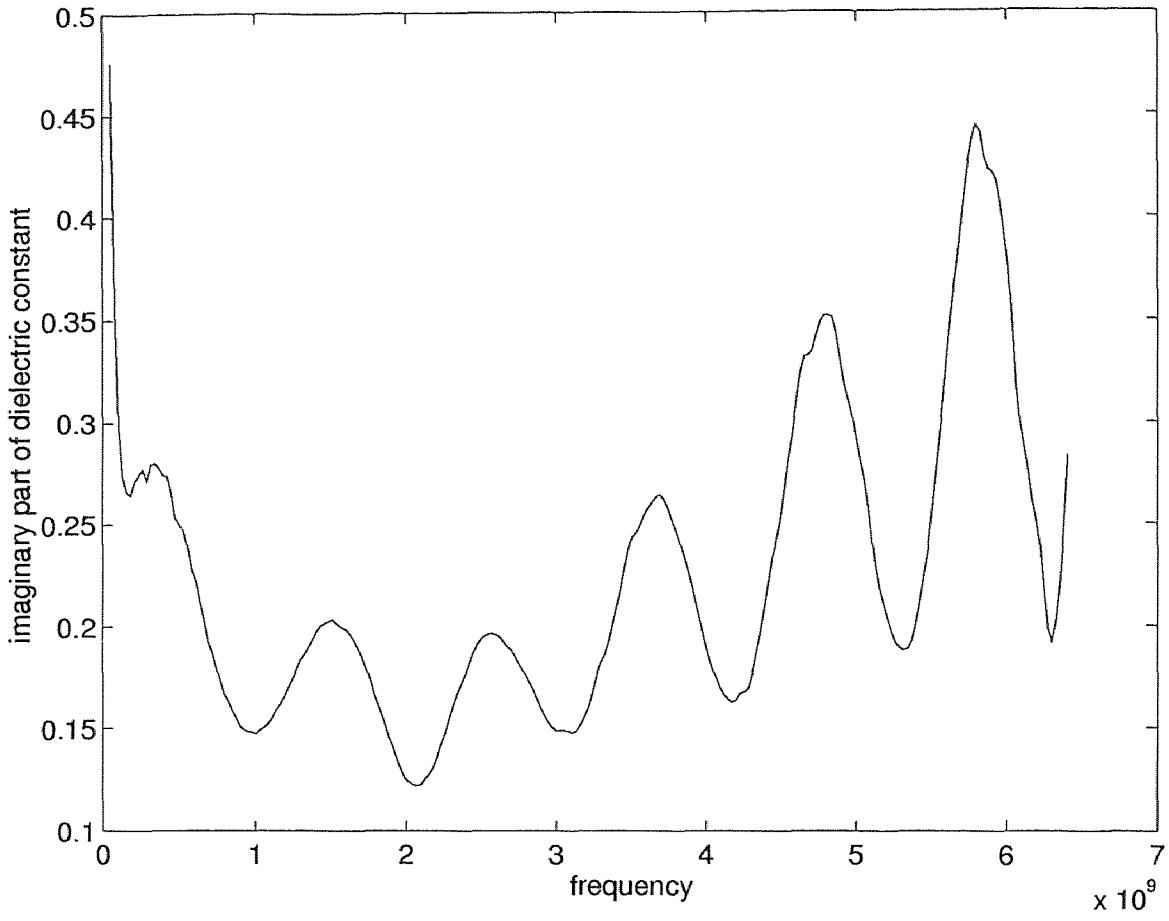

Figure B.9 Imaginary part of dielectric constant versus the frequency for PVDF loaded PMMA in which the PVDF concentration was 33.78 % by weight.

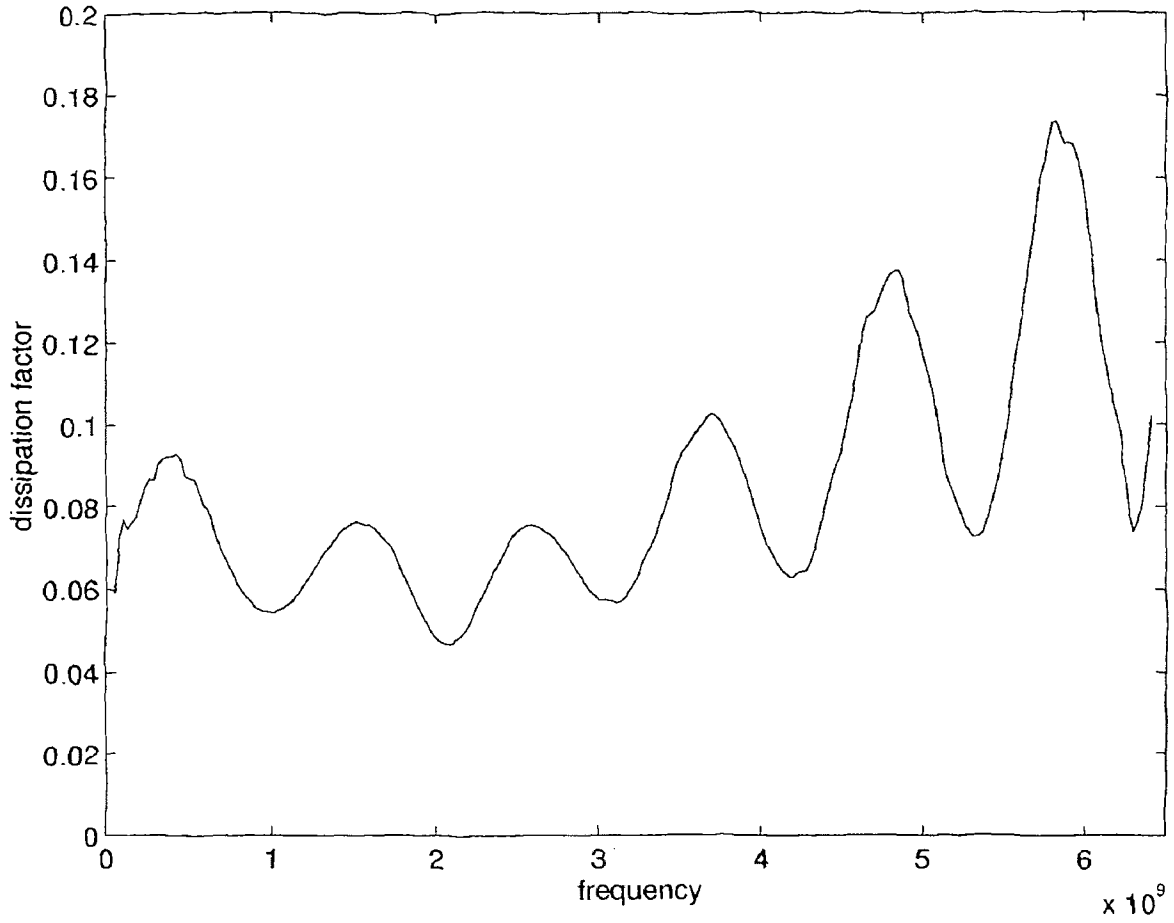

Figure B.10 Dissipation factor versus the frequency for PVDF loaded PMMA in which the PVDF concentration was 33.78 % by weight.

mixture is plotted versus frequency in figure B.10.

B.3 Figures for PVDF-graphite-PMMA composites

The real part of the dielectric constant for the blend having 0.9 % of graphite is as shown in figure B.11. The imaginary part of the dielectric constant for the blend having 0.9 % of graphite is as shown in figure B.12. The loss (dissipation) factor for the blend having 0.9 % of graphite is as shown in figure B.13. The real part of the dielectric constant for the blend having 9.5 % of graphite is as shown in figure B.14. The imaginary part of the dielectric constant for the blend having 9.5 % of graphite

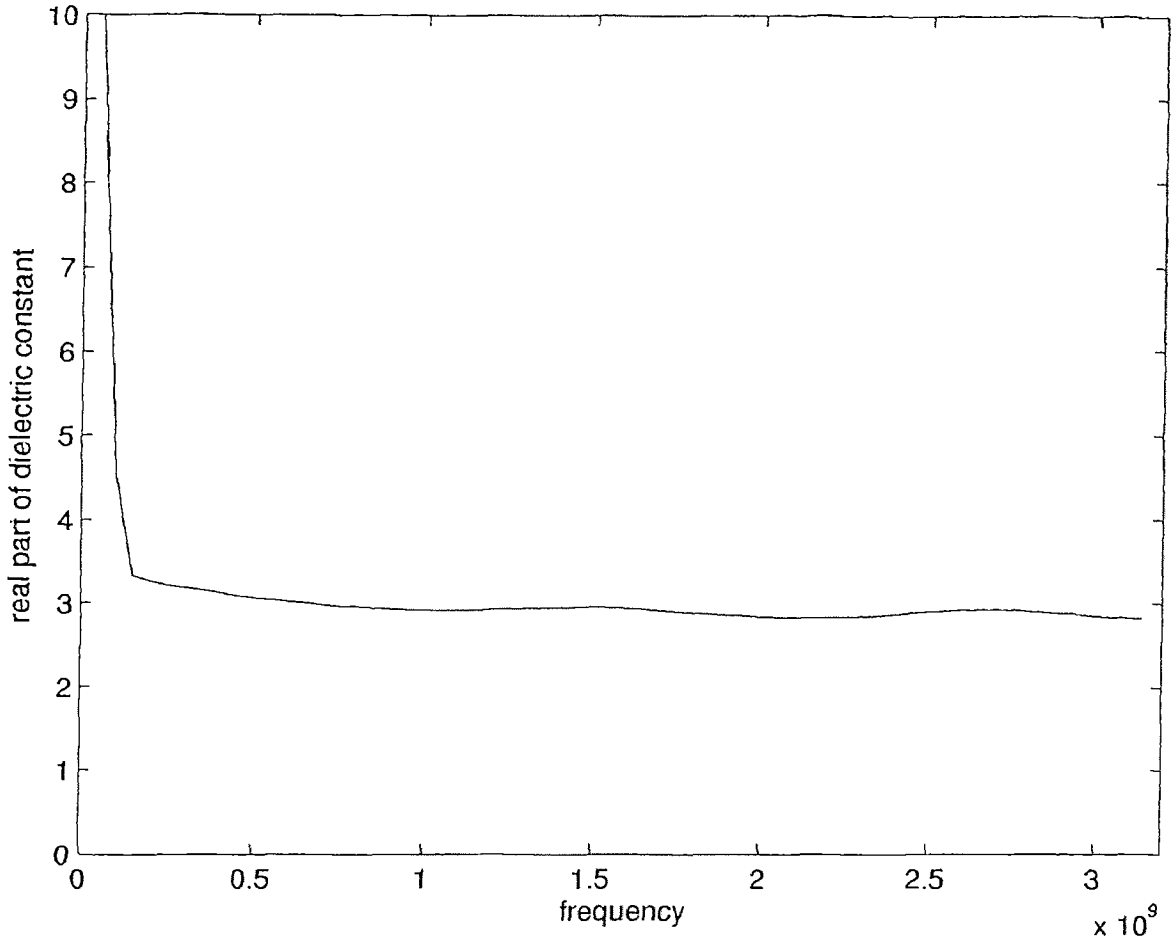

Figure B.11 Real part of dielectric constant versus the frequency for PVDF-Graphite loaded PMMA in which the PVDF concentration was 5 % by weight and the graphite concentration was 0.9 %

is as shown in figure B.15. The loss (dissipation) factor for the blend having 9.5 % of graphite is as shown in figure B.16. The data for frequencies after the point where the imaginary part changes sign (becomes negative) should not be considered as the air-line becomes multimoded beyond these frequencies. The data after that point has been included to illustrate the deleterious effect of multimoded condition on the computation of dielectric constant. The real part of the dielectric constant for the blend having 17 % of graphite is as shown in figure B.17. The imaginary part of the dielectric constant for the blend having 17 % of graphite is as shown in

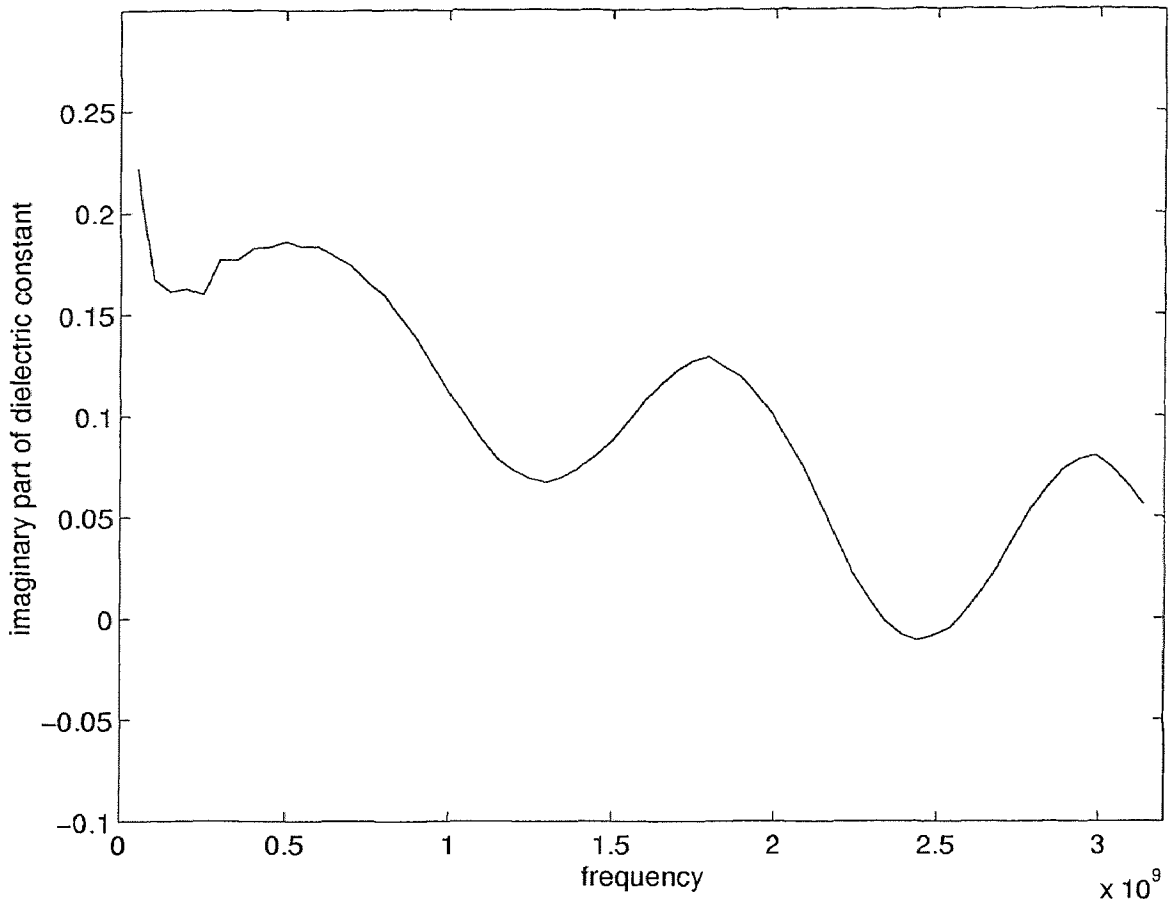

Figure B.12 Imaginary part of dielectric constant versus the frequency for PVDF-Graphite loaded PMMA in which the PVDF concentration was 5 % by weight and the graphite concentration was 0.9 %

figure B.18. The loss (dissipation factor) of the PVDF-PMMA-Graphite sample having 17 % graphite is as shown in figure B.19. The dielectric constant curves for the highest (20.5 %) graphite concentration are presented next. The noisy nature of the graphs may be due to fact that the smoothing function was was not turned on during the measurements. The real part of the dielectric constant for the blend having 20.5 % of graphite is as shown in figure B.20. The imaginary part of the dielectric constant for the blend having 20.5 % of graphite is as shown in figure B.21. The loss (dissipation factor) of the PVDF-PMMA-Graphite sample having 20.5 %

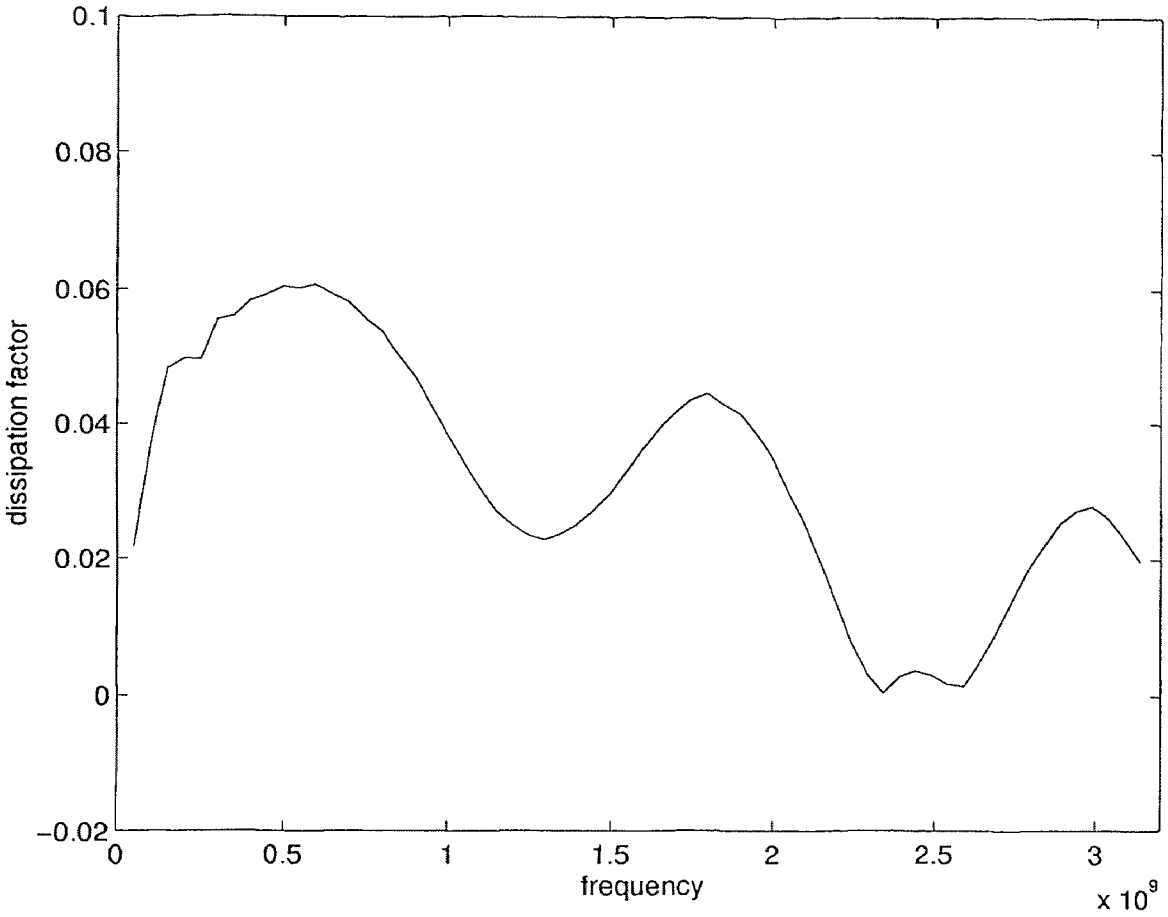

Figure B.13 The dissipation factor versus the frequency for PVDF-Graphite loaded PMMA in which the PVDF concentration was 5 % by weight and the graphite concentration was 0.9 %

graphite is as shown in figure B.22.

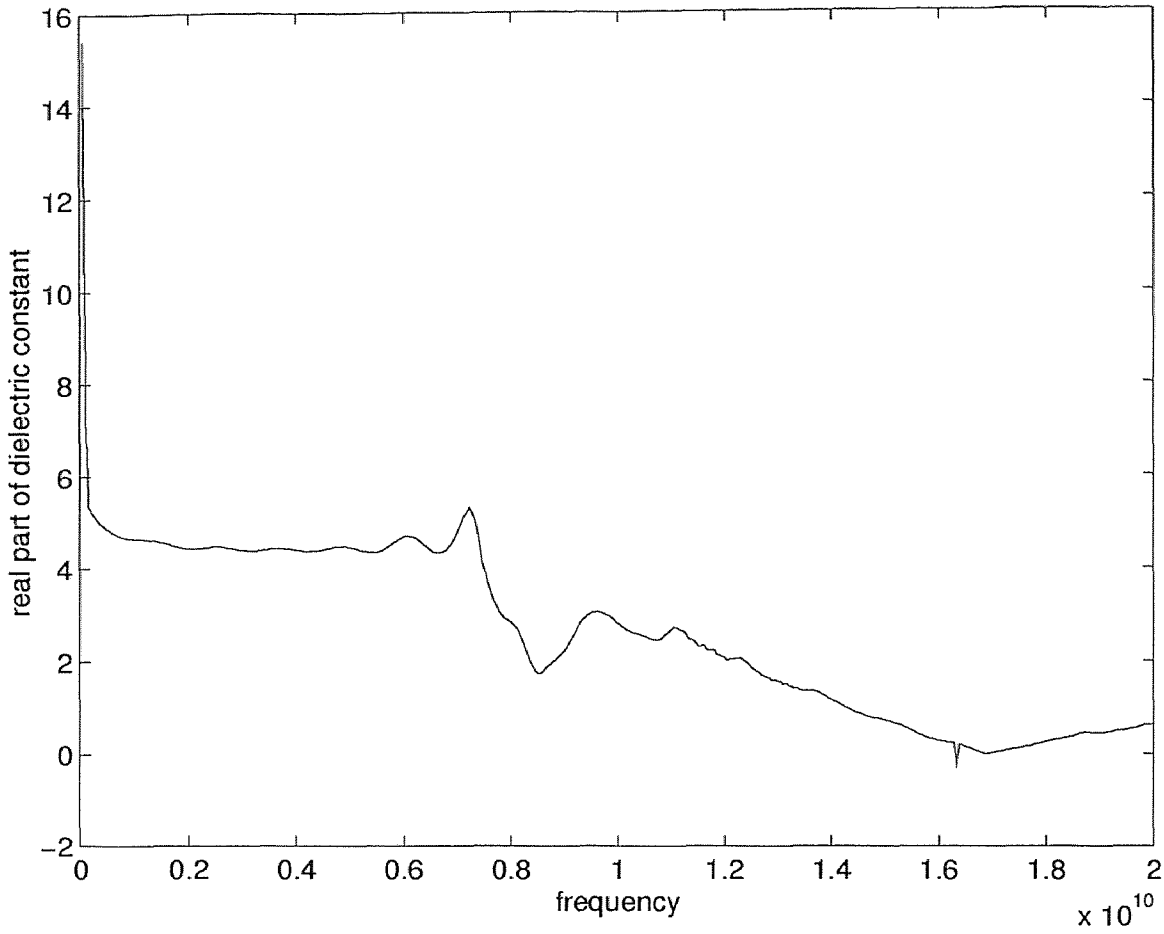

Figure B.14 Real part of dielectric constant versus the frequency for PVDF-Graphite loaded PMMA in which the PVDF concentration was 5 % by weight and the graphite concentration was 9.5 %.

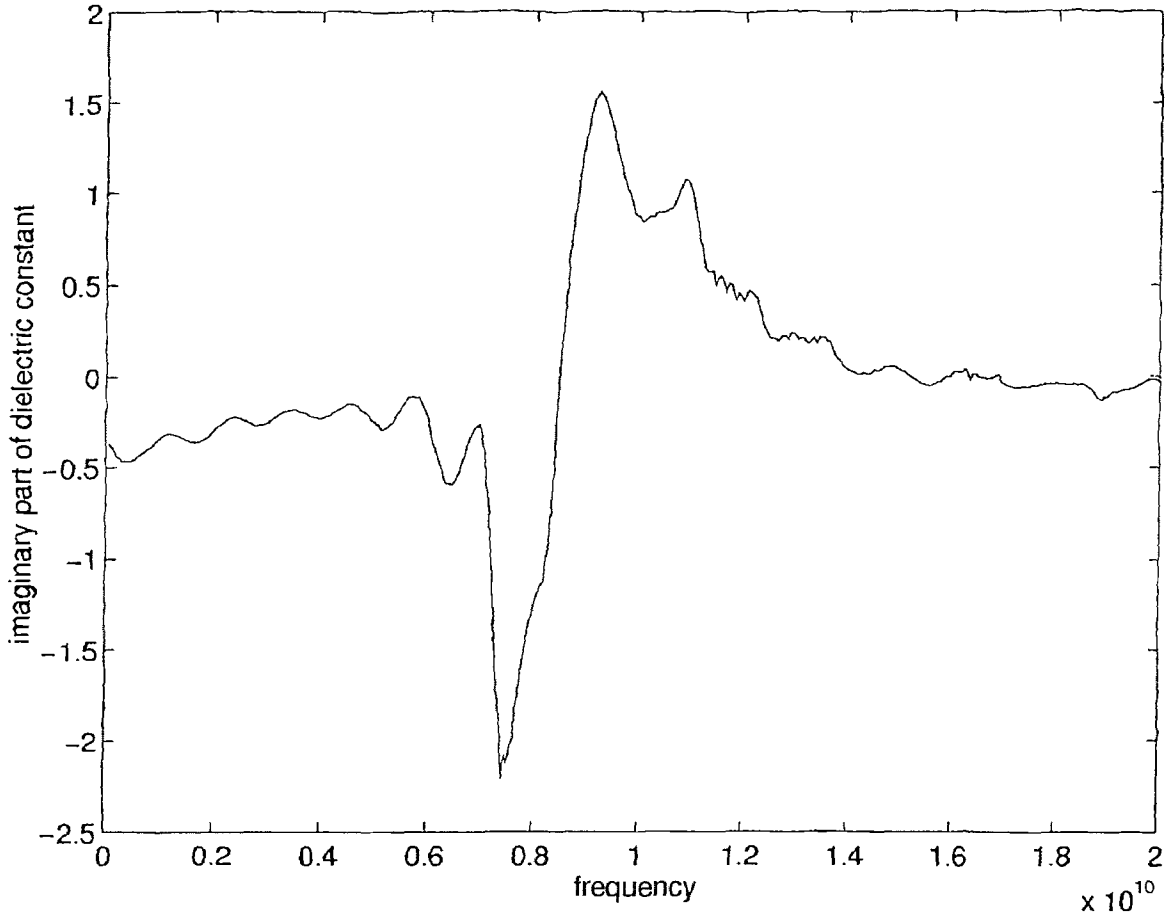

Figure B.15 Imaginary part of dielectric constant versus the frequency for PVDF-Graphite loaded PMMA in which the PVDF concentration was 5 % by weight and the graphite concentration was 9.5 %.

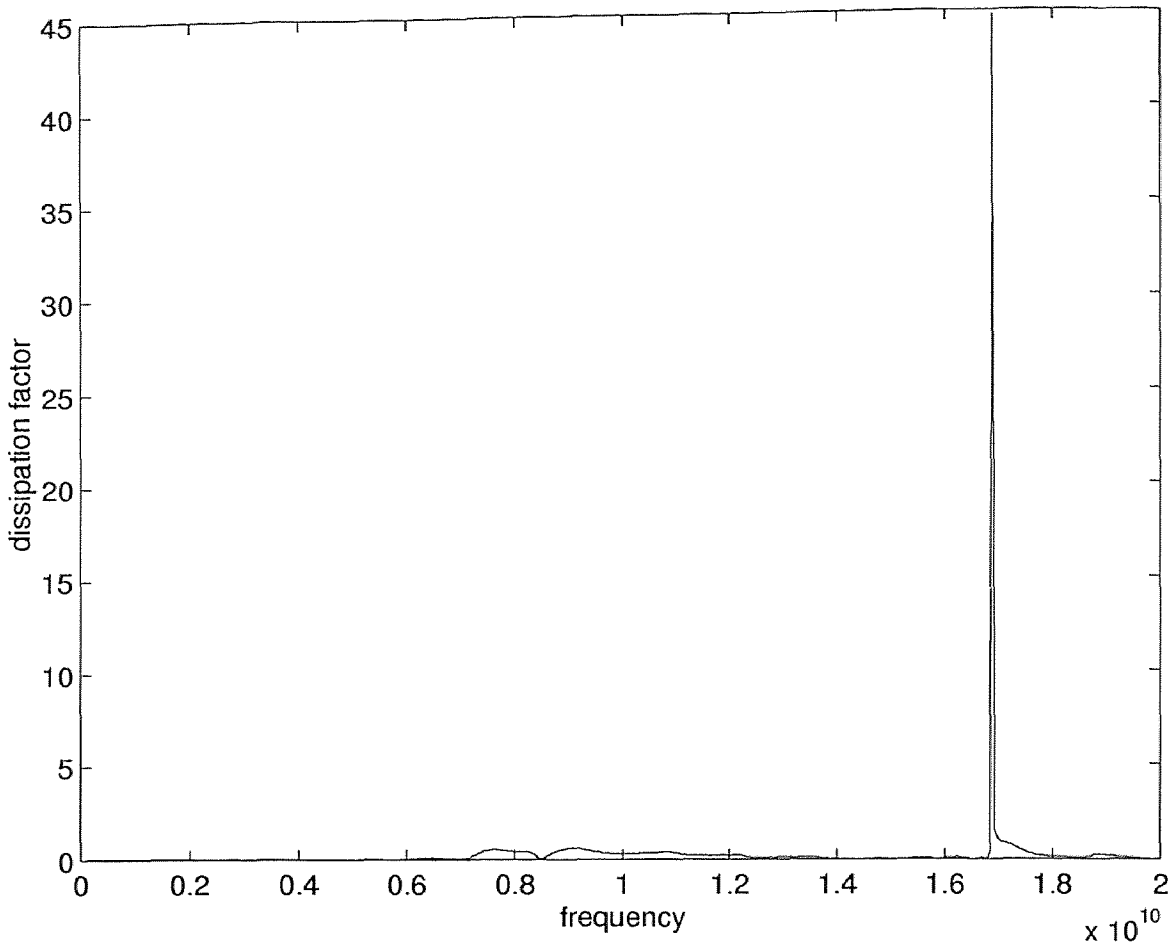

Figure B.16 The dissipation factor versus the frequency for PVDF-Graphite loaded PMMA in which the PVDF concentration was 5 % by weight and the graphite concentration was 9.5 %.

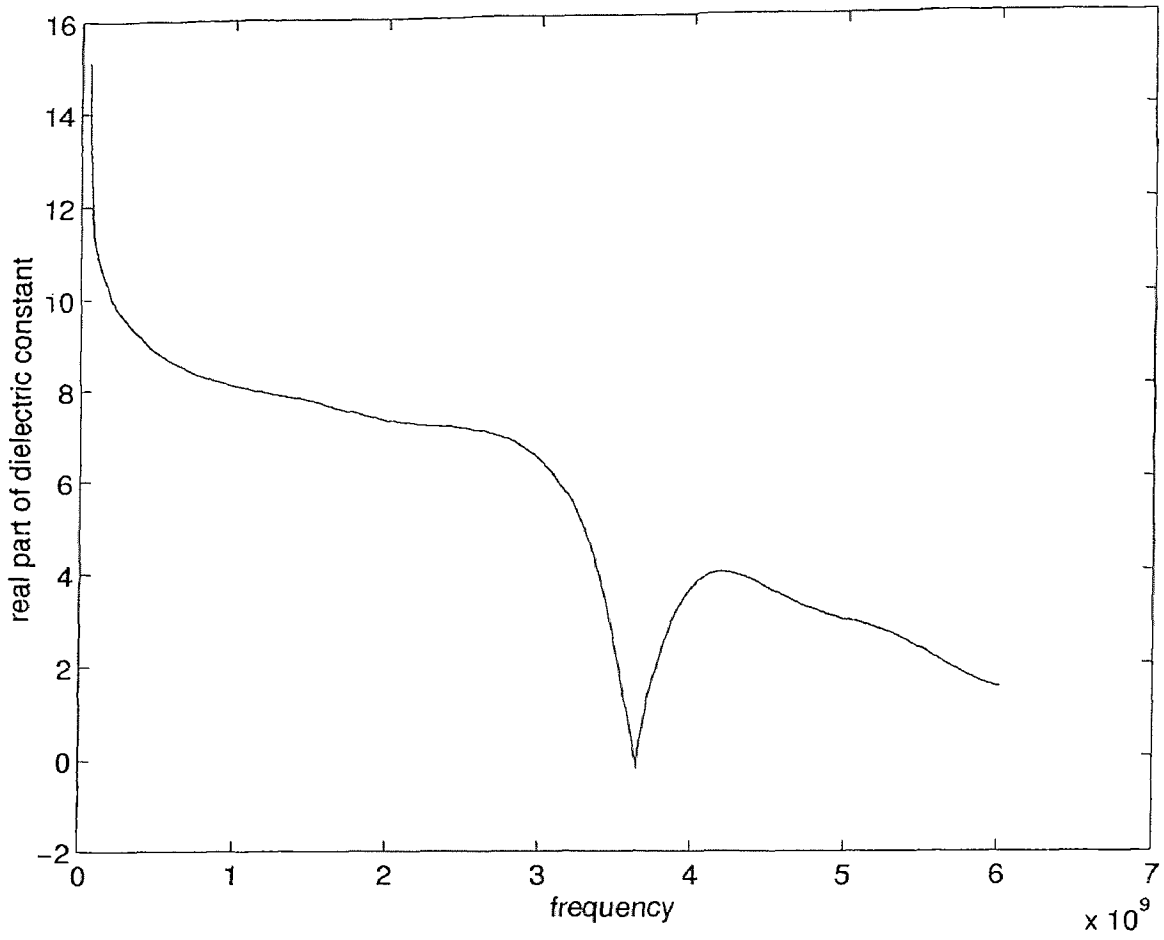

Figure B.17 Real part of dielectric constant versus the frequency for PVDF-Graphite loaded PMMA in which the PVDF concentration was 5 % by weight and the graphite concentration was 17 %.

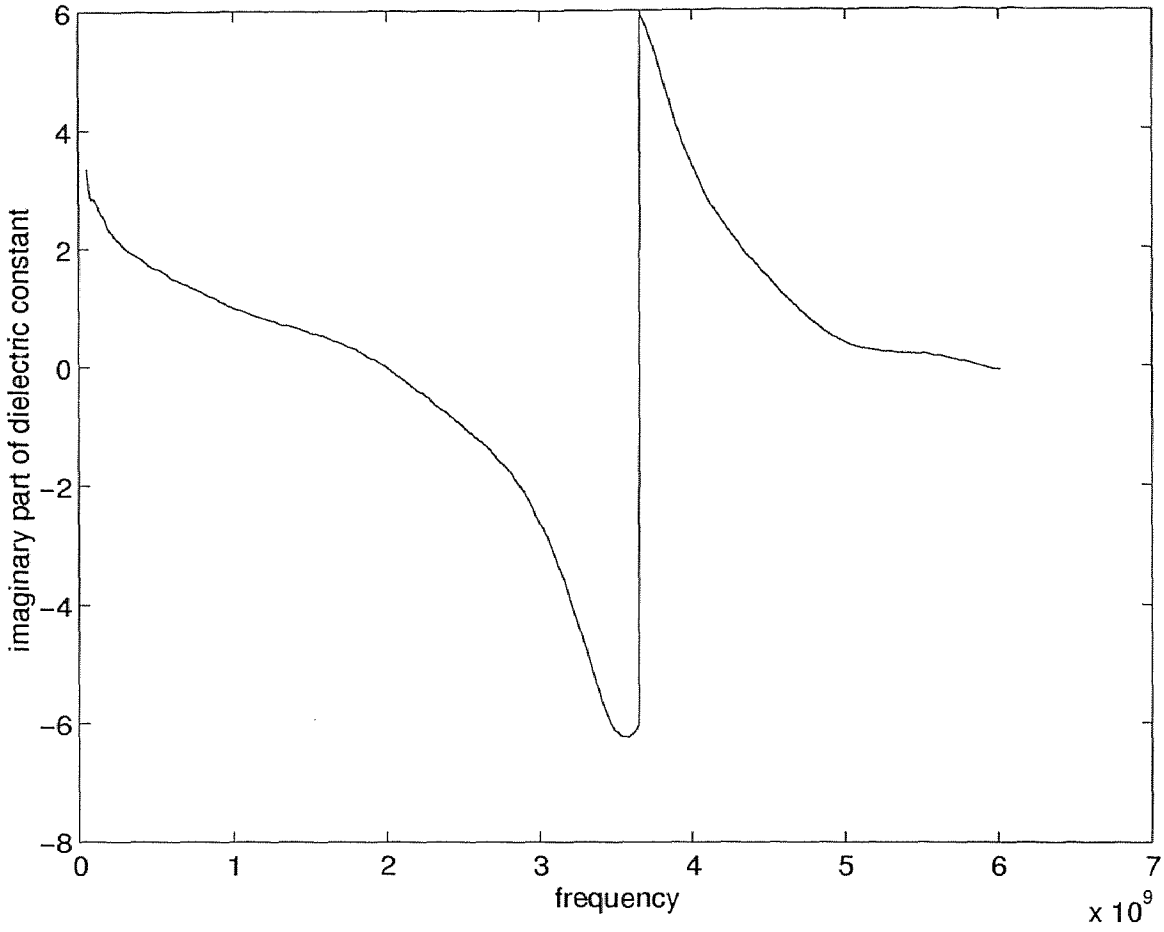

Figure B.18 Imaginary part of dielectric constant versus the frequency for PVDF-Graphite loaded PMMA in which the PVDF concentration was 5 % by weight and the graphite concentration was 17 %

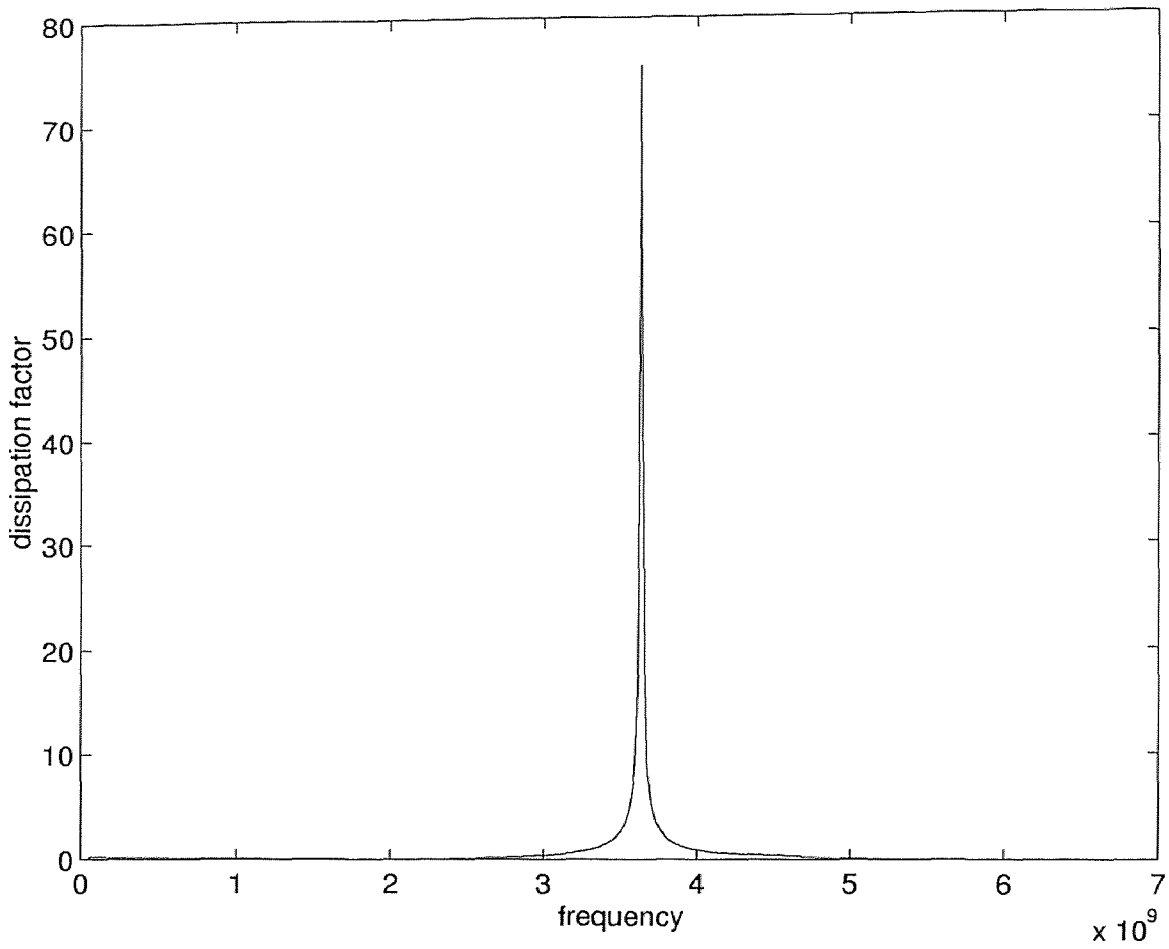

Figure B.19 The dissipation factor versus the frequency for PVDF-Graphite loaded PMMA in which the PVDF concentration was 5 % by weight and the graphite concentration was 17 %

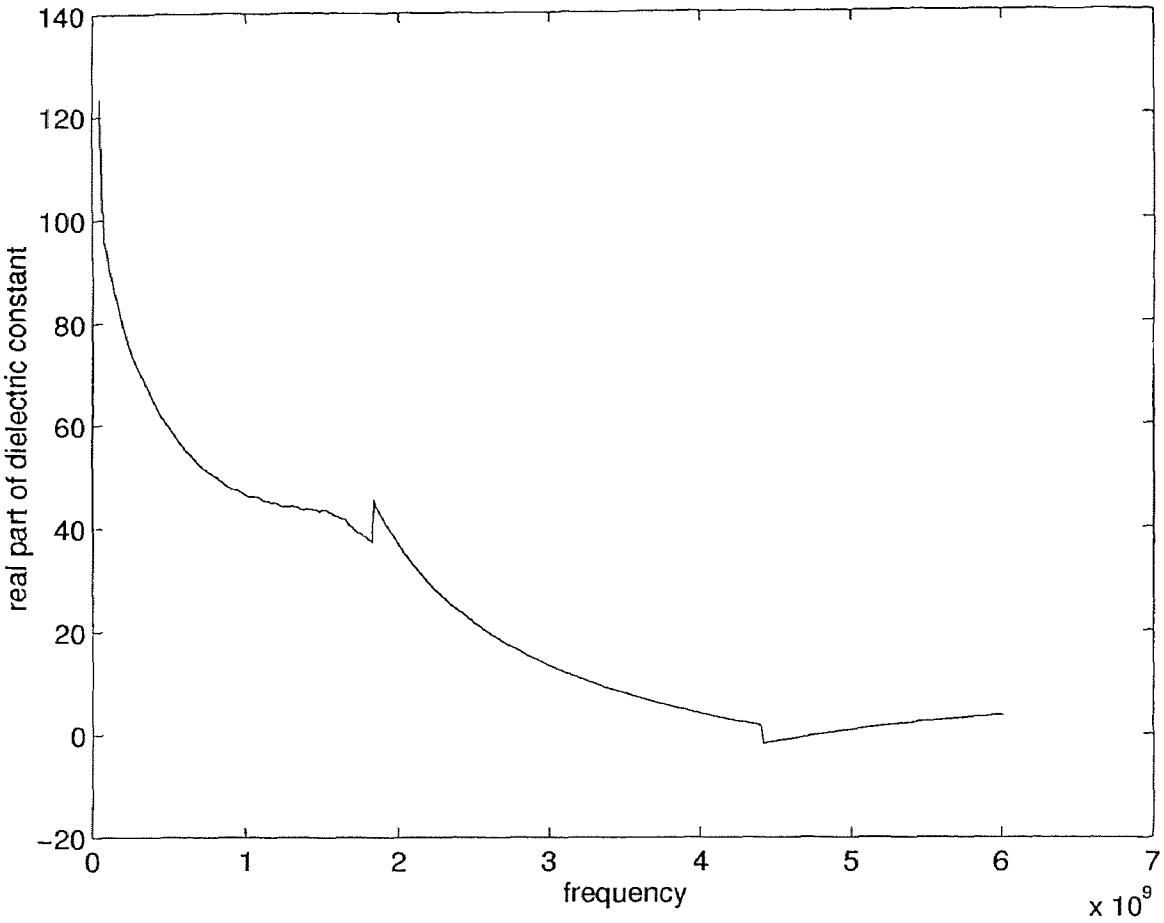

Figure B.20 Real part of dielectric constant versus the frequency for PVDF-Graphite loaded PMMA in which the PVDF concentration was 5 % by weight and the graphite concentration was 20.5 %.

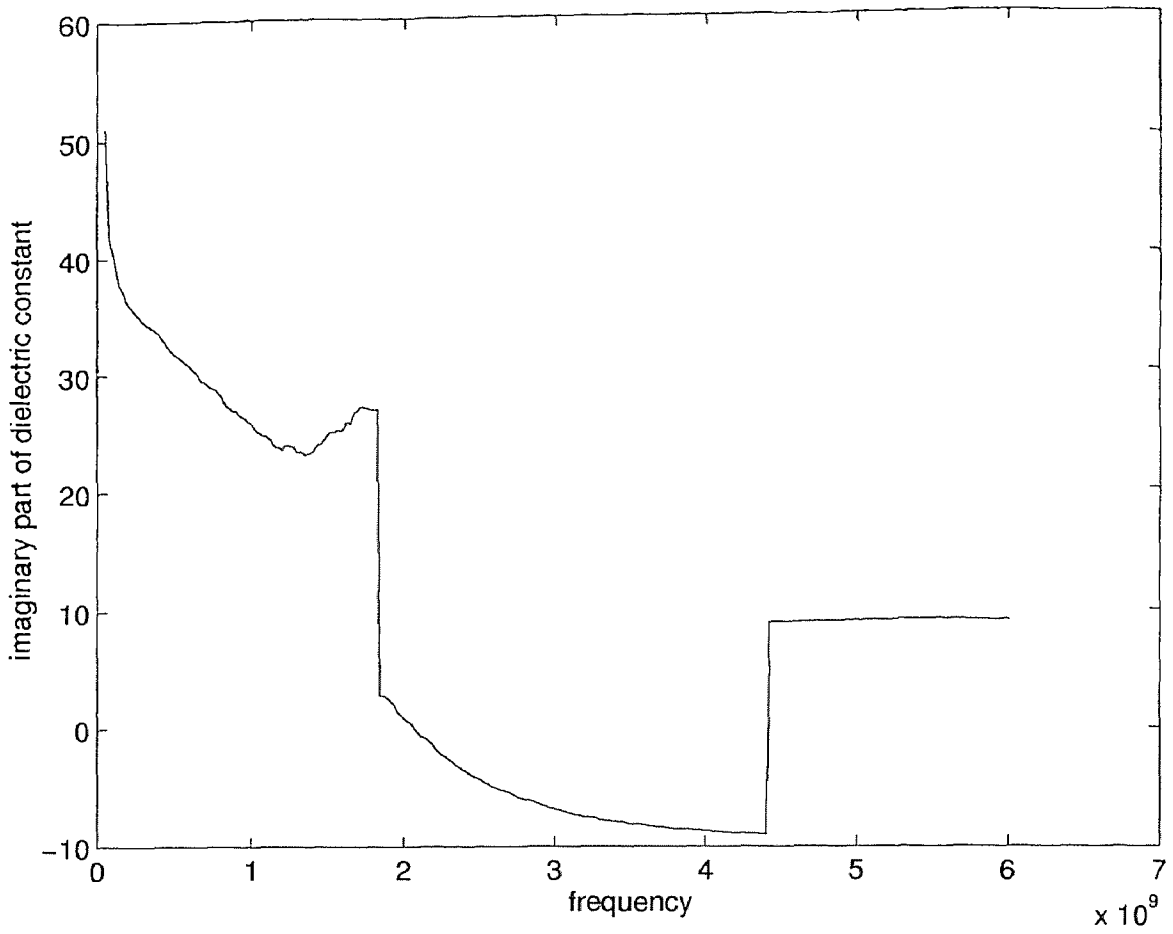

Figure B.21 Imaginary part of dielectric constant versus the frequency for PVDF-Graphite loaded PMMA in which the PVDF concentration was 5 % by weight and the graphite concentration was 17 %

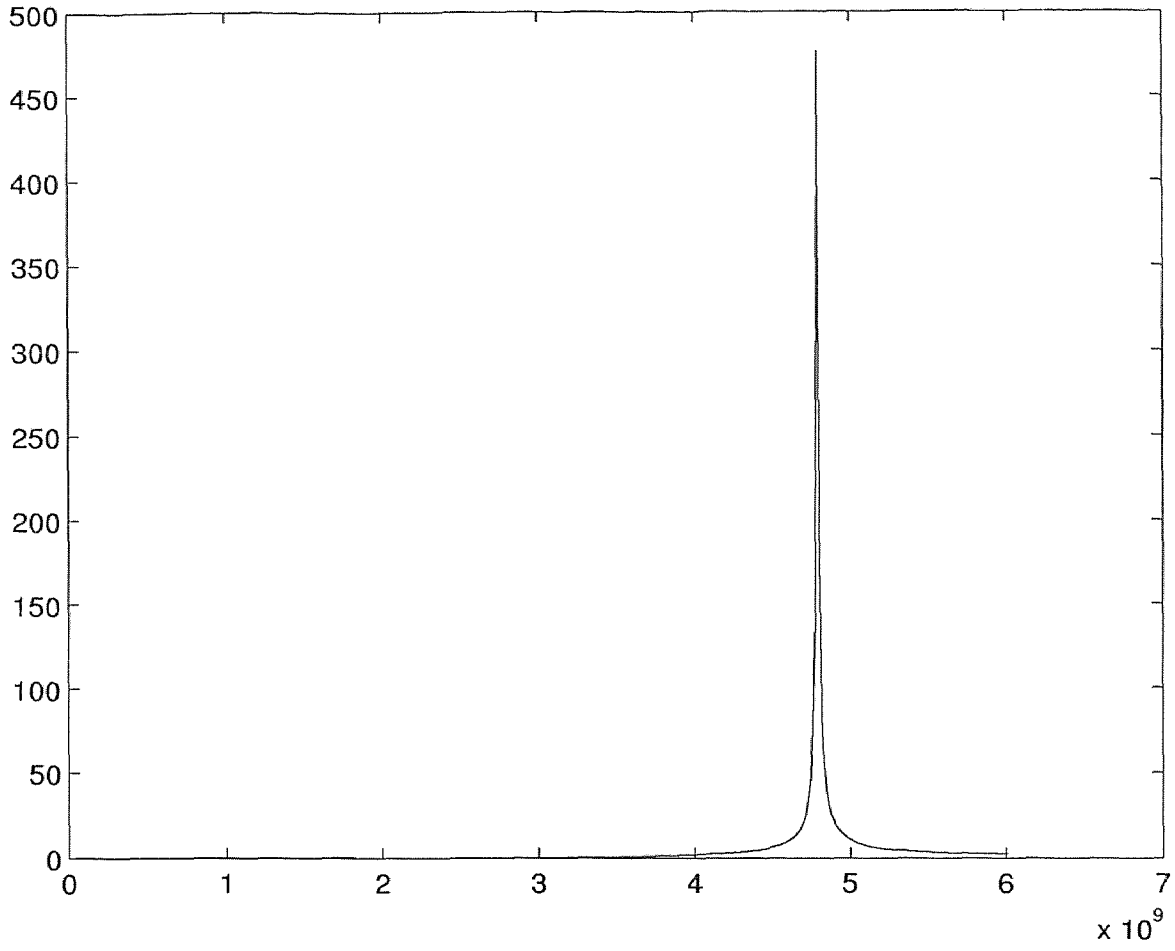

Figure B.22 The dissipation factor versus the frequency for PVDF-Graphite loaded PMMA in which the PVDF concentration was 5 % by weight and the graphite concentration was 20.5 %

REFERENCES

1. Robert E. Collin, *Field Theory of Guided Waves*, IEEE Press, Englewood Cliffs, New Jersey, 1991.

2. A. A. Zaky and R. Hawley, *Dielectric Solids*, Dover Publications Inc., New York, New York, 1970.

3. S. Ganchev, J. Bhattacharyya, S. Bhakiara, N. Qaddoumi, D. Brandenburg, and R. Zoughi, "Microwave Diagnosis of Rubber Compounds", *IEEE Transactions on Microwave Theory and Techniques*, Vol. 42, No. 1, pp. 18-24, January 1994.

4. H. Grebel and P. Chen,"Artificial Dielectric Polymeric Waveguides: Semiconductor-Embedded films", *Optical Society of America*, Vol. 15, No. 12, pp. 667-669, June 15, 1990.

5. H. Grebel and M. Jimenez,"Conditional Artificial Dielectrics: Phase and Amplitude Response at Microwave Frequencies", *IEE Proceedings-J*, Vol. 140, No. 4, pp. 232-36, August 1993.

6. T. R . Jow and P. J. Cygan,"Dielectric Breakdown of Polyvinylidene Fluoride and its Comparison With Other Polymers, *Journal of Applied Physics*, Vol. 73 (10), pp. 5147-51, May 15, 1993.

7. Naoto Tsutsumi, Yoshiaki Ueda, Tsuyoshi Kiyotsukuri, Aime S. DeReggi, G. Thomas Davis,"Thermal Stability of Internal Electric Eield and Polarization Distribution in Blend of Polyvinylidene Fluoride and Polymethylmethacrylate", *Journal of Applied Physics*, Vol. 74 (5), pp. 3366-72, September 1993.

8. T. T. Wang, M. M. Sondhi, H. von Seggern and S. Tasaka,"Dielectric hysterisis behaviour in form I poly(vinylidene fluoride), *Journal of Applied Physics*, Vol. 62 (11), pp. 4514-17, December 1, 1987.

9. Krishna Naishadham and Prasad K. Kodaba,"Measurement of Microwave Conductivity of a Polymeric Material with Potential Applications in Absorbers and Shielding, *IEEE Transactions in Microwave Theory and Techniques*, Vol. 39, No. 7, pp. 1158-64, July 1991.

10. Laurent Olmedo, Patrick Hourquebie and Franck Jousse,"Microwave Absorbing Materials Based on Conducting Polymers, *Advanced Materials*, Vol. 5, No. 5, pp. 373-77, May 1993.

11. J. Yacubowicz and M. Narkis,"Dielectric Behavior of Carbon Black Filled Polymer Composites, *Polymer Engineering and Science*, Vol. 26, No. 22, pp. 1568- 1573, December 1986.

12. American Standards of Test and Measurement, ASTM Designation: D 150-87, Standard Test Methods for A-C Loss Characteristics and Permittivity (Dielectric Constant) of Solid Insulating Materials, November 1987.

13. S. R. Seshadri, *Fundamentals of Transmission Lines and Electromagnetic Fields*, Addison-Wesley Publishing Company, New York, New York, pp. 101-121, 1971.

14. S. Roberts and A. von Hippel, "A New Method for Measuring Dielectric Constant and Loss in the Range of Centimeter Waves",*Journal of Applied Physics*, Vol. 17, pp. 610-16, July 1946.

15. A. M. Nicolson and G. F. Ross, "Measurements of the Intrinsic Properties of Materials by Time-Domain Techniques", *IEEE Trans. Instrum. Meas.*, Vol. IM-19, pp. 377-382, Nov. 1970.

16. Hewlett Packard Product Note 8510-3, "Materials Measurement : Measuring the Dielectric Constant of Solids with the HP 8510 Network Analyser", August 1, 1985.

17. Engineering Staff of the Microwave Division, Hewlett Packard Company, *Microwave Theory and Measurements*, Prentice-Hall, Englewood Cliffs, New Jersey, 1962.

18. William B. Weir, "Automatic Measurement of Complex Dielectric Constant and Permeability at Microwave Frequencies", *Proceedings of The IEEE*, Vol. 62, No. 1, pp. 33-36, January 1974.

19. A. Von Hippel, *Dielectrics and Waves*, John Wiley and Sons, Inc., New York, New York, 1954.

20. Ryogo Kyogo, Takeo Nagamiya, *Solid State Physics*, McGraw Hill Book Company Inc., New York, New York, 2nd edition, 1969.

21. S. D. Stookey and R. J. Araujo, "Selective Polarization of Light Due to Absorption by Small Elongated Silver Particles in Glass", *Applied Optics*, Vol. 7, No. 5, pp. 777-79, May 1968.

22. R. H. Doremus,"Optical Properties of Small Silver Particles",*The Journal o f Chemical Physics*, Vol. 42, No. 1, pp. 414-417, January, 1965.

23. D. Pozar, *Microwave Engineering*, Addison Wesley Publishing Co. Inc., New York, New York, 1990.